CERN-ATS-Note-2012-026 PERF
BI DCCT Note

RESULTS OF THE LHC DCCT CALIBRATION STUDIES

C. Barschel[1,2], M. Ferro-Luzzi[1], J.J. Gras[1], M. Ludwig[1], P. Odier[1], and S. Thoulet[1]

[1]CERN, Geneva, Switzerland
[2]RWTH Aachen University, III. Physikalisches Institut A, Aachen, Germany

May 24, 2012

Abstract

An important aspect of luminosity calibration measurements is the bunch population product normalization. In the case of the LHC, the treatment of this normalization can be split into three subjects: the total current measurement, the corrections from the non-perfect longitudinal distribution and the relative amplitude of the individual bunch populations. In this note, we discuss the first item in details and in the context of the 2010 and 2011 luminosity calibration measurements performed for each LHC Interaction Point. Effects Internal to the DCCT, the sensitivity to external factors, uncertainty related to the absolute calibration and comparison of two systems are all addressed. The DCCT uncertainty and numerical examples are given.

Contents

1 Introduction

Several luminosity calibration experiments were carried out in 2010 and 2011 at the LHC, with proton collisions (p-p) and with ion collisions (Pb-Pb), to obtain physics cross section normalizations at each Interaction Point (IP). Both the van der Meer (VDM) scan method and the beam-gas imaging (BGI) method were used. The experiments were carried out at the zero-momentum frame energies $\sqrt{s} = 7$ and 2.76 TeV for p-p and $\sqrt{s} = 7\,Z$TeV for Pb-Pb. A summary of the most relevant conditions of each set of VDM scans are listed in table 1.

The first measurements showed that one of the dominant uncertainties is introduced through the bunch population product normalization. As a consequence, a detailed bunch population analysis was carried out using data from the LHC Beam Current Transformers (BCTs) and from the LHC detectors (ALICE, ATLAS, CMS and LHCb). An analysis procedure was defined and bunch population uncertainties were quantified. The results of a first analysis for 2010 calibration measurements were documented in two bunch current normalization notes [1, 2] where a detailed description of the procedure used to determine the bunch populations and their associated uncertainties can be found. The precision was limited by the understanding of the BCT data at that stage. Since then, a number of additional tests were carried out which significantly improved the understanding of the bunch current measurements. The purpose of the present note and of two companion notes [3, 4] is to review the bunch population measurements and their accuracy in the light of these improvements.

Table 1: VDM luminosity calibration series for the LHC (2010 and 2011). The number of bunches in brackets indicates the number of "pilot" proton bunches in addition to the number of "main" proton bunches. Here, $\langle N \rangle$ is an indicative value of the main bunch charge in units of 10^{10} elementary charges.

Period / beams	β^* (m) IP1&5 / 2 / 8	Net angle α_{net} (μrad)	$\sqrt{s}/Z$ (TeV)	LHC fill	Nr of bunches	Colliding in IP1&5 / 2 / 8	scanned IPs	$\langle N \rangle$ ($10^{10}e$)
Apr-May 2010 p-p	2 / 2 / 2	0 / 0 / 0	7	1058	3	2 / 2 / 2	5	1.1
				1059	2	1 / 1 / 1	1, 8	1.1
				1089	2	1 / 1 / 1	1, 5	2.0
				1090	2	1 / 1 / 1	2	2.0
Oct 2010 p-p	3.5 / 3.5 / 3.5	200 / 500 / 340	7	1386	19	6 / 1 / 12	1, 5	8.0
				1422	16	3 / 1 / 12	2, 5, 8	8.0
Nov 2010 Pb-Pb	3.5 / 3.5 / 3.5	0 / 0 / -	7	1533	121	113 / 114 / 0	1, 2, 5	0.8
Mar 2011 p-p	11 / 10 / 10	0 / 710 / 1370	2.76	1653	72 (+4)	64 / 48 / 16	1, 2, 5, 8	9.0
				1658			1	10.5
May 2011 p-p	1.5 / 10 / 3	240 / 440 / 1040	7	1783	38 (+1)	14 / 16 / 22	1, 2, 5, 8	8.5
Jun 2011 p-p	1.5 / 10 / 3	240 / 440 / 1040	7	1875	1092 (+1)	1042 / 35 / 1008	5	12.0
Oct 2011 p-p	90 / 10 / 10	0/ 440 / 540	7	2234	36	4 / 16 / 16	2, 8	9.0
Dec 2011 Pb-Pb	1 / 1 / 3	240 / 120 / -	7	2335	352	344 / 324 / 0	2	1.0
				2337			1, 5	1.0

As discussed in reference [1], the LHC is equipped with a number of Bunch Current Transformers (BCTs)*. Four independent Direct Current Current Transformers (DCCTs), two per ring (called system A and B), are used to measure the total beam current circulating in each LHC ring. The DCCT is designed to be insensitive to the time structure of the beam. Two Fast Bunch Current Transformers (FBCTs), one per ring, give a measure of the individual bunch charges. The FBCT is designed to produce a signal (one per 25 ns bunch slot) which is proportional to the charge in a slot, by integrating the charge observed inside a fast

*Throughout this note, it is assumed that the measured charge for Pb beams is exactly proportional to the particle population, with 82 as proportionality factor.

gate. The IP1 BPTX button pick-up was also used to measure the relative charge in nominally filled slots. Both the FBCT and BPTX devices are "blind" to a slot charge below a given threshold. Such beam charge, if present, will be measured by the DCCT but not by the FBCT/BPTX. This is called the "ghost" charge. It is defined as the total beam population outside the nominally filled 25 ns bunch slots. Other devices , such as the Longitudinal Density Monitor (LDM) or the LHCb detector, were also used, when available, to check the relative bunch populations.

The ghost charge was mainly measured by comparing the beam-gas rates from nominally empty bunch crossings with those of crossings in which only the slot of one beam was filled with a bunch. This technique was pioneered at IP8/LHCb (though efforts are now being made to deploy it at other LHC experiments). Given the nature of the LHCb detector readout electronics, the method was limited to a 25 ns granularity. Furthemore, within the 25 ns of a nominally filled slot the bunch occupies only one of the ten RF bins. Possible "satellite" bunches may populate the other nine RF bins. Such satellite charges were indeed observed and measured in different ways with the LHC detectors (by timing or vertex reconstruction) by monitoring longitudinally displaced collisions. The amount of satellite population is generally small compared to the main bunch population, but nevertheless needs to be quantified to obtain a precise measurement of the bunch population that actually participates in the luminosity signal. At some stage, the LHC LDMs were deployed and commissioned (one per ring). The LDM allows one to obtain a precise longitudinal distribution of the beam charge with a time resolution of about 90 ps. It is now used for constraining both the ghost charge and the satellite populations.

The bunch population normalization was decomposed in three tasks: (i) determination of the total beam charge, (ii) analysis of the relative bunch populations and (iii) corrections due to the ghost charge and satellite populations. The second and third items are discussed in detail in references [3] and [4], respectively. In the present note, we concentrate on the first item, namely the determination of the total beam intensity measurement and its uncertainties. The present report is structured as follows. Section 2 provides a description of the DCCT systems and its working principle. The analysis of all factors contributing to the DCCT uncertainties are divided in the following three main categories. A schematic overview is given in Fig. 1. Section 3 reports on the analysis of effects internal to the DCCT system which may contribute to the total current uncertainty. Section 4 discusses the sensitivity to external factors and beam conditions. Section 5 focuses on uncertainties related to the absolute calibration. The difference between systems A and B observed throughout 2011 is given in Sec. 6. The DCCT uncertainties are summarized in Sec. 7 along with a few explicit numeric examples for calculating beam current uncertainties.

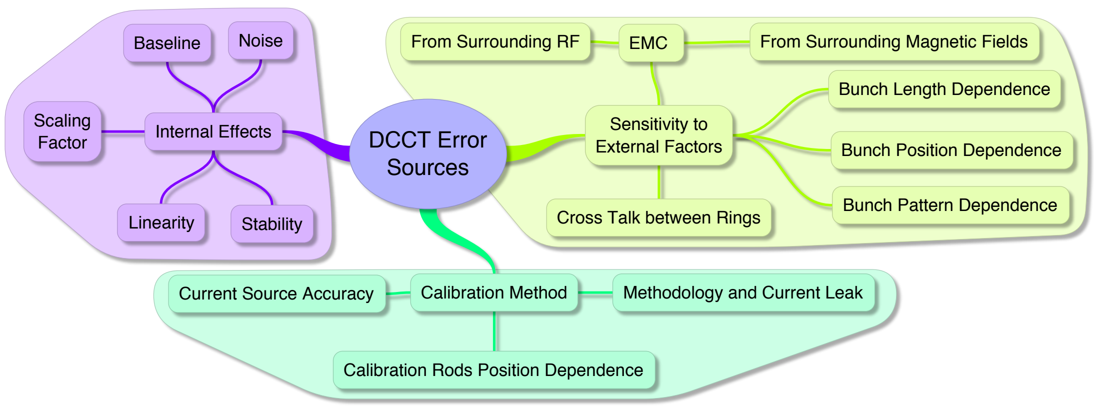

Figure 1: DCCT errors classification.

2 Description of the DCCT system

2.1 Layout

The DCCT which were designed and fabricated at CERN, are based on the principle of flux gate magnetometer and measure the mean intensity or current of the circulating beam. They can be used to measure the beam lifetime. In order to achieve the high levels of operational reliability required, two independent systems were installed on each ring (Fig. 2). Each system consists of one monitor per ring [5], one front and one back end electronics per monitor as well as one Front End Computer (FEC), housed in a VME crate, for acquisition and control purpose. The monitors and the front end electronics are located in LSS4R 152 meters away from IP4, in a region where the vacuum chamber is at room temperature, while the back end electronics and the FEC are located in the surface building SX4, which is easily accessible for performing maintenance and calibration tasks.

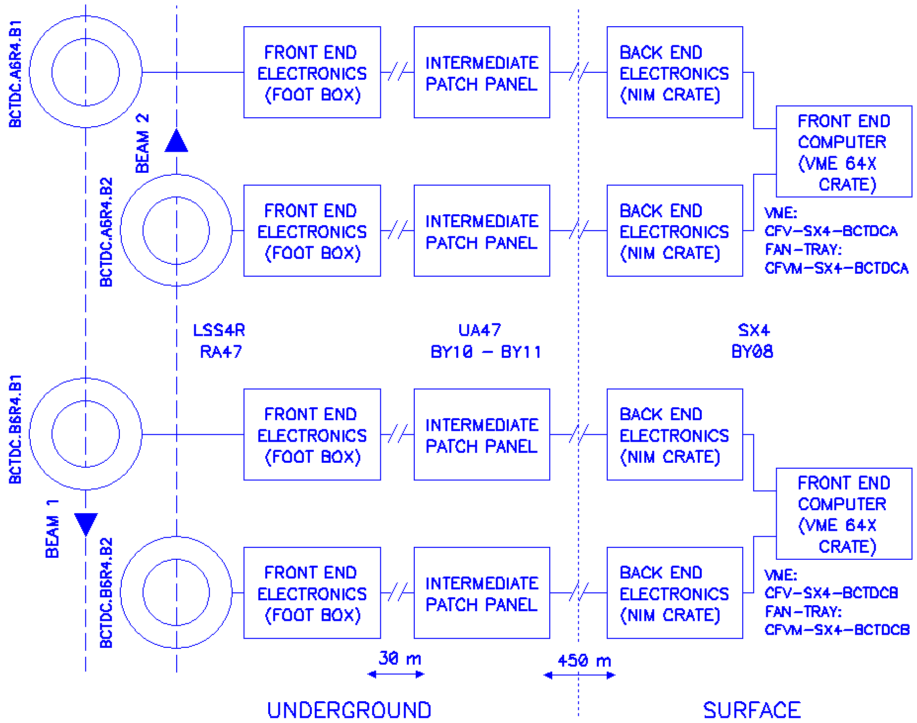

Figure 2: DCCT General Layout.

2.2 Principle

The DCCT exploits the non-linear magnetization curve of soft ferromagnetic material. Excitation coils of two cores are fed in opposite phase with a sinusoidal voltage at several 100 Hz (215Hz in this case) produced by the Modulator (Fig. 3). The modulation current of each core is distorted when the magnetic flux of the core enters into saturation. The distortion creates odd harmonics in the frequency spectrum of the modulation current. However, with the anti-phase excitation, the difference of the modulation current between both cores is zero, provided the cores are well matched. The principle is illustrated in Fig. 4. In the absence of current passing through the cores, both cores are in phase and driven simultaneously into saturation with opposing polarity. With the presence of a DC current, the core magnetization is biased with the same polarity in both cores, therefore, one core will reach its saturation before the other. In this case, the modulation current difference is not zero when one core is in saturation while the flux in the other core is still changing. A signal in the modulation current difference will appear at each polarity change i.e. at twice the modulation frequency, and the second harmonic of the modulator frequency appears in the modulation current as illustrated in Fig. 4 (right).The detection of the second harmonic is performed by synchronous detection at twice the modulation frequency. To extend the DCCT bandwidth, the detected signal is combined with an AC signal produced by a fast current transformer made of a third core. The generated common feedback current passes through the cores and cancels the magnetic field produced by the calibration or beam current. Therefore, the feedback current is equivalent to the beam or calibration current. The DCCT calibration is established with a current generator sending a known current through a dedicated coil allowing the calibration of the whole acquisition chain, from the sensor to the calibrated intensities made available digitally in the API to the control system.

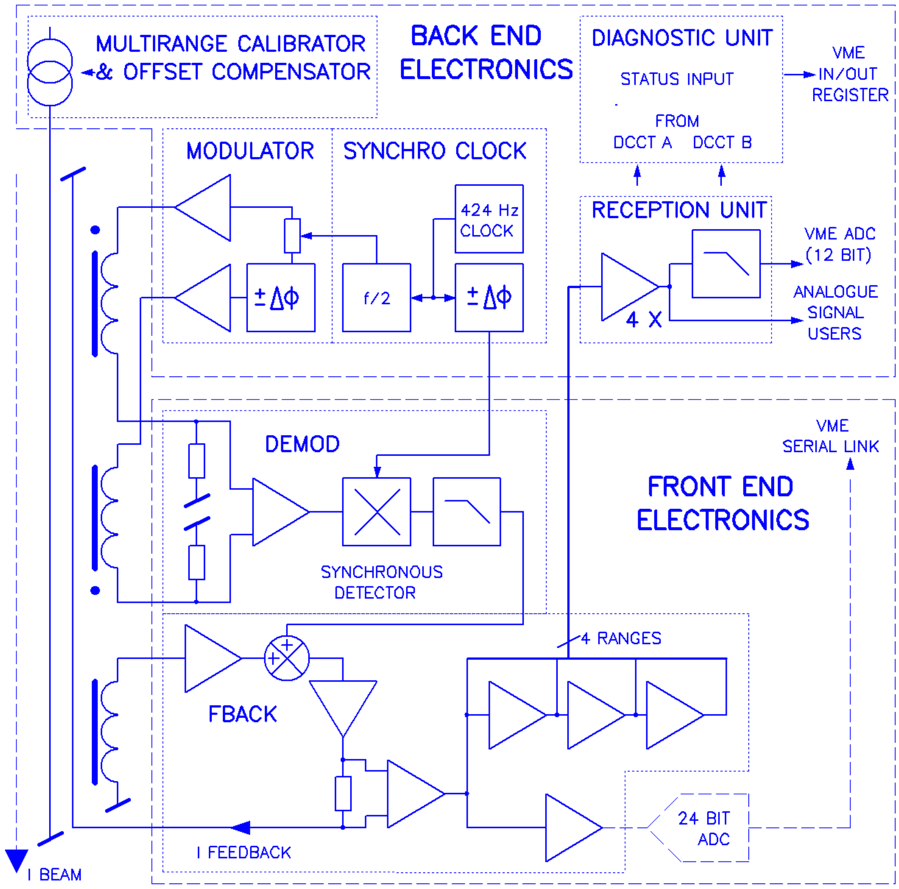

Figure 3: DCCT simplified schematics.

2.3 Implementation

The total beam population N_{tot} is extracted (for each ring separately) from the measured (raw) DCCT signals $S^{\mathrm{raw}}_{\mathrm{DCCT}}$ (in V) after correcting for the baseline offset $S^{\mathrm{offset}}_{\mathrm{DCCT}}$:

$$\begin{aligned} S_{\mathrm{DCCT}} &= S^{\mathrm{raw}}_{\mathrm{DCCT}} - S^{\mathrm{offset}}_{\mathrm{DCCT}} \\ N_{\mathrm{tot}} &= \alpha \cdot S_{\mathrm{DCCT}} = N_{\mathrm{DCCT}}\,. \end{aligned} \tag{1}$$

Here, α is the calibrated absolute scale factor of the DCCT (elementary charges/V) when fixing the absolute scale at 80% of the considered DCCT range with a precise current source. The measurement of the feedback current is made via four ranges (see Table 2), provided simultaneously, to cover the entire beam dynamic (10^9 to $5 \cdot 10^{14}$ protons). The DCCT bandwidth is limited, for noise reduction reason, to 20 Hz, even though the natural bandwidth is in the order of 20 kHz. The analogue signals of the four ranges are continuously acquired at 50Hz via a 12 bit ADC housed in a VME crate. The same ADC is used for both DCCT (beam 1 and beam 2) on one system. The choice of the pertinent range is performed by the real time program running at 10 Hz synchronously with the machine timing. The beam intensity, actually the number of circulating

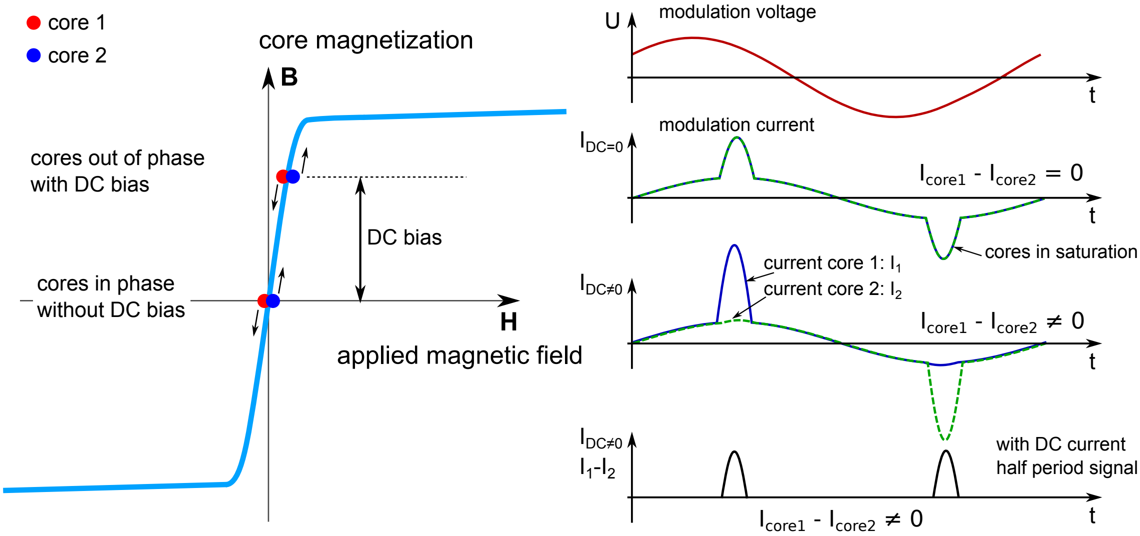

Figure 4: (left) The non-linear response of the soft ferromagnetic cores permits to drive the cores into saturation. The presence of a DC current biases the magnetization of both cores with the same polarity. (right) The non-linear magnetization of the cores distorts the modulation current; the current is higher when the core is saturated. The modulation current difference between the cores is zero when the cores are in phase; however, a signal in the modulation current appears when the cores are out of phase due to a DC current flowing though the cores. The modulation current has a phase delay of about 45 degrees.

Table 2: DCCT ranges. The scale factor for a Least Significant Bit (LSB) (charges/ADC bin) is calibrated for each range and DCCT, the last column shows the approximate value.

Range	Scaling factor (charges/V)	Full scale (charges)	LSB value (charges)
1	$1 \cdot 10^{14}$	$5 \cdot 10^{14}$	$2.5 \cdot 10^{11}$
2	$1 \cdot 10^{13}$	$5 \cdot 10^{13}$	$2.5 \cdot 10^{10}$
3	$1 \cdot 10^{12}$	$5 \cdot 10^{12}$	$2.5 \cdot 10^{9}$
4	$1 \cdot 10^{11}$	$5 \cdot 10^{11}$	$2.5 \cdot 10^{8}$

charges, after arithmetic averaging is published each second with a resolution of up to 20ms for all machine control and operation interfaces such as i.e. logging and fixed display. The beam intensity is also published at 10 Hz rate for the machine protection system. Before each LHC beam injection a DCCT offset acquisition sequence is automatically launched. This sequence starts the acquisition in a hardware module of the four ranges offset for subsequent subtraction followed by the generation of four pulses of current, each lasting 100ms, used to check the calibration of the four ranges of the four DCCT's. Any result outside the given tolerance produces an explicit message sent to the LHC operators in charge and to the DCCT experts. At the end of the sequence the residual offset $S_{\mathrm{DCCT}}^{\mathrm{offset}}$ is acquired and averaged for a period of 60 s by the real time program. The actual calibration adjustment is made manually by the DCCT experts during the technical stops.

A dependence on the filling pattern has been discovered during 2010 as described in Sec. 4.2. The problem in the front-end electronic cards have been solved in the laboratory and a new improved version of the card has been reinstalled in the DCCT front-end during the winter shutdown in early January 2011. Additionally, the RF bypass has also been improved, see details in Ref. [6]. Except for the noise studies in Sec. 3.1 and 3.3, all in-situ measurements performed for this work are done with the new hardware which is in operation since 2011. Therefore the DCCT uncertainties presented in this work are also retroactively valid for the LHC 2011 run including the first van der Meer scans in March 2011. The new electronics have been tested up to intensities corresponding to the maximal number of 50 ns spaced bunches with nominal intensity.

3 Instrumental stability and linearity

3.1 Baseline subtraction method

The DCCT data as well as all measurements performed for this study are corrected for the baseline (offset) using the method defined Ref. [1]. The offset is measured in periods without beam before and after the analyzed fill. The value of the offset $S_{\mathrm{DCCT}}^{\mathrm{offset}}$ during the fill is linearly interpolated with the two bounds and subtracted from the data as illustrated in Fig. 5. Half of the largest peak-to-peak (P2P) variation in these two no-beam periods (before and after the fill) is taken as the uncertainty on the correction. A schematic example is shown in Fig. 6.

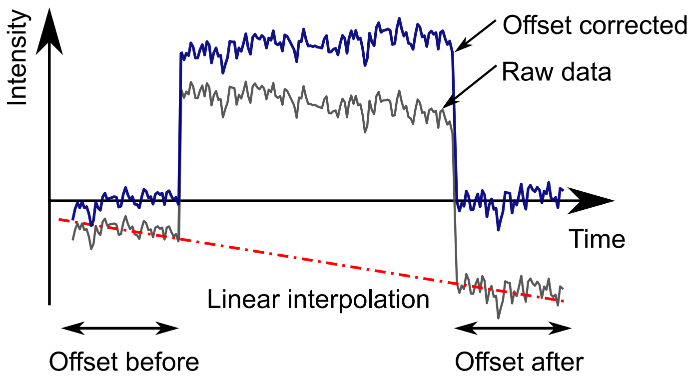

Figure 5: DCCT offset correction method. The offset $S_{\mathrm{DCCT}}^{\mathrm{offset}}$ is linearly interpolated using no-beam periods before and after the fill and subtracted from the raw signal $S_{\mathrm{DCCT}}^{\mathrm{raw}}$ to provide the final DCCT data S_{DCCT}.

A period of nine days of continuous noise have bean acquired at the end of 2010 after the last beam dump. This data is used to verify the baseline correction method over a longer time period and also to detect possible periodic fluctuations in the noise. The full data for system A/beam 1 is shown in Fig. 7, the data for the other three DCCT's is shown in Appendix A.1 (Figs. 58 to 60).

A verification of the baseline subtraction method is performed as follows (see also Fig. 6). A random gap length between 1 hour and 40 hours is taken at a random time position within nine days of data. Periods

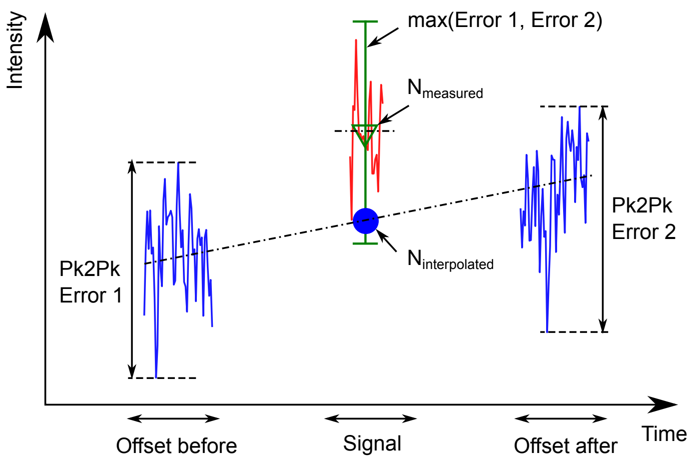

Figure 6: Offset uncertainty method. The largest peak-to-peak variation is taken as the uncertainty on the correction. The dot represents the interpolated offset, the triangle is the DCCT reading.

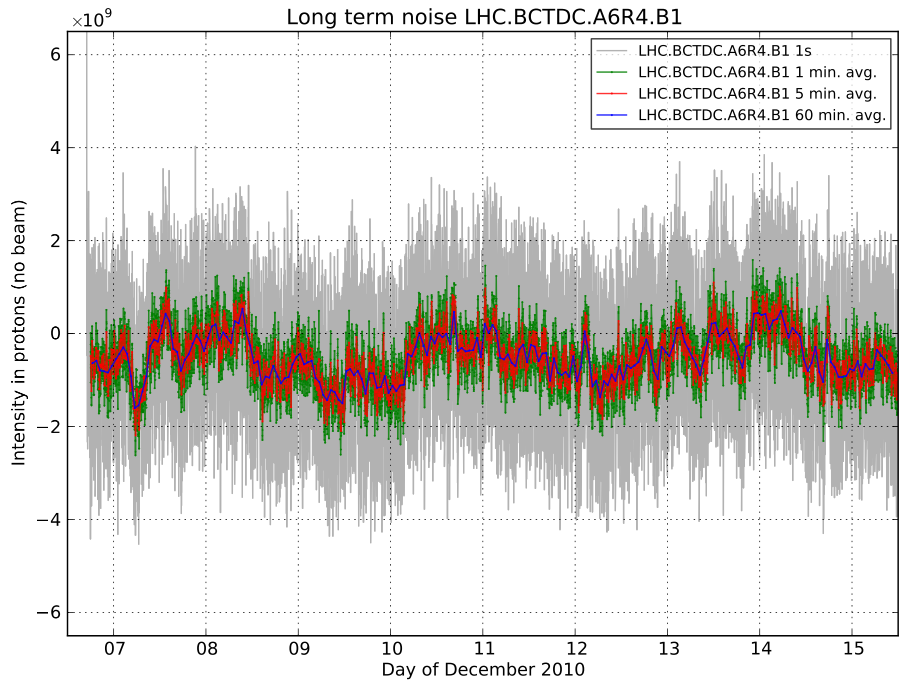

Figure 7: DCCT long term offset for system A/beam 1.

of two hours before and after the selected gap are taken as offset bounds and used to interpolate the offset $N_{\text{interpolated}}$ to the center of the gap with a linear function. The real offset N_{measured} is taken from the signal using a 1 hour average at the center of the gap and the largest peak-to-peak error from the offset bounds is taken as error for the interpolated offset. The interpolated offset $N_{\text{interpolated}}$ is compared to the measured value N_{measured} to verify that the interpolated offset lies within the given error. The test is performed 500 times for each DCCT, totaling 2000 data points. Fig. 8 shows the result for system A/beam 1 displaying only 50 out of the 500 points for better clarity. See Appendix A.1 (Fig. 61) for the result of all DCCT's. The ratio $|N_{\text{measured}} - N_{\text{interpolated}}|/(1/2\,\text{P2P error})$ for all tests and all DCCT's is combined in Fig. 9. A histogram of the largest peak-to-peak errors from all tests is shown in Fig. 10. In Ref. [1] the largest peak-to-peak error was assigned as a fixed error for all intensity measurements. As can be seen in Fig. 9, 79% of the tested offsets fall within $0.683 \cdot 1/2\,\text{P2P}$ error, which is better than for a Gaussian distribution; 8.2% are outside the expected peak-to-peak error.

In conclusion, the baseline correction method and error estimation described in [1] is valid. As seen in

Fig. 10, in general an envelope error of $\pm 1 \cdot 10^9$ charges can be assumed if the baseline has been corrected manually or if the offset is already smaller than $\pm 1 \cdot 10^9$ before and after the fill. A smaller error on the correction can be achieved by analyzing the offset manually which can be relevant for intensities acquired in range 4. For cases where the offset is not analyzed, a generic error can be used as discussed Sec. 3.2.

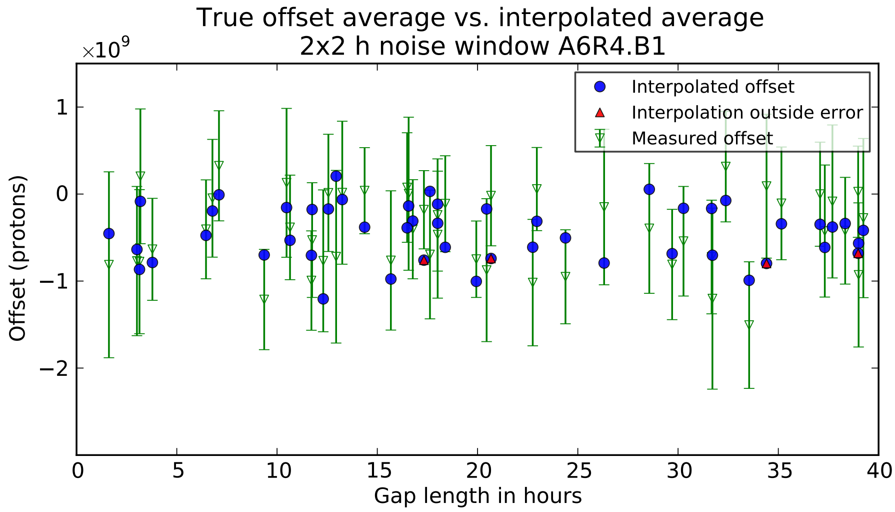

Figure 8: Offset box error test system A/beam 1 displaying 50 out of 500 points. Plain blue dots indicate an interpolated offset inside the error bar. A plain red triangle indicates an interpolated offset value outside of the expected error.

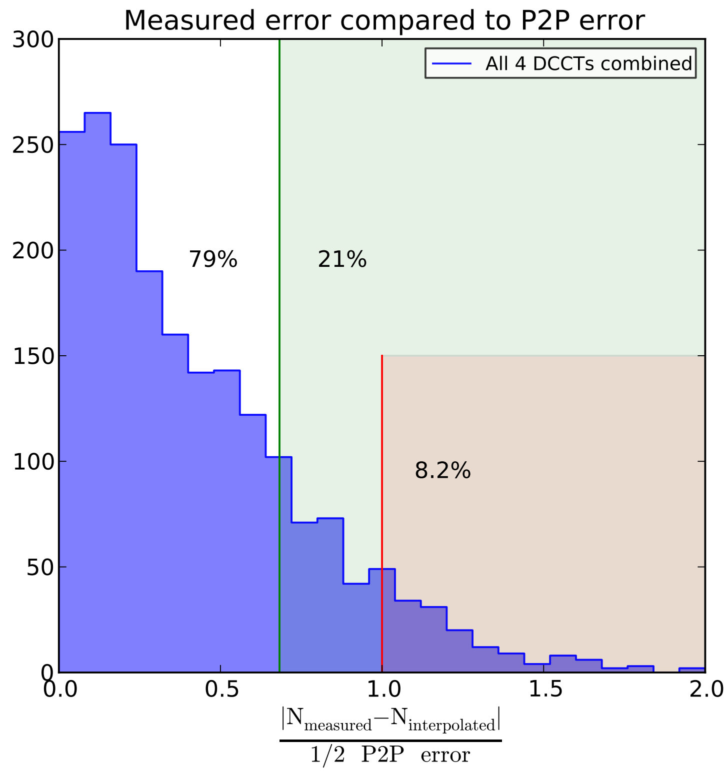

Figure 9: Offset box error histogram combining all 4 DCCT's. Entries with a ratio $|N_{measured} - N_{interpolated}|/(1/2\,\mathrm{P2P\ error}) < 1$ are tests where the interpolated offset lies within the peak-to-peak error. All values above one are tests where the measured offset lies outside the peak-to-peak error. From the 2000 tests, 79% have a ratio 0.683 indicated by the left vertical line. If the peak-to-peak error would be truly a Gaussian distribution, 68.3% of the tested offsets would lie below 0.683.

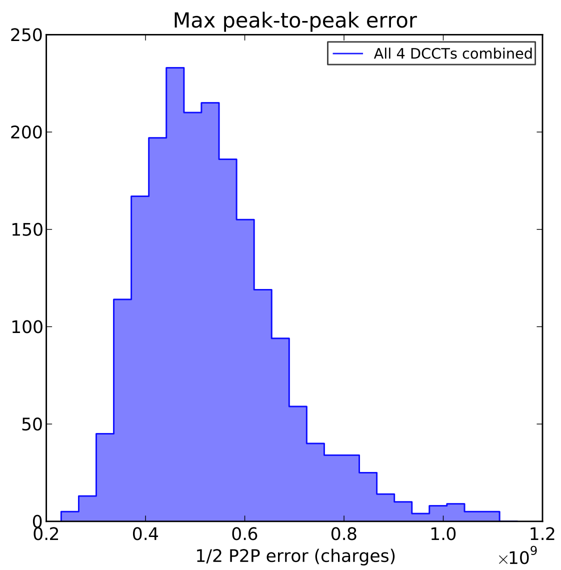

Figure 10: 1/2 P2P error observed within two hours or noise with samples of 5 minutes average. The histogram represents the expected distribution of the half peak-to-peak error attributed to the baseline correction.

3.2 Automatic baseline correction

The baseline is automatically corrected before each fill in the preparation sequence of the DCCT's. A first rough correction using an 80 ms average is performed at the hardware level before the signal acquisition, a second correction using a 60 s average is performed in the acquisition software such that every range is set at zero at the beginning of each fill. If the baseline is not analyzed manually as described in Sec. 3.1, a generic uncertainty of the baseline can be used which is based on the results of the following analysis.

An analysis has been performed to evaluate the offset deviation from zero at the end of fills. The baseline values for each range and DCCT were measured at the end of each fill in 2011[†]. The ADC raw data of every range is averaged over 10 minutes immediately after the beam dump and the offset correction which is measured automatically in the preparation sequence is applied to the average. Ideally the offset is zero when the beam is dumped. For each range, the absolute offset values of all DCCT's observed in 2011 are combined in a histogram as shown in Fig. 11.

Based on the histograms in Fig. 11, an error covering 68.3% and 99% offset deviations is provided in Table 3. This systematic error due to the offset has to be added to the DCCT uncertainty if the baseline is not corrected or analyzed manually as described in Sec. 3.1.

Table 3: Observed offset deviation at the end of fills for each range. The indicated offset error includes 68.3% (left column) and 99% (right column) of the measured fills.

Range	Absolute offset error (charges) 68.3% of samples	Absolute offset error (charges) 99% of samples
1	$\pm 7.0 \cdot 10^9$	$\pm 6 \cdot 10^{10}$
2	$\pm 2.1 \cdot 10^9$	$\pm 7 \cdot 10^9$
3	$\pm 1.3 \cdot 10^9$	$\pm 4 \cdot 10^9$
4	$\pm 1.3 \cdot 10^9$	$\pm 4 \cdot 10^9$

[†]Only fills declared for physics were analyzed.

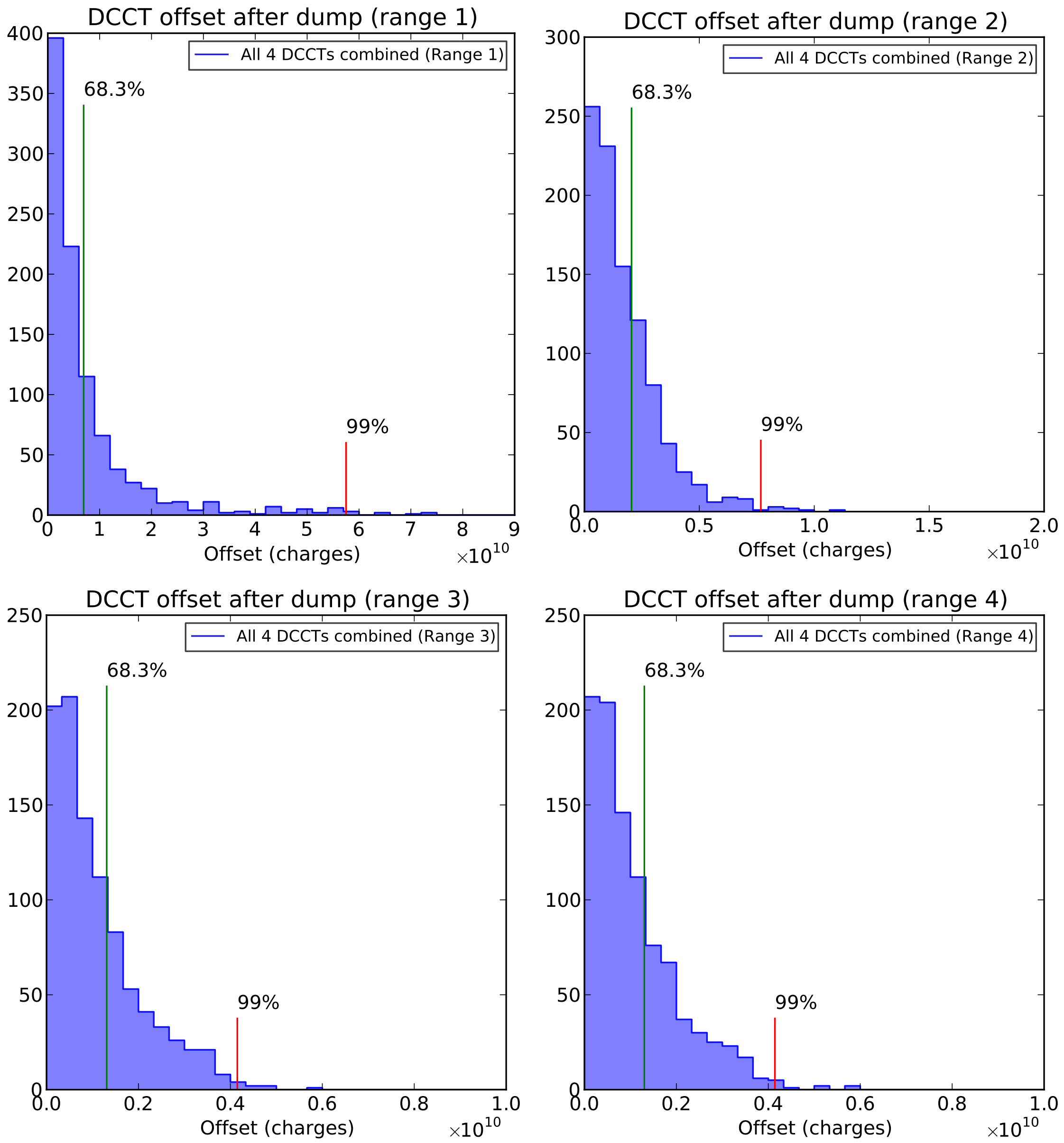

Figure 11: Measured offsets after a fill dump for all physics fills in 2011. The averaged offset over 60 seconds was automatically subtracted from the raw values in order to correct the baseline down to zero at the beginning of each fill. The deviation observed at the end of each fill was taken as a 10 minutes average starting 10 s after the dump.

3.3 Fourier analysis of the noise

Periodic fluctuations of the noise can be detected with a Fourier analysis of the available data. A Fast Fourier Transform (FFT) of the nine days of data with a 60 s sampling average is shown on Fig. 12 for the four DCCT's. The highest detectable frequency is 2 min^{-1} and the lowest detectable frequency is about 3 days^{-1} as a minimum of 3 periods are needed to detect a frequency. The power is highest at low frequencies < 24 h^{-1} indicating a possible long term drift or a period longer than 9 days. There is, however, no frequency peak visible in the available range.

The FFT method used in Fig. 12 was verified by analyzing a simulated signal with known frequencies. The raw signal and resulting FFT are shown in Fig. 13. The simulated signal is a superposition of a linear function, 4 sine waves and random values as static. The points are generated with a 1 s resolution over 10 days and are averaged into 60 s time bins before the Fourier transformation as with the DCCT noise. The linear function simulates a slow downward drift starting at 1 at T = 0 and ending at -2 after 10 days. The four sine waves have a frequency of 360^{-1} s, 3600^{-1} s, 24^{-1} h and 30^{-1} days with amplitudes of 0.5, 1, 0.5 and 5 respectively. A random value between ± 10 is added to the final signal to simulate some static noise. The top plot shows the resulting signal over 10 days, the x axis is the time in s; the 24^{-1} h is clearly visible and the 30^{-1} days period is responsible for the long curvature. The peaks at 360 s, 3600 s and 24 h (86400 s) are clearly visible, however the long term period of 30^{-1} days could not be detected with 10 days of data. The high power towards the low frequencies is due to the slow drift and 30^{-1} days period.

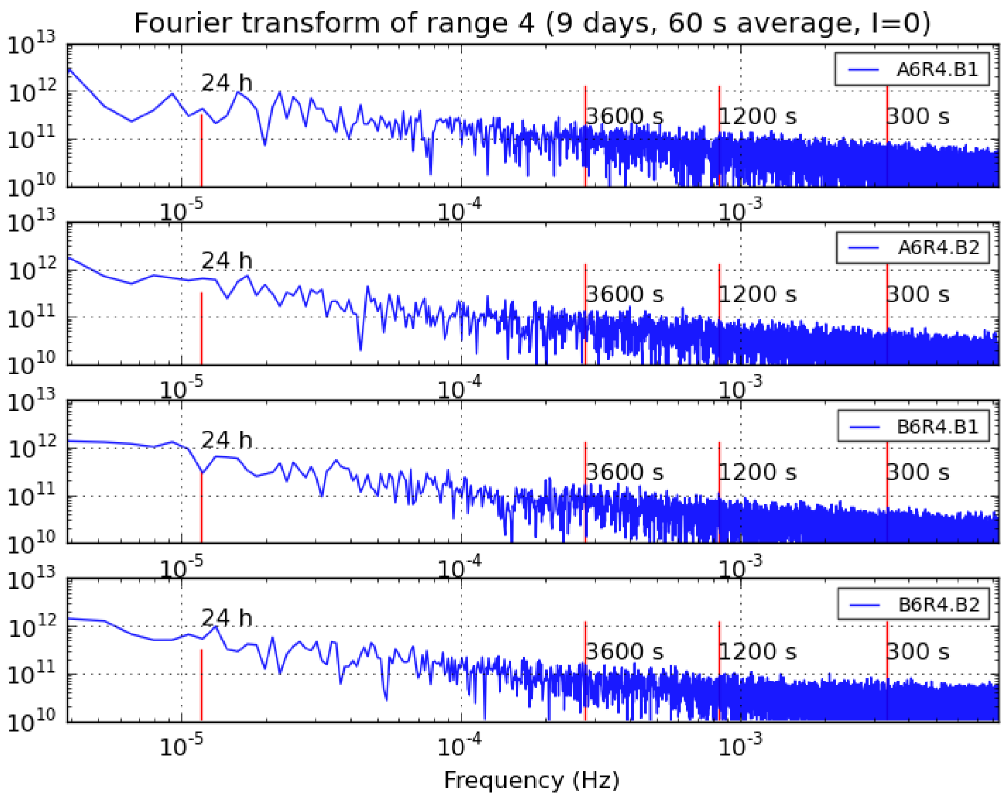

Figure 12: Fast Fourier transform of the DCCT noise. The DCCT signal was acquired with range 4 (the most sensitive). The x axis represents the frequency on a logarithmic scale. For reference, the frequency value for 300^{-1}, 1200^{-1} and 3600^{-1} seconds and of 24^{-1} hours are indicated with a vertical line as example.

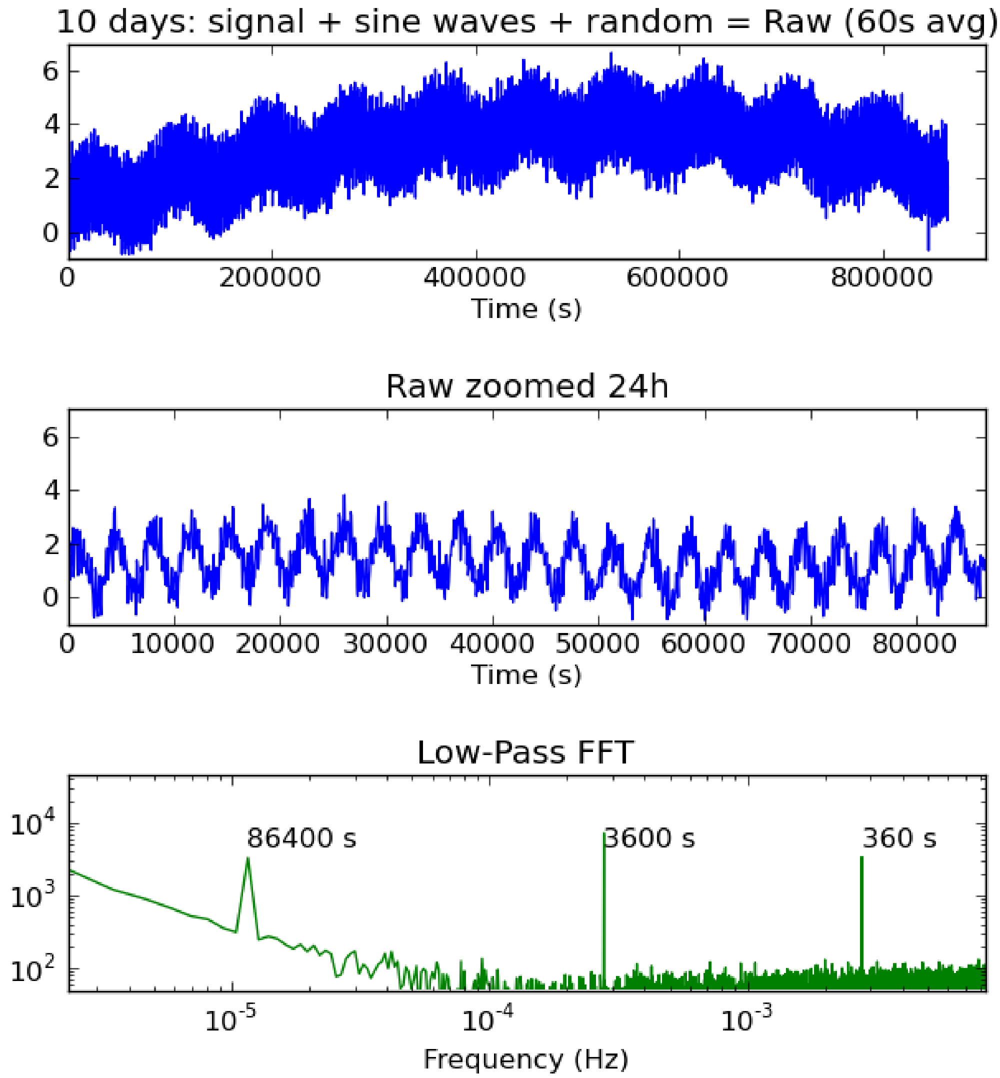

Figure 13: Fast Fourier transform of simulated noise. The first graph shows the raw signal over 10 days. The second plot shows a zoom in a 24 h period, here the 3600^{-1} (1 h) period is clearly visible but not the 360^{-1} period. The FFT of the raw signal is shown on the bottom plot, the highest detectable frequency is 120^{-1} s due to the 60 s binning.

3.4 In-situ tunnel measurements

A set of measurements have been performed with the DC current source placed in the tunnel near the DCCT's. The aim was to evaluate the DCCT stability with and without current over a long term period of 12 hours, also the linearity away from the calibration point and the calibration method were analyzed in-situ. The setup is summarized in Fig. 14. The current source[‡] was controlled by a labview program which set the desired current in predefined time steps. The cable connected to the DC source passed through all four DCCT's in two loops, therefore the current seen by the DCCT's was twice larger than the injected current. A 100 Ω resistance (Sfernice RE3 RH50 5%, 50 W) was connected in series. Because the measurement were performed during an access-restricted period, the planned sequence could not be modified once started. The incentives to place the source near the DCCT's were the following:

- The DC current seen by the DCCT's is exactly the same at all times. Therefore, any difference between the DCCT's can not be due to the source.

[‡]Yokogawa GS200 is also used for the precise calibration

- One measurement can be performed with all DCCT's at the same time. This was important for the long term measurements which required 5 days to test all ranges.
- A current leak in the 500 meter cables from the surface back-end electronics to the DCCT's in the tunnel can be excluded by comparing the calibrations with the source in the tunnel and on the surface.

The normal acquisition chain was used to record the DCCT values; however, an additional software feature has been added to the DCCT acquisition software to be able to record the raw ADC value of each DCCT range. The ADC values of each DCCT range were sampled at 50 Hz; however, only one value out of the 50 was sent to the logging database for diagnostic purposes. The special software flag computed a 1 Hz average of the 50 Hz DCCT values and wrote the averages in a file. The system was therefore independent of the central logging database and provided a 1 Hz average of the raw values from all ranges.

The absolute scale calibration was performed as a first measurement in the 7 days sequence. A known current was injected at about 80% of each range and was used to measure the value of 1 ADC Least Significant Bit (LSB) for each range from all DCCT's. This calibration was used throughout all subsequent measurements to convert the DCCT signal into charges.

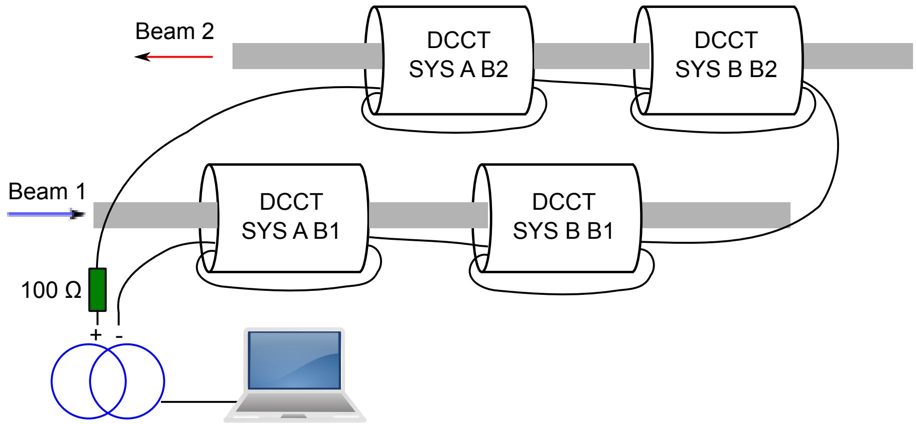

Figure 14: Tunnel setup.

3.4.1 Long term stability over 12 hours

The long term stability of the DCCT was verified with two measurements of 12 hours per range separated by 3.5 days using a constant current. Short term fluctuations within 12 hours are expected to be due to a variation of the baseline instead of the scale factor and depend on the averaging time. Furthermore, periods longer than 12 hours could yield larger fluctuations while shorter periods will reduce the fluctuations. Therefore the uncertainties deduced from this measurement are valid for fills of less than 12 hours and are provided for measurements averaged over 1 minute or 1 hour.

Each range was tested with a current near its full scale; the injected currents are listed in Table 4. The time evolution of the DCCT response during both 12 hours measurements is shown in Fig. 15 for system A/beam 1 range 3 and Fig. 16 for system B/beam 1 range 1 as examples. The results for all DCCT's and all ranges are shown in Appendix A.2 (Figs. 62 to 65). In all cases, the measurements use the same calibration factors determined at the beginning of the tunnel sequence.

There is no visible systematic drift or long term daily fluctuation visible. An oscillation with a 30 minute period is visible on range 1 which is probably due to a digitalization artifact due to the low noise of the signal for this range. The Fourier analysis for range 1 for all DCCT's is shown in Fig. 17 and confirms the oscillation with a frequency of about 1800^{-1} s^{-1}, no other frequency is visible in the spectrum. The amplitude of the oscillation is < 0.02 ADC bin and can be ignored. In all other ranges the current is stable and no pattern or daily effect can be observed.

For each DCCT and range, the raw ADC values are projected in a histogram to evaluate the spread of the signal over 12 hours at different currents. Each measurement, for a given range, taken during one of the 12-hour periods, is centered around its average during that period. An example histogram for system A/beam

1, range 3 is shown in Fig. 18. The histograms for all ranges and different currents are grouped in Fig. 19 for the DCCT system A/beam 1, the remaining DCCT's are shown in Appendix A.2 (Figs. 66 to 68). The histograms taken without current (bottom line) use 5 hours of data instead of the normal 2×12 hours.

The current intensity flowing through the DCCT does not affect the spread of the signal. For a given range and using 1 minute and 1 hour time bins, the largest observed standard deviation and the largest half peak-to-peak value from any current and from all DCCT's are given in Table 5. The conversion into charges is calculated before rounding and uses the calibration factor of the corresponding DCCT.

The RMS and largest observed deviation from the average taken from Table 5 reflect the error induced by the baseline fluctuation even after baseline correction. The fluctuation depend on the averaging time: as expected, averaging the signal over a longer time period reduces both the RMS and peak-to-peak spread, therefore a 1 minute measurement will have a larger baseline induced uncertainty as a 1 hour measurement. In a typical precise van der Meer fill the DCCT signal is averaged over about 1 hour.

The intrinsic DCCT noise can improve the ADC resolution below $1/\sqrt{12}$ LSB; this is probably the case for range 3, and possibly for range 2 (for range 4 the noise level exceeds the ADC resolution). This assumption, however, is not true for range 1 which has a low noise level and quantization effects are visible during the slow beam decay if the signal sampling is too short. An example demonstrating this effect is shown in Fig. 20 where a step-like structure is visible in the beams intensity decay. This step wise decay can be observed in all fills with intensities covered by range 1. In this case the noise level is too low to improve the ADC resolution below $1/\sqrt{12}$ LSB and the ADC is limiting the precision of range 1.

In conclusion, the uncertainty induced by the baseline fluctuation within a fill depends on the signal averaging time and acquisition range. A signal averaged over 1 hour or more will have smaller fluctuations compared to an average of 1 minute only. The corresponding absolute half peak-to-peak fluctuations are provided in Table 5. Furthermore, the long term fluctuations are independent of the intensity within a range.

Table 4: Injected currents per range used during the long term measurements of two times 12 hours. For range 1 the 200 mA maximal current or the source was used. The DCCT sees twice the current due to the two loops of the cable.

Range	Injected current (mA)	Equivalent charges	Relative range scale
1	400	$2.22 \cdot 10^{14}$	44.4 %
2	80	$4.44 \cdot 10^{13}$	88.8 %
3	8	$4.44 \cdot 10^{12}$	88.8 %
4	0.8	$4.44 \cdot 10^{11}$	88.8 %

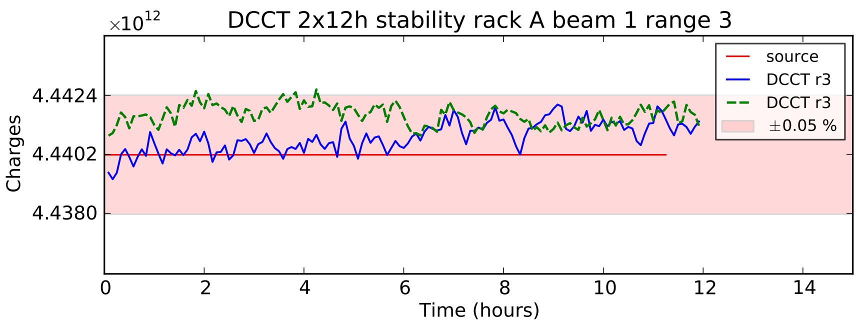

Figure 15: Long term stability under load for system A/beam1, range 3. The data is averaged in 300 s time bins. The first 12 hours measurement is plotted as a solid blue line, the second measurement taken 3.5 days later is plotted as a dashed green line.

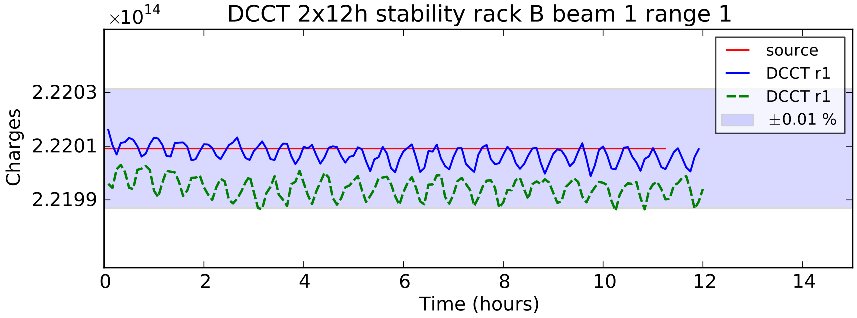

Figure 16: Long term stability under load for system B/beam1, range 1. A 30 minutes oscillation is clearly visible on range 1 and is probably due to digitalization and averaging effects with a low noise signal.

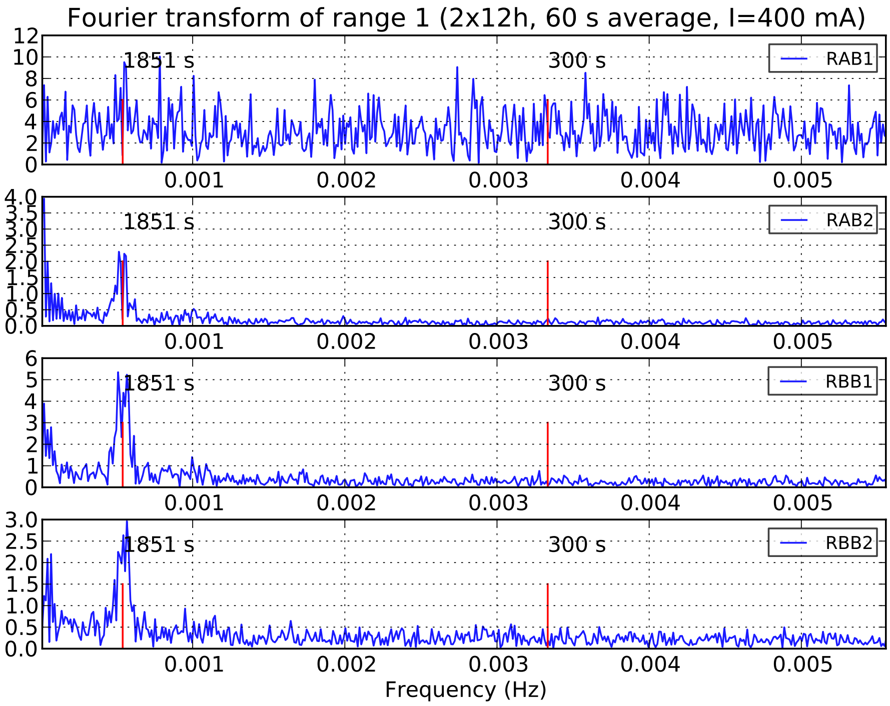

Figure 17: Fourier analysis of range 1. The small oscillation visible on range 1 is visible at a frequency of 1851^{-1} s^{-1}. As reference the frequency of 300^{-1} s^{-1} is indicated with a vertical line.

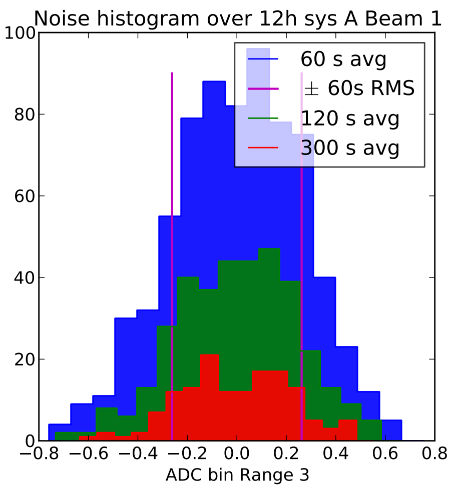

Figure 18: Histogram of ADC values for system A, beam 1, range 3 recorded during two 12-hour periods at 88% of the maximum intensity for that range. The zero ADC bin is set to the average of the 12-hour measurement; both periods are accumulated in the same histogram. The signal in averaged in time bins of 60 seconds (blue), 2 minutes (green) and 5 minutes (red). The two vertical lines indicate the RMS value of the 60 s time averages.

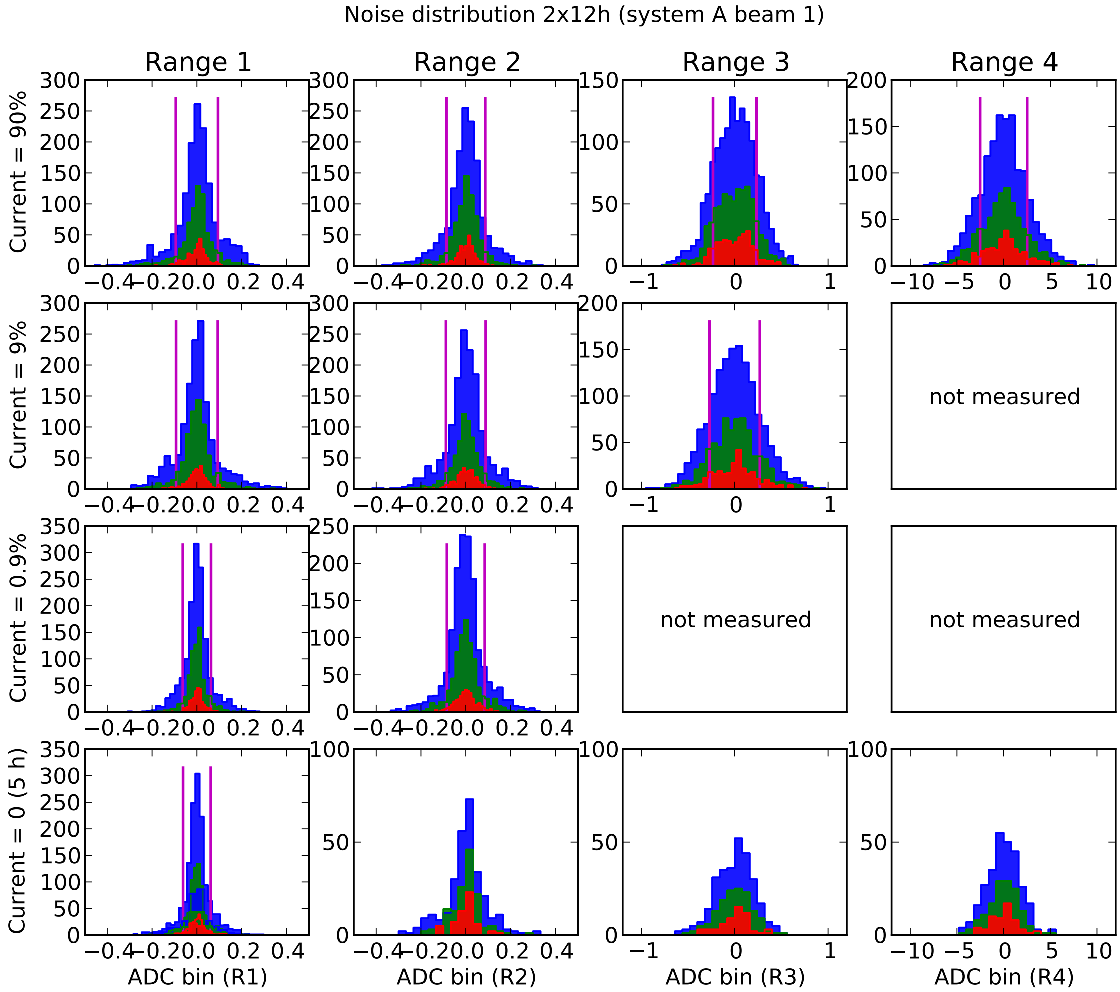

Figure 19: Histograms of 2×12 hours of all ranges for system A/beam 1. The ranges are sorted per column, each row represents a current intensity relative to the total scale of the range. The first row is measured with a current intensity equivalent to 90% of the range and the lower row is measured without current. Due to time constrains the histograms without current contain only 5 hours of data instead of 2×12 hours. For this reason the histogram for range 1 at zero current (bottom left frame) uses instead the current of range 4 at 90%, which corresponds to 0.09% of range 1. The lowest current used during the long term measurements corresponds to 90% of range 4; values below this intensity have therefore not been measured and the corresponding frames are marked accordingly.

Table 5: Observed standard deviation and largest half peak-to-peak deviation of 1 minute and 1 hour average over two periods of 12 hours. For each range, the largest RMS and half peak-to-peak deviation from any intensity and from all DCCT's is selected. The LSB conversion into charges is done before rounding.

Range	Averaging time	Absolute RMS (LSB)	Absolute RMS (charges)	Absolute P2P (LSB)	Absolute P2P (charges)
1	1 min.	$\pm$ 0.1	$\pm 2.3 \cdot 10^{10}$	$\pm$ 0.4	$\pm 1.1 \cdot 10^{11}$
2	1 min.	$\pm$ 0.1	$\pm 2.2 \cdot 10^{9}$	$\pm$ 0.4	$\pm 1.0 \cdot 10^{10}$
3	1 min.	$\pm$ 0.3	$\pm 6.7 \cdot 10^{8}$	$\pm$ 0.9	$\pm 2.4 \cdot 10^{9}$
4	1 min.	$\pm$ 2.5	$\pm 6.3 \cdot 10^{8}$	$\pm$ 9.4	$\pm 2.3 \cdot 10^{9}$
1	1 hour	$\pm$ 0.01	$\pm 2.8 \cdot 10^{9}$	$\pm$ 0.03	$\pm 7.3 \cdot 10^{9}$
2	1 hour	$\pm$ 0.02	$\pm 5.2 \cdot 10^{8}$	$\pm$ 0.05	$\pm 1.1 \cdot 10^{9}$
3	1 hour	$\pm$ 0.2	$\pm 4.8 \cdot 10^{8}$	$\pm$ 0.4	$\pm 1.1 \cdot 10^{9}$
4	1 hour	$\pm$ 1.9	$\pm 4.7 \cdot 10^{8}$	$\pm$ 4.1	$\pm 1.0 \cdot 10^{9}$

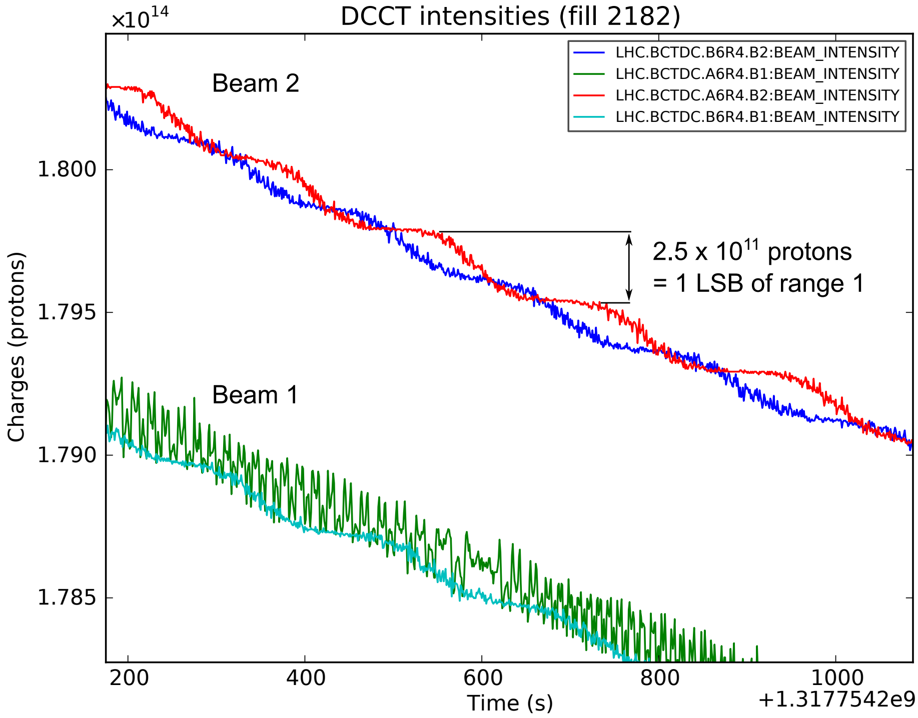

Figure 20: The quantization of the 12-bit ADC response is apparent on range 1 as the beam-2 intensity slowly decays. DCCT system A/beam 1 is more noisy and the step pattern is less visible. The difference between two steps corresponds to the scale factor of one ADC bin of range 1. The resolution of the DCCT 12-bit ADC is not improved by the noise for range 1.

3.4.2 Long term stability under load over 24 hours

An additional long term measurement has been performed during 24 hours with a current of 400 mA to test for possible thermal effects in the front-end electronics. The DCCT injects a current equivalent to the measured intensity to cancel the total current; therefore, this generated current could warm up the electronic components over time and induce a slow drift. The DCCT response of range 1 during 24 hours averaged over 300 seconds time bins is shown in Fig. 21 for all DCCT's. The small oscillation pattern observed in Sec. 3.4.1 is also visible here. No thermal effect or systematic drift can be observed, only a slow downward drift on system A/beam 2 can be observed with a total amplitude of about 0.01% in 24 hours. Range 1 reaches about 890 ADC bins with a current of 400 mA, therefore, 1 LSB represents about 0.11% at this intensity.

In conclusion, no thermal or daily effect can be observed within 24 hours with a current intensity of 44% of range 1. The observed signal is within $\pm$ 0.1 LSB, therefore, the accuracy of the measurement is limited by the 12-bit ADC.

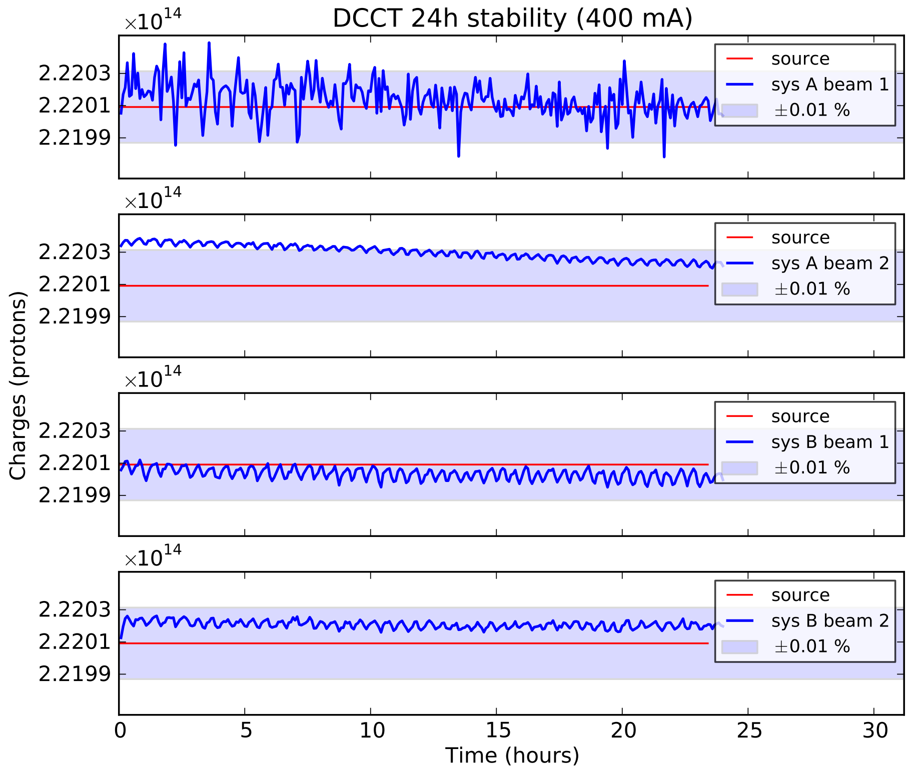

Figure 21: Long term stability under load for range 1. A current of 400 mA ($2.22 \cdot 10^{14}$ charges, 44% of range 1) is injected during 24 hours. The data is averaged in 300 s time bins, the calibration was performed 48 hours before the measurement

3.4.3 DCCT Linearity

The linearity of the DCCT response away from the calibration point was studied with three measurements performed in the tunnel. The first two measurements were spaced by 48 hours and took 5 minutes per step with 8 steps per range. The third measurement was performed 5 days later taking 2 minutes per step with 5 steps per range. Zero-current intervals separated one period from the next, in order to correct the offset with the method described in 3.1. All values used the same calibration performed at the beginning of the tunnel measurements. All linearity measurements were done with the new 2011 front-end electronics which solved the bunch pattern dependence observed in 2010 (see Sec. 4.2). The acquisition chain together with the ADC remained unchanged from 2010. The 12-bit ADC is shared and multiplexed in a system, that is, the same ADC acquires all ranges for beam 1 and 2 for a given system. An example of the current sequence used to test the four ranges is shown in Fig. 22. As an example, Fig. 23 shows the DCCT response in all ranges for system A, beam 1.

The residual fraction $1-(\mathrm{N}_{\mathrm{DCCT}}/\mathrm{N}_{\mathrm{source}})$ $(\%)$ for each range is shown in Fig. 24 for system A/beam 1. The plots for the remaining DCCT's are shown in Appendix A.3 (Figs. 69 to 71). Due to technical reasons, the second measurement was lost for system A.

A positive residual, i.e. the DCCT underestimates the actual current, is observed for the ranges 1, 2 and 3 of all DCCT's. The noise level of range 4 limits the accuracy of the measurement. This observed non-linearity, however, is within 1 LSB as indicated by the dashed line. A standard precise calibration performed at 14% of range 2 instead of the usual 80% is compared to the linearity measurements for range 2 in Fig. 25. The green dots show the combined three linearity measurements according to the calibration performed in the tunnel. The red star shows the result of the standard precise calibration performed at 14% of range 2 and is in accordance with the expected non-linearity.

In conclusion a non-linearity of the DCCT response of the order of 1 LSB is observed for all ranges and DCCT's. The non-linearity measurement is inconclusive for range 4 due to the noise level; however, it is expected to be the same as for the other ranges as all ranges are acquired with the same ADC.

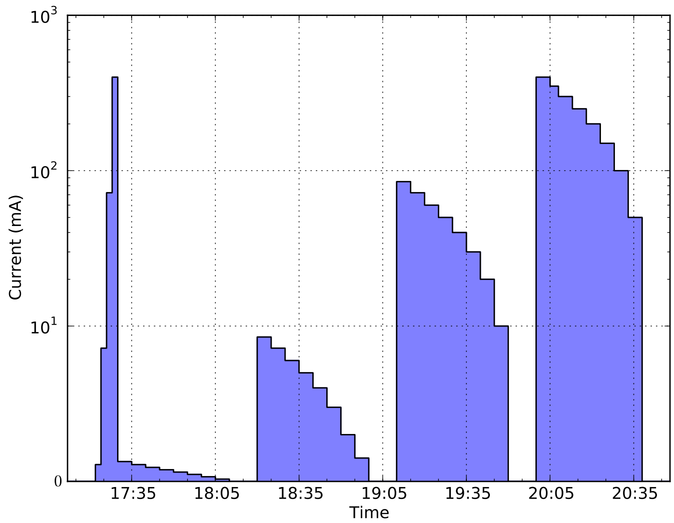

Figure 22: Current sequence used for the linearity measurement. A period of 10 minutes separated each sequence to correct the offset. The low intensity steps were also used in the less sensitive ranges. The first four steps were used for the calibration which were kept throughout all measurements in the tunnel.

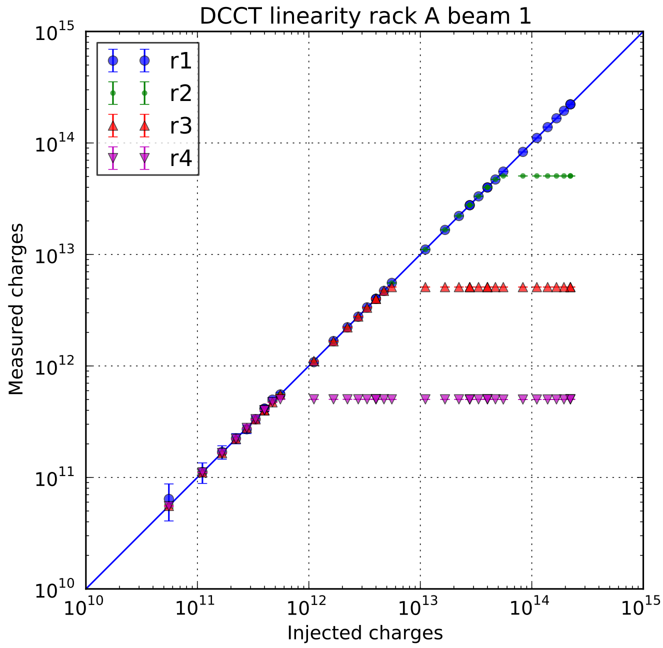

Figure 23: Injected current versus measured current for the DCCT system A/beam 1. With increasing intensity, the ranges 4, 3 and 2 enter in saturation and the response is constant.

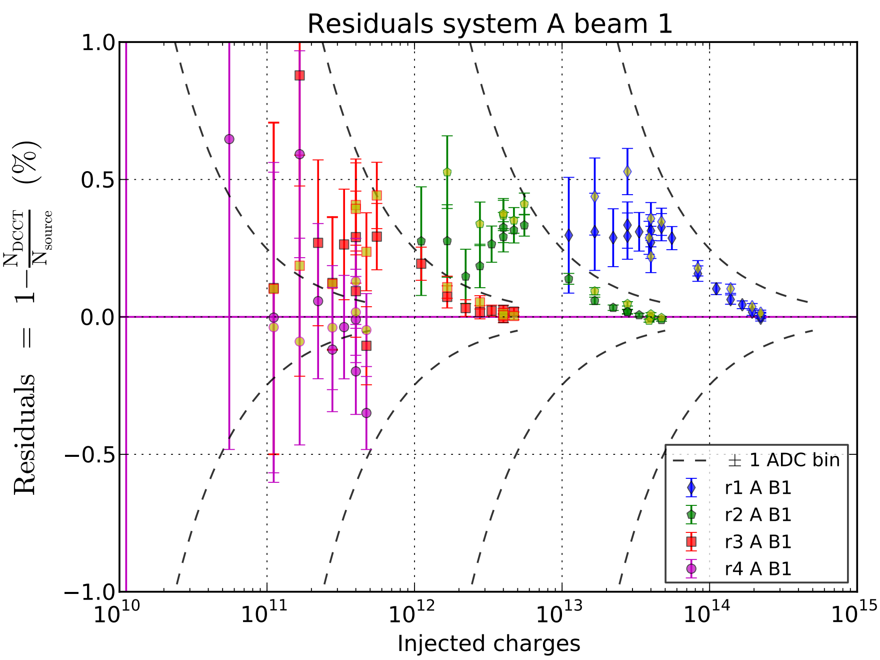

Figure 24: Linearity residuals for system A/beam 1 combining values from the first measurement (plain dots) and third measurement (yellow faced dots). Intensities below 2% of the range (about 40 ADC bins) are not shown. The residuals corresponding to ± 1 ADC bin are indicated by dashed lines.

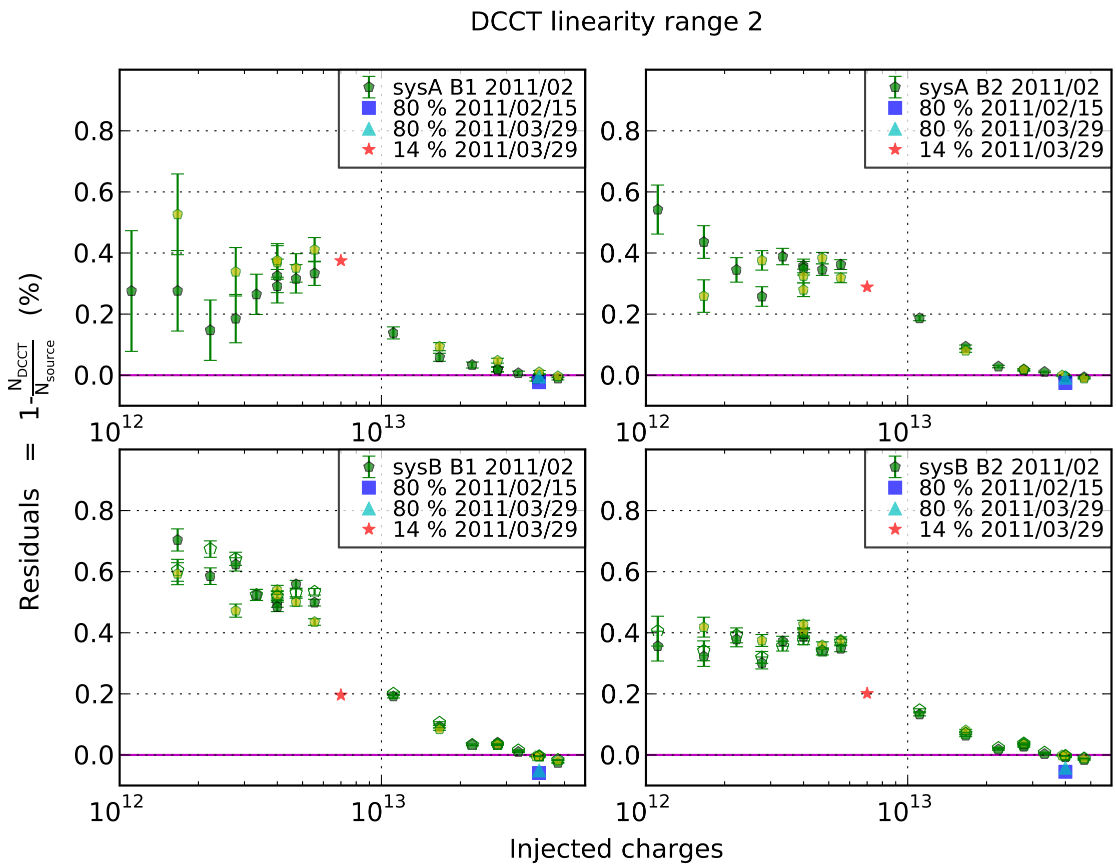

Figure 25: Linearity residuals for range 2 compared to standard calibrations.

3.5 DCCT Linearity verified with alternate ADC

In an effort to disentangle the origin of the non-linearity between the DCCT and the acquisition chain, an additional linearity measurement was performed with an alternate ADC recording the DCCT signal in parallel to the normal acquisition. The second ADC from National Instruments was a 16 bit ADC model NI USB-9162 with a connector block NI 9215 with 4 BNC and was used in the bipolar range of $\pm$ 10 V.

3.5.1 Reference response of NI ADC

A reference response of the NI ADC has been measured in the laboratory with the same source and was used as a control reference. The goal was to generate a signal between 0 and 5 V by using four different ranges of the source by selecting an appropriate resistance. The voltages were acquired with the NI ADC for each range to quantify the residuals. To avoid any thermal effects, the maximal power dissipated was kept below 1% of the nominal power of the resistance configuration; furthermore, the measurement was performed twice, once with an increasing current and once with a decreasing current (see Fig. 26). The resistances used to test each range are listed in Table 6; the last column lists the current range used at the source. Each voltage generated from a current step was acquired during 20 s with a 10 Hz sampling.

The residual fraction $1 - (\mathrm{N_{ADC}}/\mathrm{N_{source}})$ (%) for each range is shown in Fig. 27. the source was used over its full range and the non-linearity pattern is similar for all ranges, therefore, the systematic negative non-linearity points towards a non linearity of the ADC instead of the source.

Table 6: Resistance used to test the NI ADC. The symbol "//" means "parallel".

Range	Resistance configuration	Measured resistance	Nominal power	Maximal power used	Resistance model	Current range used (A)
4	4×100 kΩ in //	25.05 kΩ	1.4 W	1 mW	Philips MRS 25 0.4 W	$0 - 2 \cdot 10^{-4}$
3	11×26 kΩ in //	2.37 kΩ	1.4 W	10 mW	Sfernice 25 k RS63Y 0.25 W	$0 - 2 \cdot 10^{-3}$
2	4×100 Ω; 2 in // 2 in series	250 Ω	25 W	0.1 W	Sfernice 100 Ω RH50 5% 50 W	$0 - 2 \cdot 10^{-2}$
1	4×100 Ω in //	25 Ω	200 W	1 W	same as in 2	$0 - 2 \cdot 10^{-1}$

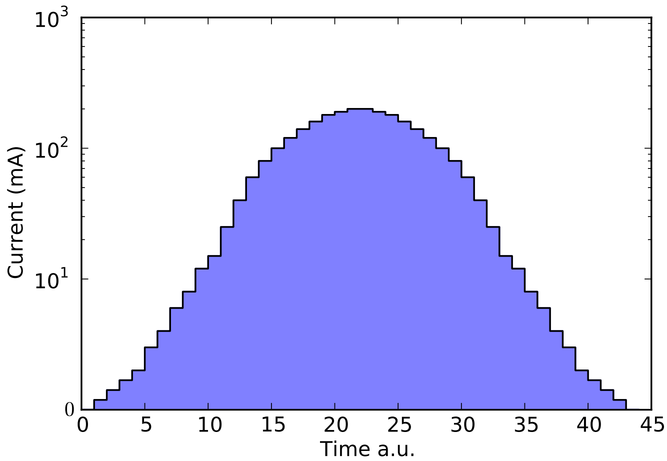

Figure 26: Current steps used to characterize the NI ADC. The pyramidal measurement permits to check for a possible thermal effect of the resistances. This sequence example with a maximal current of 200 mA used a similar current range as used to measure the linearity of range 1 of the DCCT.

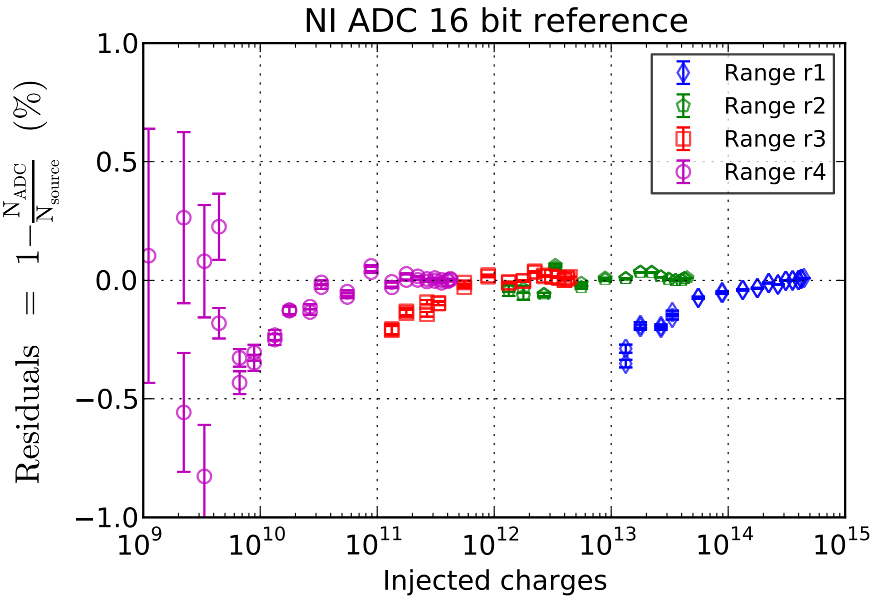

Figure 27: Reference response of the NI ADC.

3.5.2 DCCT Linearity compared with NI ADC

The setup used to acquire the DCCT signal with the two ADC's is sketched in Fig. 28. Each range of beam 1 and beam 2 of one system provided a signal between 0 and 5 V in the front-end electronics. The signals were send to the surface and decoupled with a unity gain module. The 12-bit ADC of a system acquired the 8 signals from the unity gain module with a multiplexer. The same signals were also acquired in parallel at the unity gain module with the 16 bit ADC.

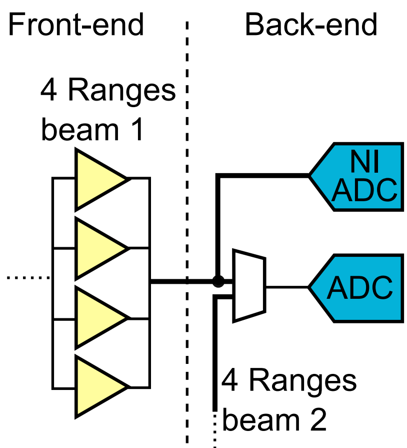

Figure 28: Setup with parallel ADC. Each DCCT range sends a signal between 0 and 5 V to the surface. The signals were acquired through a unity gain module by the normal 12-bit ADC and also a 16 bit ADC from NI. Therefore, both ADC's acquired the signal from the same source.

The results of the linearity measurement acquired with both ADC's in parallel is shown in Fig. 29 for system B/beam 2 range 1. The DCCT response measured with the NI ADC follows closely the laboratory reference of the NI ADC. As in the previous measurements, the 12-bit ADC shows a positive non-linearity. The same measurement performed on all DCCT's and all ranges is shown in Appendix A.3 (Fig. 72).

In conclusion the observed non-linearity appears to originate from the acquisition chain, most probably from the 12-bit ADC and not from the DCCT itself. The ideal working point for a precise measurement of the beam intensity is close to calibration point. In addition to the above linearity measurements, a similar measurement has been performed one year later with the new single range 24-bit ADC. The results are shown in Appendix A.3.2 (Figs. 73 to 76) This new 24-bit acquisition system is still in a testing phase at this time; however, the results confirm that the DCCT is linear within the measured range. The noise level and baseline fluctuations limit the accuracy at low intensities below 10^{11} charges.

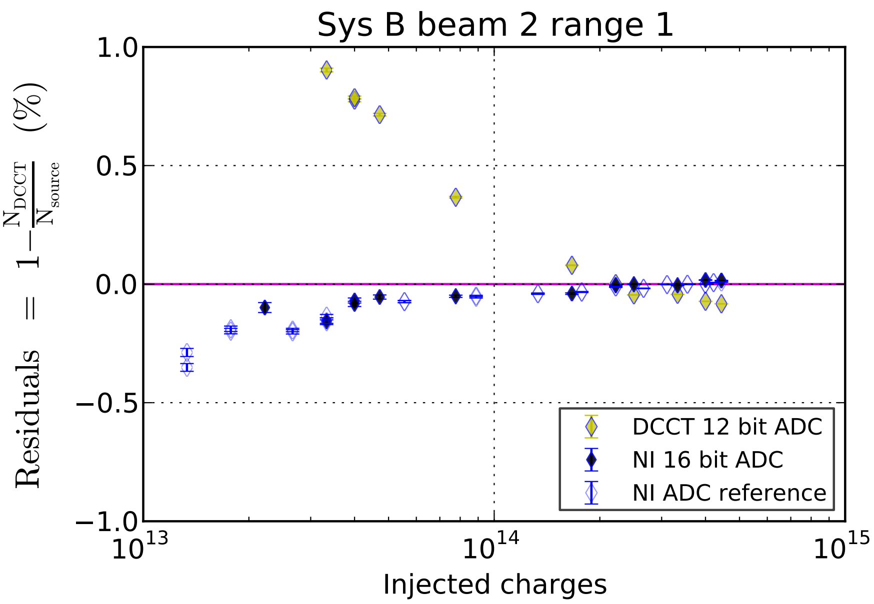

Figure 29: Linearity measurement with NI ADC acquired in parallel to the DCCT 12-bit ADC. The open dots are the reference response of the NI ADC measured in the laboratory. The filled blue dots are the DCCT response measured with the NI ADC and the filled yellow dots are the DCCT response measured with the 12-bit ADC. The DCCT response measured with the NI ADC follows the reference response of the ADC.

3.6 Absolute Scale

The stability over time of the scale factor (Sec. 2.3) was the main source of uncertainty affecting the measured beam intensities in 2010. A difference of up to 1.6% was observed between the two precise calibrations performed in 2010 at two different times. A precise calibration has been performed during all technical stops in 2011 to assert the stability of the scale factor over the year. The history of the scale factors over nine month is shown in Fig. 30. The scale factors for the ranges 1 to 3 are contained within an envelope of $\pm$ 1 ADC bin which corresponds to a relative error of $\pm$ 0.06%. The scale factors of range 4 are contained in an envelope of $\pm$ 4 ADC bins which corresponds to a relative error of $\pm$ 0.24%. The stability of range 4 is compatible with the intrinsic noise of the DCCT which is of the order of 4 ADC bins (10^9 charges). The ranges 1 to 3 are probably limited by the ADC resolution similarly to the long term measurements in Sec. 3.4.1.

The scale factor could be sensible to the temperature of the electronics or of the monitor, however, no seasonal fluctuation is visible over the full year. A view of the inlet ventilation temperature for different sections around the DCCT's is shown in Fig. 32, the location of the section is provided in Fig. 31. Fluctuations of $\pm$ 2°C are present, but there is no seasonal change in the tunnel or service sections.

In conclusion the scale factors are stable within $\pm$ 1 LSB for the ranges 1 to 3 and within the intrinsic noise level of range 4. Therefore, an uncertainty envelope of $\pm$ 1 LSB and $\pm$ 4 LSB has to be assumed for the ranges 1 to 3 and 4 respectively.

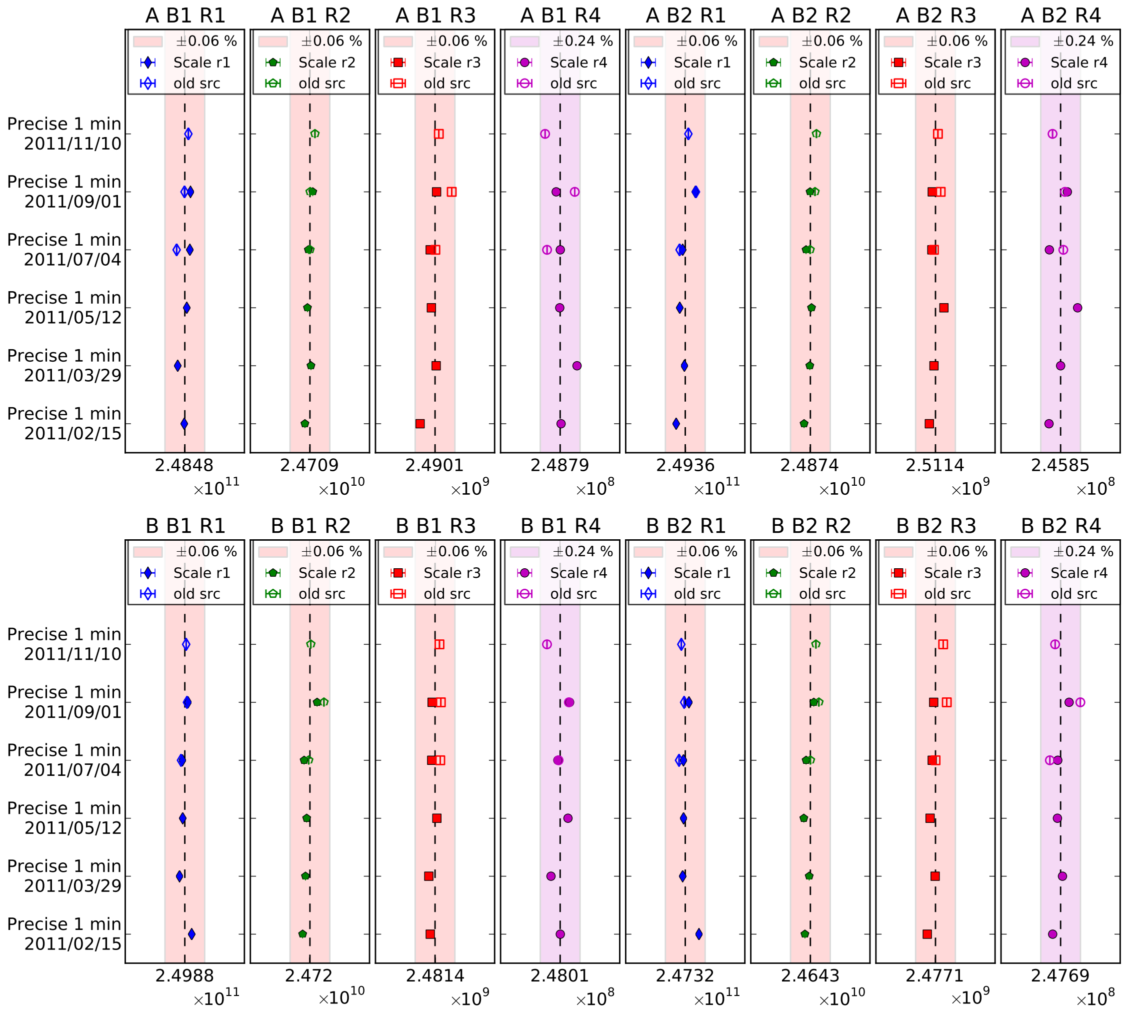

Figure 30: Precise calibrations preformed during the six technical stops in 2011 using the standard BI procedure. The top plot shows the scale factors for each range of system A, the bottom plot shows system B. The scale factor of a range is the value of charges for 1 LSB and is expressed in units of charges/ADC bin. The vertical dashed line is the average of all scale factors of the corresponding range. Most of the calibrations are done with the more recent source Yokogawa GS200 (see also Sec. 5.1) and are indicated with plain markers. The last three measurements indicated with an empty marker are done with the old source Yokogawa 7651. The pink band shown in ranges 1 to 3 has a width of $\pm$ 0.06% (equivalent to $\pm$ 1 LSB), the magenta band shown in range 4 has a width of $\pm$ 0.24% (equivalent to $\pm$ 4 LSB)

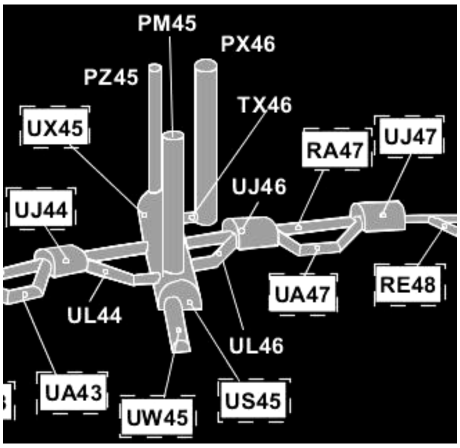

Figure 31: Synoptic of LHC point 4 shafts. The DCCT's are located in the section RA47.

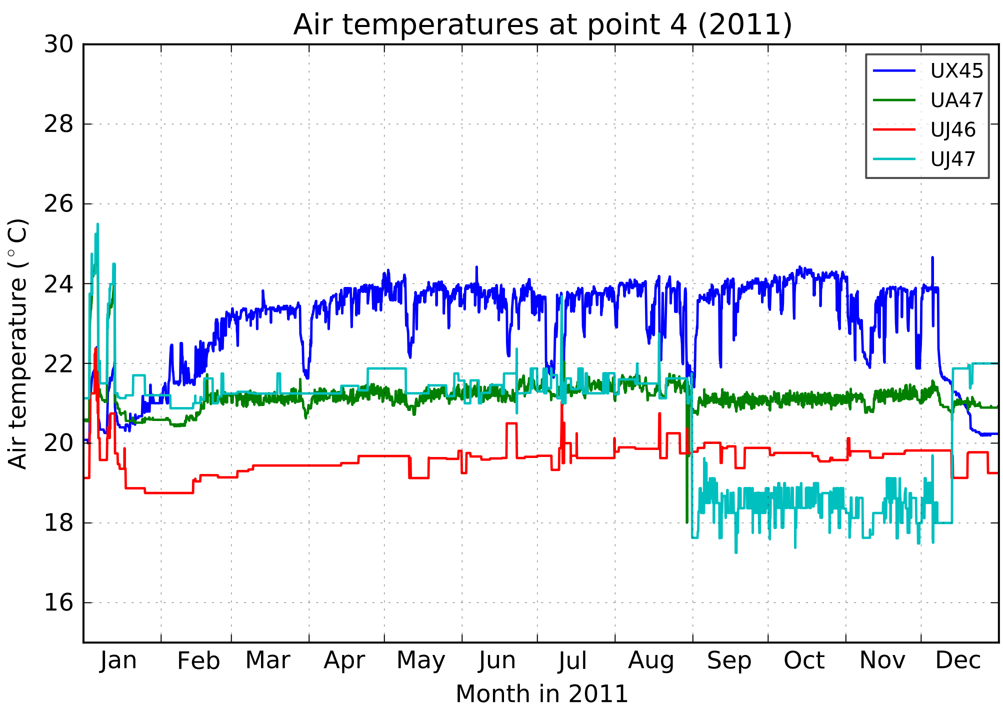

Figure 32: Air temperature around the straight section 4-5 at the LHC point 4 where the DCCT's are installed, see Fig. 31. The values are taken at the ventilation inlet; the values for UX45 and UA47 are an average of 12 sensors. The temperature of UJ46 is probably the most representative of the values found in the tunnel section RA47 where the DCCT's are located.

4 Sensitivity to beam conditions and other external factors

4.1 Cross talk between rings

A possible cross-talk effect between the rings of beam 1 and beam 2 has been analyzed with special machine development (MD) fills. Five fills have been identified in 2010 where only one beam was circulating with a large intensity in the order of 10^{13} protons, while the other ring was empty. The DCCT's of the empty ring were automatically set to range 4 and were therefore sensitive to a potential cross-talk effect when the other beam is dumped. The noise behavior of the empty ring before and after the dump time was analyzed. An example of a beam dump with only one beam is shown in Fig. 33. The difference in noise levels recorded 60 s before and 60 s after the beam dump are shown in Fig. 34 for the five fills. Detailed plots of the other fills are shown in Appendix A.4 (Fig. 77).

In conclusion there is no evidence of a cross-talk effect between rings, the difference in noise before and after the dump lies within $\pm 0.5 \cdot 10^9$ charges for both system A and system B. Such spread is expected with a typical noise level of $\pm 1 \cdot 10^9$ charges.

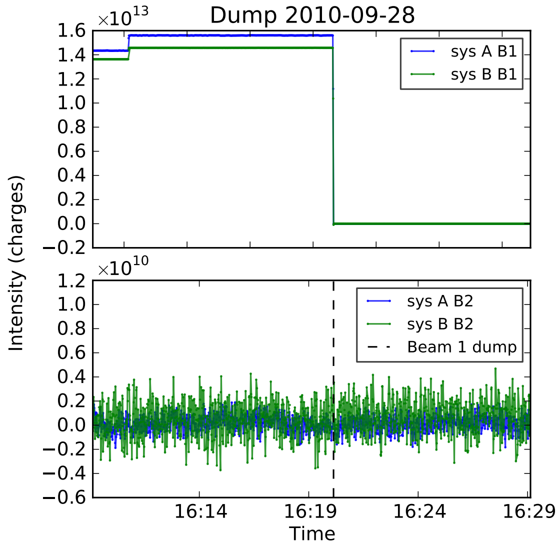

Figure 33: Crosstalk example. Beam 1 is circulating with $\approx 1.5 \cdot 10^{13}$ protons (top plot) while beam 2 is empty (bottom plot). The noise level of beam 2 remains constant when beam 1 is dumped.

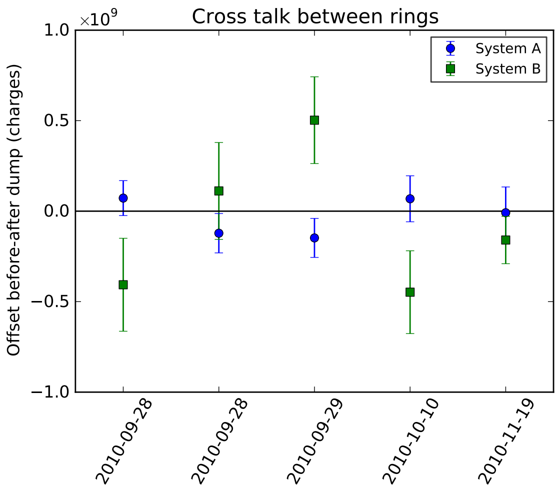

Figure 34: Crosstalk between both rings at dump time. For a given fill on the x axis, the data point shows the difference of the noise level $|N_{\mathrm{before}} - N_{\mathrm{after}}|$ at the time of the dump. The indicated error is the standard deviation of the 60 points used for the average.

4.2 Bunch pattern dependence

A misbehavior of the DCCT related to the filling pattern has been discovered in 2010. The problem was observed with bunch train fills with bunch spacings of 150 ns and 50 ns. The problem has been identified in the laboratory and corrected in the 2011 hardware [6]. The misbehavior was due to saturation effects in the front-end amplifiers. An example showing the effect of the bunch pattern dependence is provided in Fig. 35. The left plot shows a fill for beam 1 in 2010 injected with bunch trains. The DCCT responses between systems A and B are inconsistent at each train injection and do not follow the FBCT signal. The right plot shows a bunch train injection in 2011 with the corrected hardware.

Three measurements have been performed to test the DCCT dependence on the bunch pattern. A laboratory measurement simulating high intensity bunch trains is given in Sec. 4.2.1. A measurement with beam debunching is shown in Sec. 4.2.2. Finally the sensitivity to an injected RF sine wave is presented in Sec. 4.2.3.

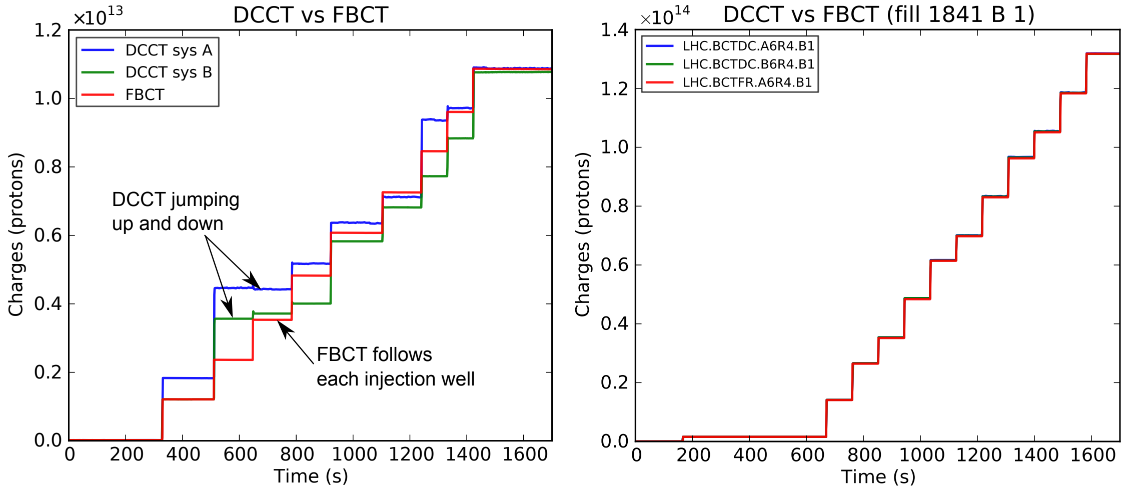

Figure 35: Example of difference between system A and B in 2010 (fill 1459, left) and 2011 (fill 1841, right). The DCCT misbehavior is clearly visible in 2010.

4.2.1 Laboratory measurements

The new front-end cards have been tested in the laboratory with a spare DCCT. The configuration in the laboratory was identical to that in the LHC tunnel including the beam pipe section and high-frequency (HF) bypass. However, the acquisition of the DCCT signal was different and used a portable 16 bit ADC. In 2010 the bunch trains used in the LHC filling scheme were composed of several close bunches with 150 ns or 50 ns spacing. One bunch occupied a 25 ns slot but had a width of 2.5 ns dictated by the LHC RF cavities (400 MHz). The generation of 2.5 ns or 25 ns high intensity pulses was not possible in the laboratory, only the shape of bunch trains could be simulated. However, the DCCT bunch pattern misbehavior was due to the presence of bunch trains combined with a high intensity. That is, the large mean intensity of a bunch train as a whole was the source of the problem, rather than the shape, the number of trains or the bunch structure within a train. The laboratory setup could therefore reproduce the faulty DCCT behavior and was a valid test for the new hardware.

The setup used to test the bunch pattern dependence is shown in Fig. 36. A computer controlled scope generated a voltage pattern over time with a maximal amplitude of 1 V. The generated pattern, which represents one or more bunch trains simulating an LHC filling pattern, was repeated at a frequency of 11245 Hz. The different patterns tested are shown in Fig. 37. The filling pattern signal from the pico scope was fed to a custom made “shaper” which amplified the signal up to 20 V. The amplified signal was carried through the DCCT via the beam pipe antenna and was terminated with a 50 Ω - 200 W resistance. The repeated pattern created a net current flowing through the DCCT with the shape of the given pattern. The current intensity depends on the pattern shape and the amplification of the “shaper”. The voltage drop at the 50 Ω resistance is a measure of the average current flowing through the DCCT; the signal was reduced with a 1/2 divider to stay within the acquisition range. The signals were acquired with a 16 bit ADC with a sampling rate of 1 s. A low-pass 1 Hz filter was used for each channel to smooth the signal before acquisition.

All measurements were averaged over 60 s. One measurement with zero current was used to correct the DCCT offset. The ratio between the injected current pattern ($I_{pattern}$) and the DCCT response (I_{DCCT}) must be constant for all tested patterns and intensities. A comparison of the DCCT response between the 2010 and 2011 hardware at low intensity is shown in Fig. 38. The 2010 misbehavior is clearly visible (bottom plot), while the ratios taken with the new 2011 settings are constant within $\pm 1\%$. The accuracy of the measurement is limited by the low voltage drop at the 50 Ω resistance and by the noise-induced fluctuations. The same measurement performed with the maximal intensity is shown in Fig. 39. The higher current intensity improved the measurement accuracy. The ratio $I_{pattern}/I_{DCCT}$ is constant within a 0.1% band for all tested patterns. The DCCT range 2 is saturated for some measurements, the data points are therefore missing.

In conclusion the improved DCCT front-end electronics are stable for all tested patterns and the measurement accuracy is limited by the instrumentation and electronic components. While it is not feasible to test all possible patterns, this measurement confirms the correct DCCT behavior with bunch trains up to the tested intensities. Indeed the saturation effects on some amplifiers, responsible for the misbehavior, are visible as soon as a large mean intensity is grouped in a continuous train, regardless of its length, shape or number of bunches. High intensities worsen the misbehavior effect; this measurement simulates intensities of up to 1200 nominal bunches. Testing the bunch pattern ratio to simulate the higher intensities reachable with 25 ns trains will require a new dedicated experiment.

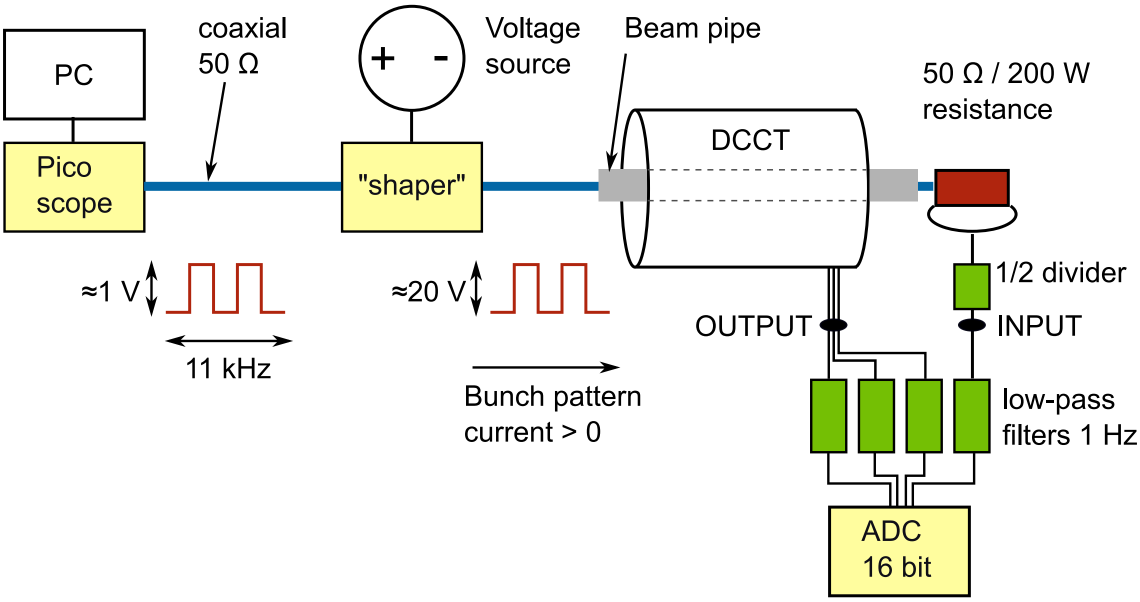

Figure 36: Setup in the laboratory to verify the bunch pattern dependence. A computer controlled scope generated a 90 μs filling pattern which was repeated at 11 kHz. The signal was amplified by a custom made “shaper” and fed through the DCCT. The resulting net current intensity was measured through the voltage drop of the 50 Ω resistance terminating the circuit. The DCCT signals and the input current were acquired with a NI 16 bit ADC.

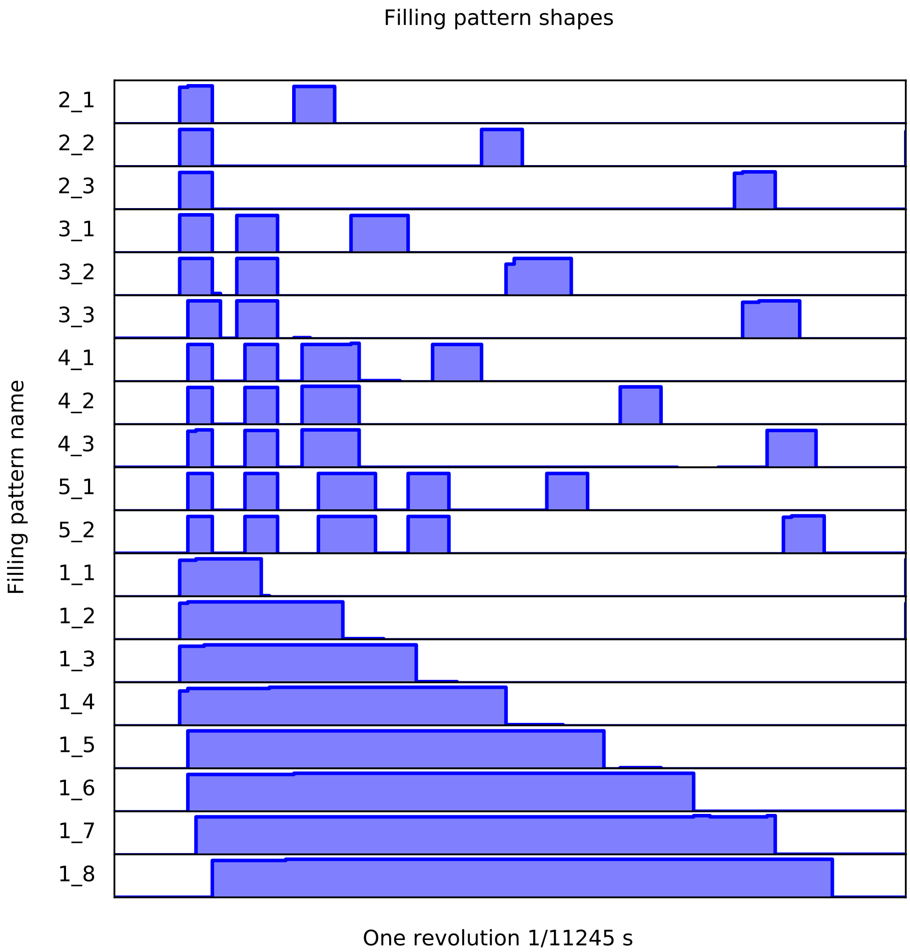

Figure 37: Bunch pattern used in laboratory tests of the DCCT. The shape was measured at the output of the Pico scope with an oscilloscope; each line represents a different pattern. The first number in the pattern name (y axis) is the total number of trains in the pattern, the second number enumerates the different positions or sizes of the trains. The x axis represents the time with a total length of one LHC revolution (90 μs). The filled and empty regions are the time when the signal carries 1 V and 0 V, respectively. Within the hardware limitations, the shortest possible train is about 2.8 μs (e.g. first train in 4)

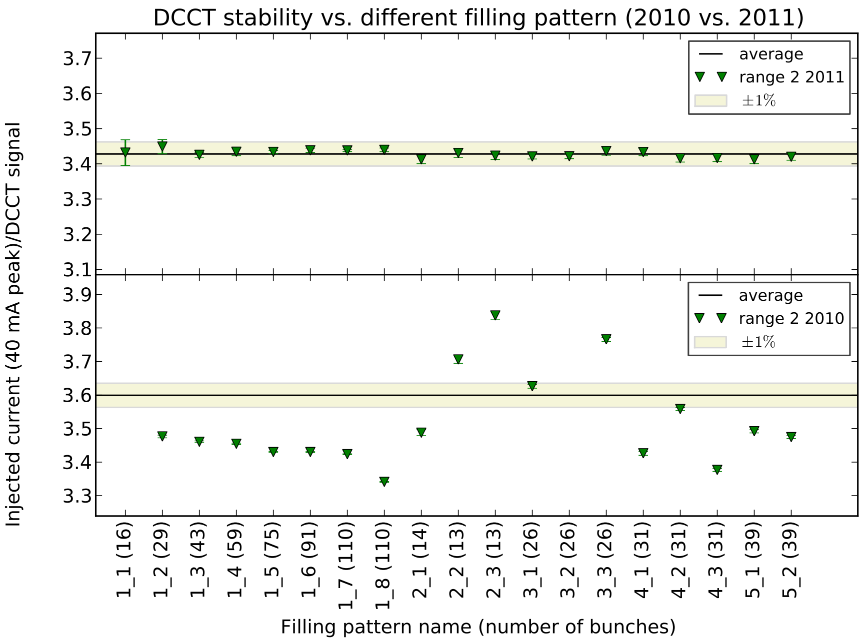

Figure 38: Comparison of the DCCT sensitivity to different bunch patterns at low beam intensity, in 2010 and 2011. The different filling pattern names are listed on the x axis with an estimation of the equivalent number of bunches with 10^{11} protons indicated in parentheses. The y axis represents the ratio $I_{pattern}/I_{DCCT}$. For those measurements, the "shaper" amplified the signal to 2 V resulting in a peak current of 40 mA. The spread in the 2010 data points (bottom plot) is due to the bunch pattern dependence, the ratio for the 1_1 pattern is off-scale. The indicated errors include only the noise fluctuations of the data within the 1 minute measurement.

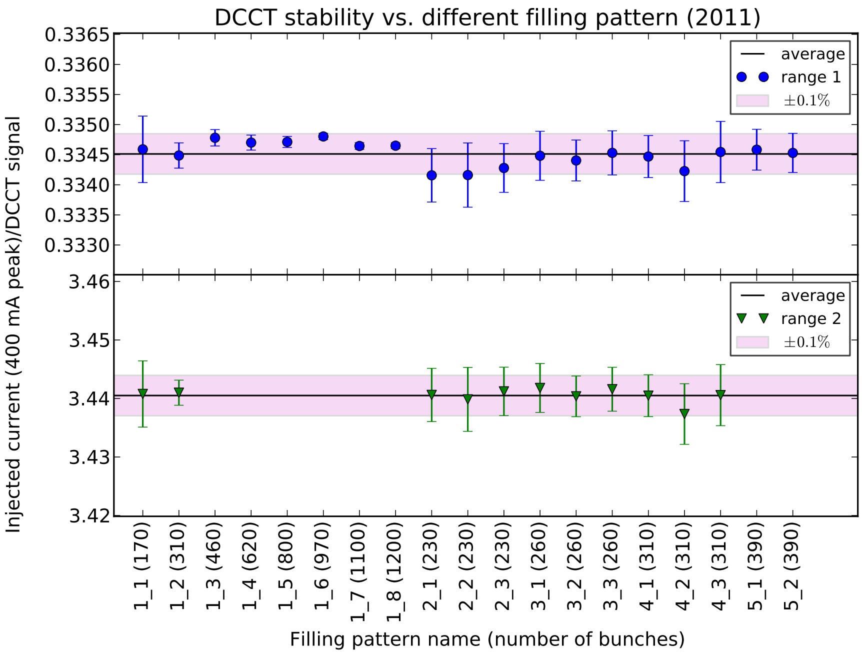

Figure 39: Bunch pattern dependence at high intensity. The "shaper" amplified the signal to 20 V resulting in a peak current of 400 mA. Some data points are missing on range 2 due to saturation, because the value is above the range maximum. The indicated errors include only the statistical fluctuation of the data within the 1 minute measurement.

4.2.2 Measurement with beam

The pattern-related misbehavior was only observed during fills with bunch trains and a large mean intensity. A bunch train generates different frequency harmonics compared to single bunches: the power spectrum is stronger at lower frequencies with a bunch train compared to a single bunch. High-frequency harmonics from single bunches are masked by the 80 kHz HF by-pass of the DCCT. In principle the DCCT is not affected by single bunch pattern.

A beam debunching measurement has been performed on 30 June 2011. Both beams where filled with five nominal bunches plus one pilot bunch before the RF was switched off. Without RF capture, the bunched protons quickly populated the whole beam circumference eventually forming an unbunched, continuous beam. The DCCT was therefore subjected to a continuously changing frequency pattern. Provided that the unbunched protons remain in the beam, the DCCT signal must be constant during the debunching process which takes less than 15 minutes. The results of the debunching measurement are shown in Fig. 40. The debunching process is evidenced by the fall of the FBCT signal towards zero in the first 600 to 800 seconds after the RF was switched off. During this time the DCCT was stable within the noise level. On beam 2 an intensity decay is visible; however, the decay is starting before the RF was switched off and the FBCT signal is stable during this time. Therefore, the decay is probably due to a drift of the DCCT offset.

In conclusion the DCCT is not affected by the bunch length or the filling pattern; however, the low intensity of the beam limits the significance of the measurement.

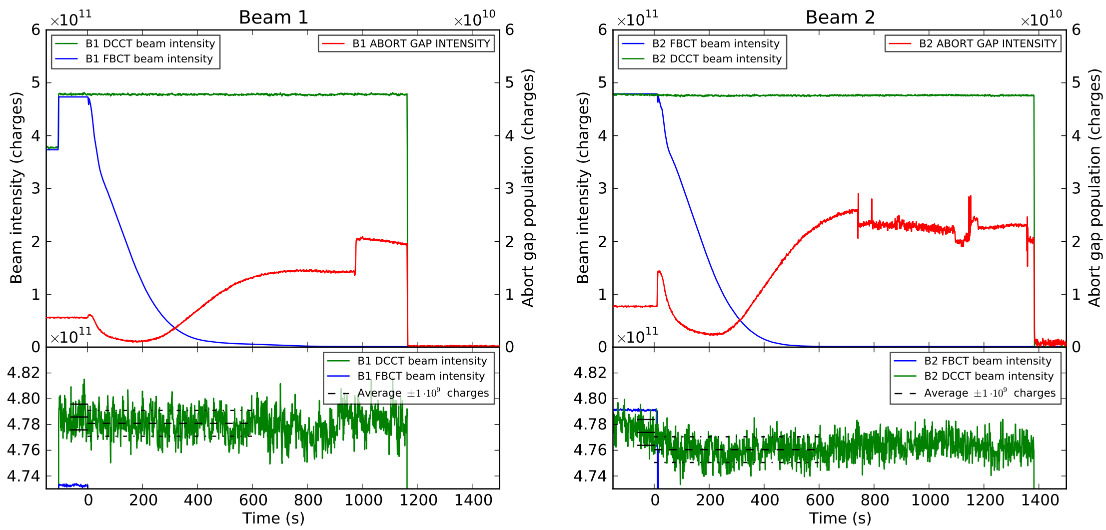

Figure 40: Stability of the DCCT during beam debunching for beam 1 (left) and beam 2 (right). The LHC RF was switched off at T=0 at which point the FBCT signal dropped quickly. The beam was fully unbunched after about 12 minutes; at this time the FBCT signal reached zero and the abort gap population reached its maximum. The lower plot shows the DCCT intensity in a narrow intensity range. The average DCCT value taken 60s before and 600s after turning off the RF is indicated as an horizontal line. A boundary of $\pm 10^9$ charges is shown as dashed lines. The stability of the DCCT during the debunching of the beam is compatible with the typical noise value of $\pm 10^9$ charges.

4.2.3 Sensitivity to an injected RF sine wave

The DCCT is exposed to various frequency spectra depending on the number of circulating bunches and the filling pattern. A circulating bunch will create harmonics in the frequency domain; the amplitude of the harmonics are related to the beam intensity. The frequencies and number of harmonics depend on the number of circulating bunches and their arrangement in trains. While it is not possible to reproduce in the laboratory the same spectrum and power generated by a 200 MJ beam, a single harmonic can be shown as an RF wave with high amplitude. In this measurement the DCCT was exposed to an RF sine wave which was swept over a wide frequency range to test if the DCCT is sensitive to a specific harmonic.

The Gaussian pulse created by a circulating bunch of N protons with a width σ_z at a revolution frequency ν_{rev} is described in the time domain as

$$I(t) = Q \cdot \sum_{n=-\infty}^{\infty} \frac{1}{\sqrt{2\pi}\,\sigma_t} e^{-\frac{(t-nT)^2}{2\sigma_t}} \tag{2}$$

with

$$T = \frac{1}{\nu_{rev}};\ Q = N \cdot e;\ \sigma_t = \frac{\sigma_z}{c}. \tag{3}$$

The Fourier transform of the pulse takes the form of a Dirac comb

$$I(\nu) = Q \cdot \nu_{rev} \cdot e^{-\nu^2 \cdot \sigma_t^2 \cdot 2\pi^2} \sum_{k=-\infty}^{\infty} \delta(\nu - k\nu_{rev});\ k = 0, \pm 1, \pm 2, \dots \tag{4}$$

The harmonics form a Dirac comb $\sum_{k=-\infty}^{\infty} \delta(\nu - k\nu_{rev})$ with a Gaussian envelope $e^{-\nu^2 \cdot \sigma_t^2 \cdot 2\pi^2}$ and the DC component $Q \cdot \nu_{rev}$ as amplitude. An example of a bunch pulse and the resulting harmonics is shown in Fig. 41. The pulse width of 2.25 μs is arbitrarily large to demonstrate the effect of the Gaussian envelope which reduces the high frequency harmonics. A wide pulse has a stronger spectrum power at lower frequencies while a narrow pulse of 2 ns has a flat power spectrum with for example 97% intensity at 200 kHz. Therefore a nominal bunch creates a similar harmonic spectrum to an RF wave considering that the 80 kHz HF by-pass of the DCCT cuts the high-frequencies.

An RF wave with a frequency ν_0 can be described as

$$I_{RF}(t) = I_{peak} \cdot \cos(2\pi\nu_0 t). \tag{5}$$

The Fourier transform of the RF is

$$I_{RF}(\nu) = I_{peak} \cdot \frac{1}{2} \left(\delta(\nu - \nu_0) + \delta(\nu + \nu_0) \right). \tag{6}$$

The power of a single bunch pulse can be compared to an RF wave with (4) and (6):

$$Q \cdot \nu_{rev} \approx \frac{1}{2} I_{peak} \tag{7}$$

with the peak intensity of an RF wave defined as

$$I_{peak} = \sqrt{2} \cdot I_{RMS} = \sqrt{\frac{2P}{R}}. \tag{8}$$

The DCCT has been tested against the effect of radio frequencies (RF) using the setup depicted in Fig. 42. An RF wave generated by a network analyzer was fed trough the DCCT with a coaxial antenna. The net current produced by the RF, which is expected to be zero, was measured in parallel by the DCCT and with the 50 Ω resistance. The network analyzer scanned a given frequency range during 4000 seconds in a continuous logarithmic sweep, i.e. more time was spend at low frequencies. The ADC acquisition was sampled at 1 Hz and the data was offset corrected with a linear function taking a 5 minutes offset before and after the sweep using the same method as described in Sec. 3.1. The baseline correction of about 40 mV ($\approx 2 \cdot 10^{10}$ charges) was substantial but not unexpected in the laboratory DCCT. Furthermore the large ambient temperature variation in the laboratory during the summer days influenced the offset during the measurement. The DCCT offset has an estimated temperature dependence of ≈ 5 μA/°C ($\approx 2.5 \cdot 10^9$ charges/°C) [7]. The laboratory DCCT is uncalibrated, therefore, the DCCT signal conversion into charges was approximated with the theoretical scale of 1 V $\approx 10^{11}$ charges.

The DCCT response signal during the frequency scan from 1 kHz to 250 kHz is shown in Fig. 43. In this frequency range the RF signal was taken directly from the network analyzer without amplifier. The DCCT is unaffected by the RF and only the typical random noise pattern of range 4 is visible. Using equations (7) and (8), the equivalent bunch charge for this RF power is about

$$N_{30mW} \approx \frac{35 \cdot 10^{-3}}{2} \cdot \frac{1}{10^4} \cdot \frac{1}{1.6 \cdot 10^{-19}} \approx 10^{12} \text{ protons}. \tag{9}$$

The measurement from 250 kHz to 110 MHz was performed with an additional amplifier resulting in an RF power of about 10 W. The scan was performed once without DC current as in Fig. 43 and once with a 80 mA DC current passing through the DCCT. The results of both scans are shown in Fig. 44. Without DC current (top plot) the DCCT 10 seconds average stays mostly above the expected zero line at a value of about 10^9 charges. Such deviation is however compatible with range 4 with a typical noise level of $\pm 10^9$ charges. The bottom plot in Fig. 44 shows the same measurement with the addition of an 80 mA DC current flowing through the DCCT. The acquisition was performed with range 2. The signal has less noise and remains within a $\pm 0.1\%$ band around the expected value. Here with (7) and (8), the equivalent bunch charge for this 10 W RF power is about

$$N_{10W} \approx \frac{0.6}{2} \cdot \frac{1}{10^4} \cdot \frac{1}{1.6 \cdot 10^{-19}} \approx 1.6 \cdot 10^{14} \text{ protons.} \tag{10}$$

In conclusion, the DCCT proved to be unaffected by all tested RF frequencies from 1 kHz to 110 MHz and no resonance has been found. In all measurements the DCCT signal is compatible with the noise of the selected range.

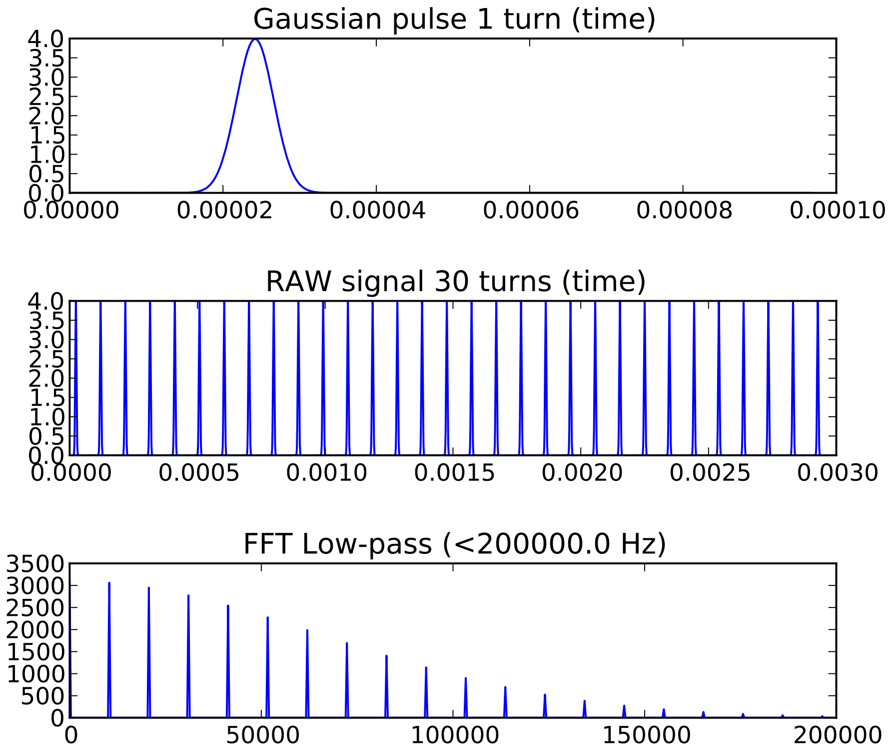

Figure 41: Fourier transform example with a wide Gaussian pulse. The first plot (top) shows a 2.25 μs wide pulse in the time domain. The full width of the x axis represents 100 μs, approximately one LHC revolution. The second plot shows the resulting signal of the pulse during 30 revolutions also in the time domain. The Fourier transform of this signal is shown in the bottom plot, the x axis represents the frequency. The harmonics are places at 10 kHz intervals. The effect of the Gaussian envelope is clearly visible for a wide pulse and the power is close to zero at 200 kHz.

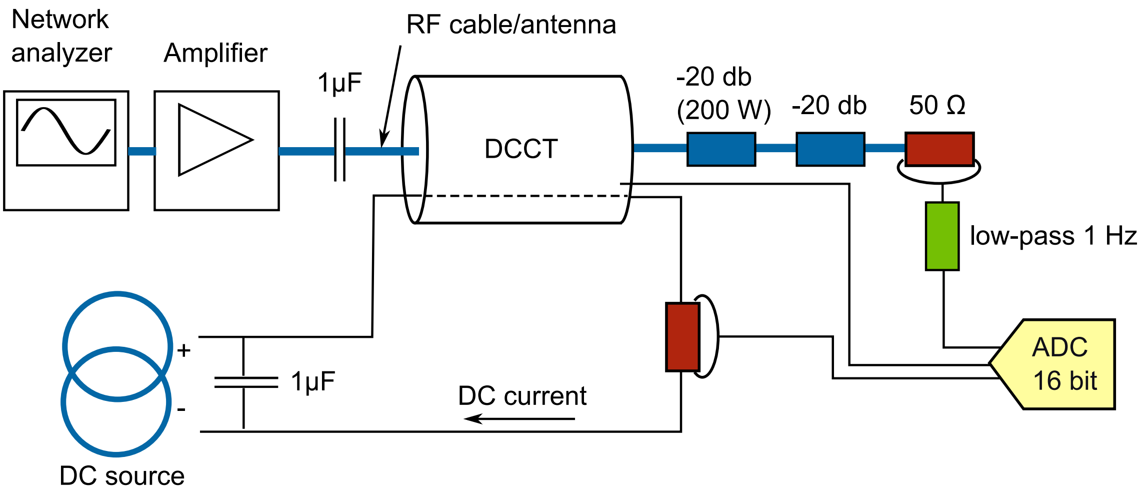

Figure 42: Sensitivity to RF setup. A network analyzer and an amplifier send an RF wave through the DCCT. The wave was guided through a coaxial cable and then through the beam pipe antenna and finally two -20 db RF attenuators. The cable was terminated with a 50 Ω resistance; furthermore, a 1 μF capacitance was placed after the amplifier to avoid any direct current flowing through the RF cable, for example due to a ground differential. The voltages at the resistances and from the DCCT were acquired with a 16 bit ADC. Additionally, for one measurement, a DC current was fed through the DCCT in parallel to the RF. The voltage drop in a 14.7 Ω resistance (3 W; ±5%) was used to verify the DC current.

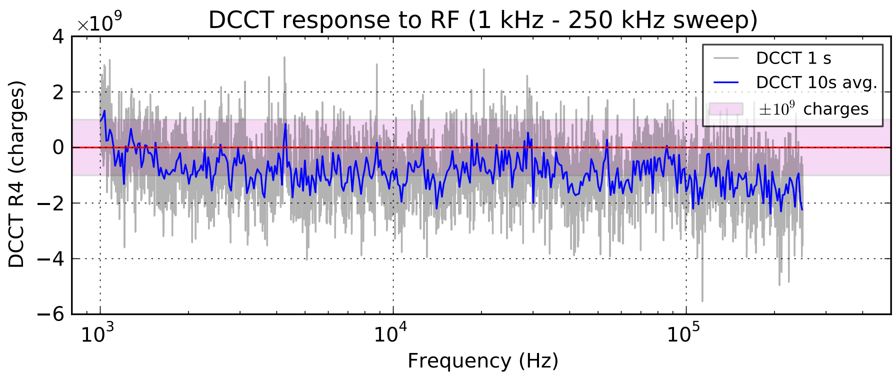

Figure 43: DCCT response to RF between 1 kHz and 250 kHz. The range was scanned in 4000 seconds in a logarithmic sweep. The average RF power was about 30 mW by using the network analyzer directly at its maximal output (signal unamplified).

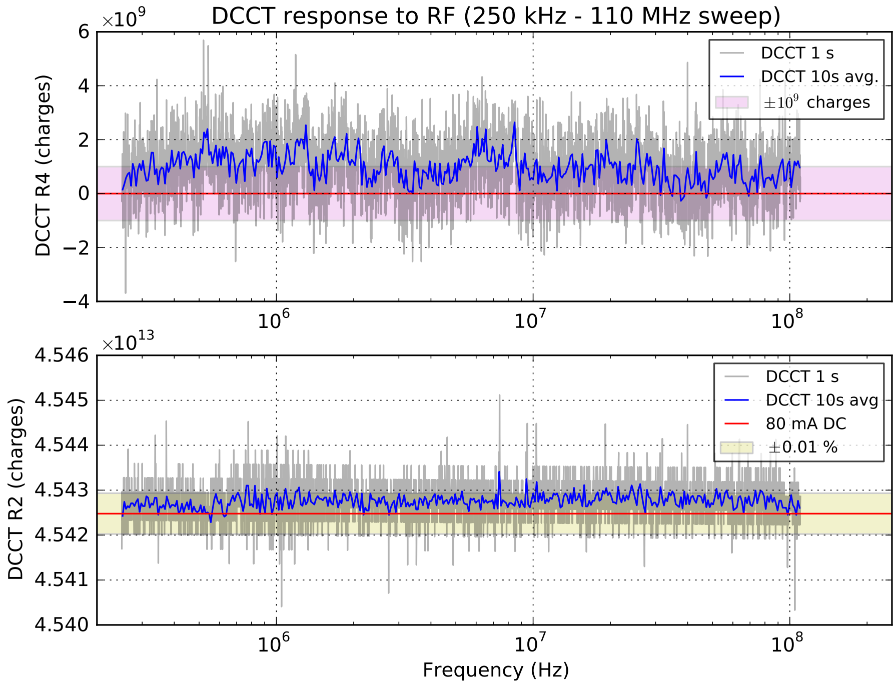

Figure 44: DCCT response to RF between 250 kHz and 110 MHz. The range was scanned in 4000 seconds in a logarithmic sweep. The RF was amplified with an RF amplifier ENI (Electronic Navigation Industries) 310L with a range of 250 kHz - 110 MHz resulting in an average RF power of about 10 W. The top plot shows the DCCT range 4 during the sweep, without an additional DC current. The bottom plot shows the DCCT range 2 during the sweep with an additional current of 80 mA passing through the DCCT.

4.3 Bunch position dependence

The fast BCT's have a known sensitivity to the bunch position. The sensitivity of the DCCT with respect to the bunch position has been tested by moving each beams in the vertical and horizontal planes during a machine development (MD) fill[§]. The DCCT signal and beam position over time are shown in Fig. 45 for beam 1 and Fig. 46 for beam 2. No correlation with the beam position can be seen in the beam decay.

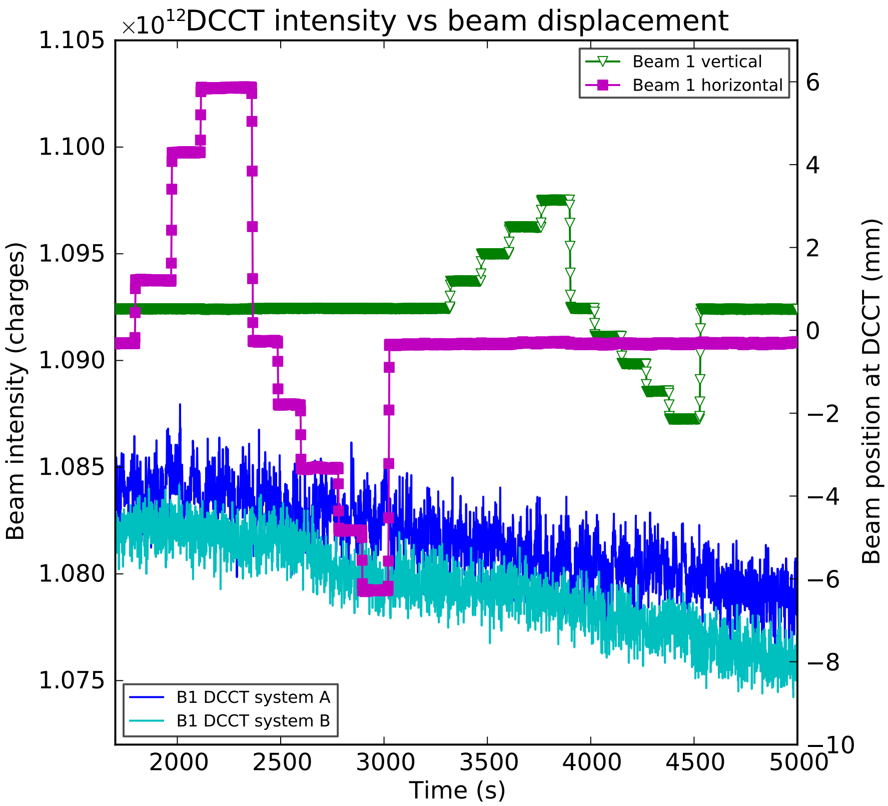

Figure 45: Bunch position dependence beam 1.

[§]Fill 1910 on 30 June 2011.

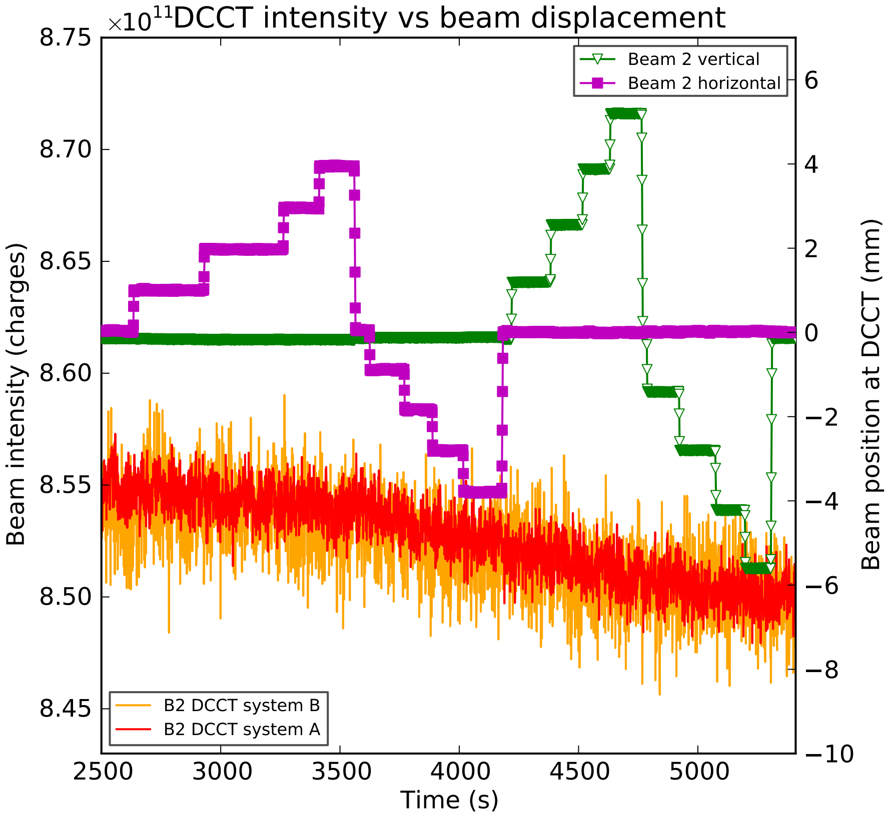

Figure 46: Bunch position dependence beam 2.

4.4 Interference from Accelerator Systems

4.4.1 Interference from magnetic field

A possible interference between the LHC magnetic fields present at high energy and the DCCT response has been analyzed for all physics fill in 2011. The DCCT's are placed in straight section 45 and the nearest magnet is located xx meters away (TODO: find numbers). During the energy ramp down, after a fill has been dumped, the DCCT is at its most sensitive range and the signal is expected to be zero or compatible with the typical offset of $\pm 5 \cdot 10^9$ charges. For this verification, the correlation between the DCCT signal and the LHC energy has been analyzed for all physics fills in 2011. The DCCT signal and LHC energy are averaged over 60 seconds time bins during the ramp down period from 3500 GeV to 450 GeV followind the beam dump. The correlation between the LHC energy and the DCCT signal without beam is shown in Fig. 47 for the four DCCT's. This analysis is biased by the fact that the energy is always ramped down from high to low energies, and the high energy data is therefore always taken shortly after the dump, while the low energy data is always taken 15 to 20 minutes later. A possible correlation with the time or an other time changing parameter can not be disentangled from the LHC energy with this method. However, the offset during the energy ramp down stays within $\pm 5 \cdot 10^9$ charges for all DCCT's and is compatible with the typical offset drift as seen in Sec. 3.2.

For system A/beam 1 the offset is systematically larger at 3.5 TeV compared to lower energies, while for system B/beam 1 the offset is often smaller at higher energies. This effect can be observed in some fills where, immediately after the beam dump, a downward drift for system A/beam 1 and a similar upward drift for system B/beam 1 can be observed. The full drift amplitude is typically of the order of $2-5 \cdot 10^9$ charges over 10 minutes after which the signal is flatting out. This drift is not always present and is also observed when the LHC energy remains constant before the start of the ramp down, it is therefore not correlated with the LHC energy.

In conclusion, no correlation with the LHC energy is observed and the baseline is always within the $\pm 5 \cdot 10^9$ charges as observed in Sec. 3.2. A drift during the first 15 minutes following the beam dump is sometime observed in beam 1; the drift is downward for system A and upward for system B. The drift amplitude is smaller than $5 \cdot 10^9$ charges and is not correlated with the LHC energy.

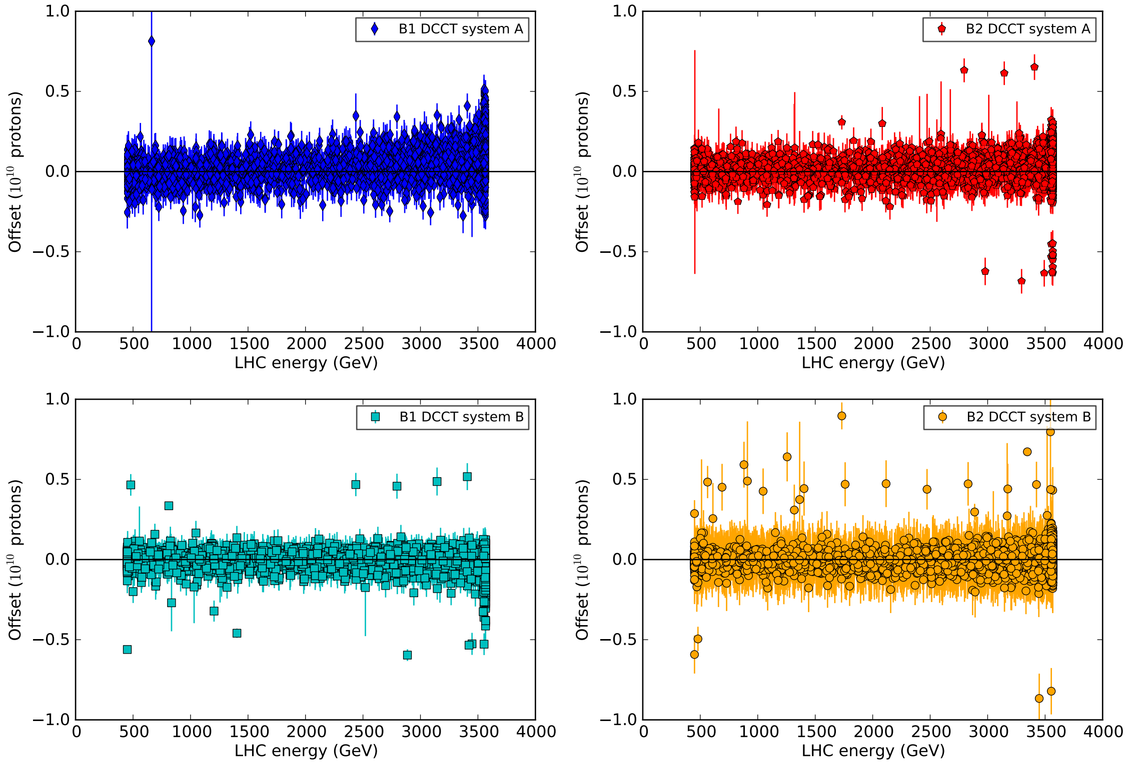

Figure 47: Offset versus LHC energy during ramp down for all physics fills in 2011. Each point is a DCCT average of 60 seconds placed at the average LHC energy for this time. The indicated error is the standard deviation of the 60 values.

4.4.2 Interference from RF

The LHC RF system is located on each side of the interaction point 4 (IP4), about 200 m away from the DCCT's. The accelerating cavities are composed of 8 single-cell cavities per ring operated at a constant frequency of 400 MHz. During a fill setup, and before the first beam injection, the field from each cavity is ramped up from 0.02 MV/m (RF_{off}) to about 0.75 MV/m (RF_{on}).

The following analysis evaluates a possible interference between the RF field variation and the DCCT signal by evaluating the DCCT offset over 120 seconds before and after the RF field is switched on. An example showing the RF cavity transition is provided in Fig. 48. In the absence of interference from the RF system, the offset should remain constant regardless of the RF cavity field and the difference Offset(RF_{on}) - Offset(RF_{off}) must be zero within the noise level of range 4. The RF is not always switched off between fills, furthermore the automatic offset correction, which is part of the LHC setup sequence, can occur within the averaging time window, therefore not all fills can be used to verify the offset change. From all physics fills in 2011, 86 fills had a clear RF transition and could be used for this analysis. The offset difference observed between the time periods RF_{on} and RF_{off} is shown in the histograms in Fig. 49 for beam 1 (left) and beam 2 (right), combining both systems A and B. The offset difference amounts to $0.5 \cdot 10^8$ and $-0.1 \cdot 10^8$ charges for beam 1 and 2 respectively.

In conclusion the DCCT's are unaffected by the cavity field of the RF accelerating system located at IP4, the DCCT offset in its most sensitive range is not sensitive to the LHC RF.

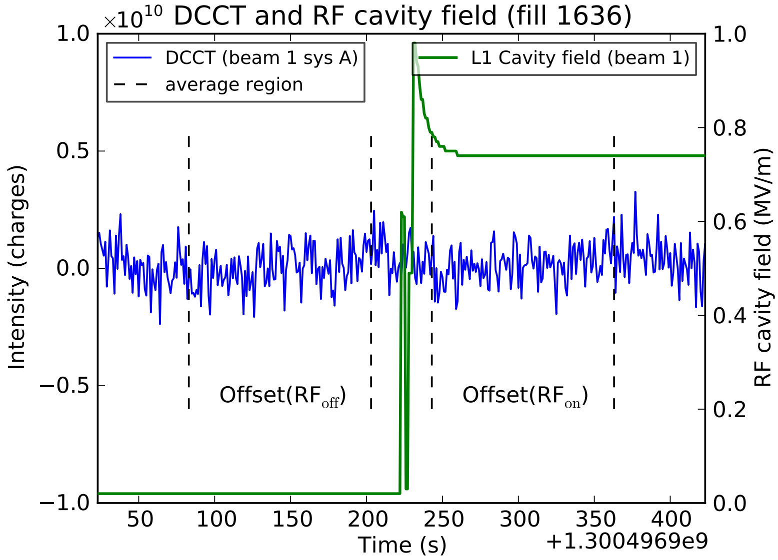

Figure 48: Example plot showing one DCCT (beam 1 system A) offset evolution when the RF cavity field is switched on. For better clarity, only 1 out of the 16 cavities is shown. The left y axis shows the beam intensity measured by the DCCT, the right y axis indicates the RF cavity field. The vertical dashed lines indicate the bounds used to average the DCCT offset before and after the RF field ramp.

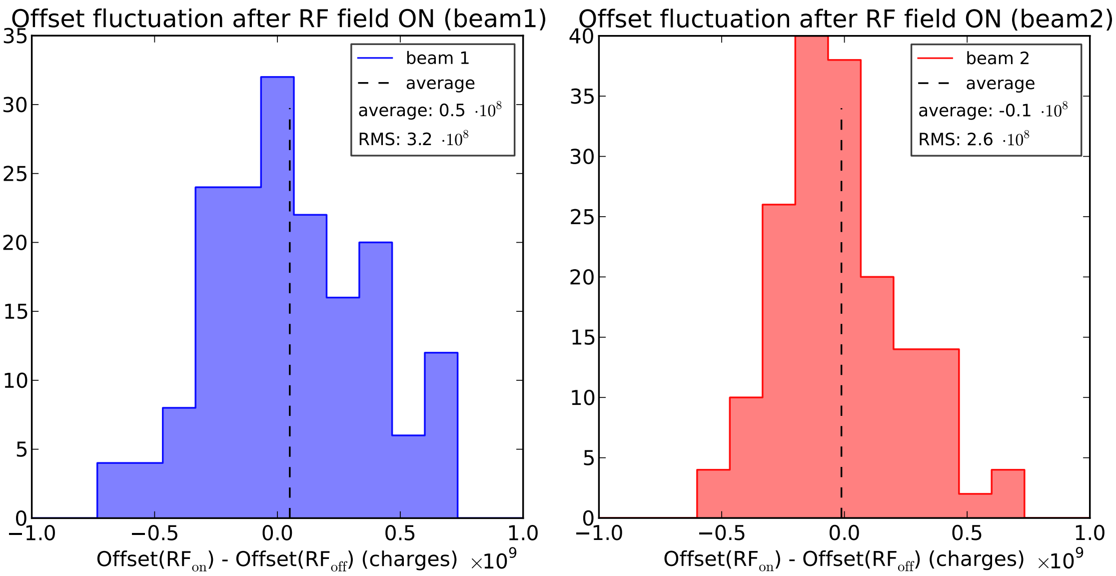

Figure 49: Offset versus LHC RF field. The offset is measured for 120 s before and after the RF field has been switched on. The offset difference Offset(RF_{on}) - Offset(RF_{off}) is evaluated at each ramp up of the cavities in the pre-injection setup.

5 Calibration Method

The stability of the scaling factor during the year seen in Sec. 3.6 shows that the reproducibility of the calibration method combined with the stability of the scaling factor are limited by the resolution of the ADC only. The following sources of uncertainty related to the calibration itself are discussed below:

- The precision of the current source used for the calibration
- The position of the calibration rods

- The methodology of the standard BI calibration procedure
- Current leak between the surface and the tunnel

5.1 Current source accuracy

The absolute scale for each transformer is calibrated with a precise DC current source. Two sources are available: the model Yokogawa 7651 was used for the 2010 calibrations and the model Yokogawa GS200 was used for the 2011 calibrations. The sources manufacturers quote a 90-day accuracy of 0.02%. Both sources have been tested with common laboratory multimeters or voltmeters. While the results are compatible with the expected uncertainties, those methods were not able to reach a precision of the order of a permille. The most precise measurement was reached by measuring the voltage drop across a known precise resistance. The measurement was performed with a soldered 4-wire (Kelvin) setup (Fig. 50) to eliminate both wiring and contact resistances. This precise measurement could not reach the claimed accuracy of the sources; however, it can be used as systematic uncertainty for the calibration of the DCCT's. The following components were used:

- A 100 Ω precise foil resistance with a tolerance of ±0.01%, ±5 ppm/°C and power rating of 0.6 W. RS catalog number 201-9848.
- A Voltmeter Solartron / Schlumberger 7060 multimeter with a quoted accuracy of 0.002%. The lowest measurements of 0.1 mA and 0.18 mA were limited by the last digit of the voltmeter.

The measured currents for both sources are shown in Fig. 51. For reference, the calibration currents used for the ranges 4 to 1 are: 0.18, 1.8, 18 and 120 mA, respectively. The 100 mA measurement dissipated 1 W of heat which is above the maximal power of the resistance quoted at 0.6 W. Therefore, the measurement was performed quickly as to avoid a temperature drift or damage to the resistance. The last digit of the voltmeter, equivalent to 10 μV, limited the accuracy of the lowest measurement of 0.1 mA to ±0.1%. At 0.18 mA, which is the current used to calibrate range 4, the uncertainty is still dominated by the last digit and amounts to 0.06 %.

In conclusion, the current used for the calibration of range 4 is verified with an accuracy of 0.06% which is dominated by the last digit of the instrument, the higher currents agree within an error of ±0.05%. Therefore, an envelope error of ±0.05% has to be taken for the total beam intensity. Because the same source is used for all DCCT's, the error is correlated between both beams. Furthermore, there is no precision advantage of using one source over the other.

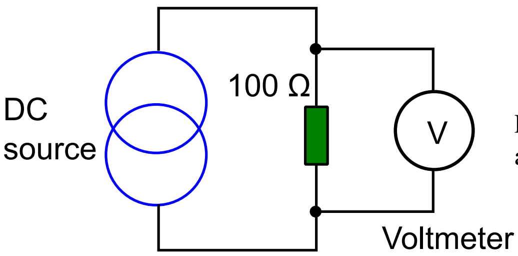

Figure 50: 4-wire (Kelvin) setup to measure the DC source accuracy. The resistance and wires are soldered.

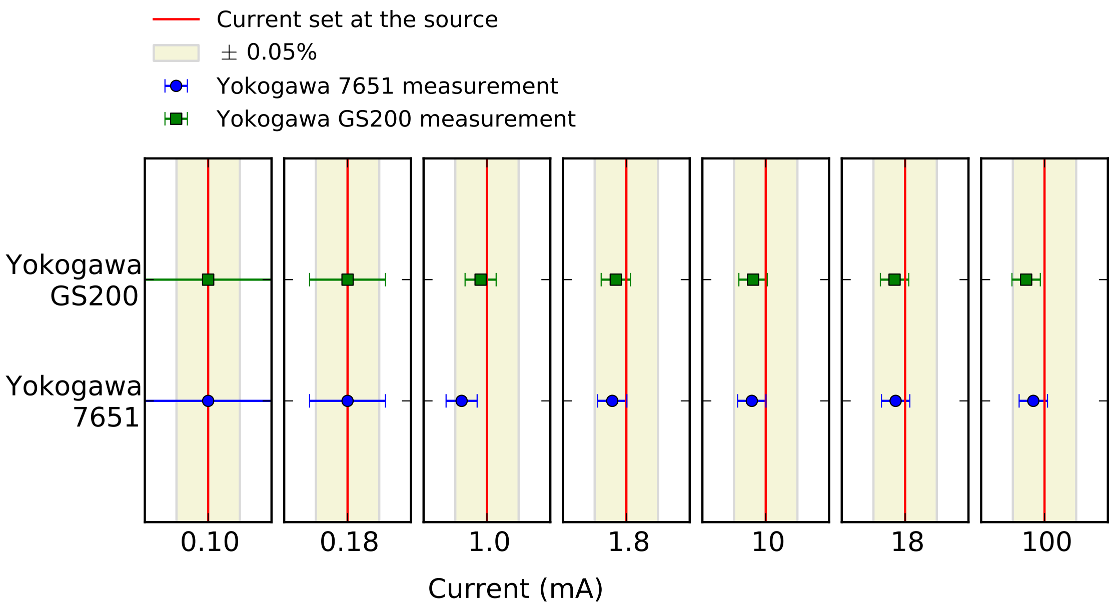

Figure 51: Accuracy verification of the precise DC sources. The vertical lines indicate the current set at source; the measured current is indicated by a square for the GS200 source (top) and by a circle (bottom) for the 7651 source. The error bars include the resistance uncertainty of $\pm 0.01\%$ plus a maximal temperature variation of 40°C and the voltmeter uncertainty of 20 ppm and last digit resolution. The vertical band shows an envelope of $\pm 0.05\%$. The uncertainty of the two smallest values (0.1 and 0.18 mA) are dominated by the last digit of the voltmeter.

5.2 Position of the calibration rods

The calibration current is injected through 4 rods placed symmetrically around the internal opening of the DCCT for the beam pipe. The wiring configuration is such that the DCCT sees four times the current which is injected with the current source. Measurements in the laboratory confirmed that the position of the cable carrying the DC current has no influence on the DCCT response. The DCCT signal was identical regardless of the cable position inside the DCCT opening and the signal was exactly multiplied by four when injected through the calibration rods.

In conclusion, for a DC current, the DCCT is not sensitive to the cable position and no error is introduced by the fact that the calibration current is not injected at the center of the DCCT.

5.3 Methodology and current leak

The standard precise calibration procedure which is regularly carried out during technical stops is performed in the following way. The current source is connected to the back-end electronic rack on the surface. The DCCT control software first acquires the offset for all ranges of the given DCCT while the source is set to zero current. For each range the calibration current (shown in Table 7) is injected in the DCCT while the digital signal is acquired for 60 seconds. The scaling factor is the offset corrected average signal over 60 seconds divided by the equivalent charges specified by the operator.

To validate the standard procedure, a series of independent "self" calibrations has been performed using the measurements in the tunnel; in addition, one "self" calibration was carried with the source on the surface. For those independent calibrations, the source was controlled by a computer and the raw DCCT data was saved offline for analysis (as in Sec. 3.4). The offset was subtracted using a period before and after the signal as described in Sec. 3.1. The LSB value (i.e. the scaling factor) is given by the ratio (Injected charges)/(measured ADC signal). The measurements dedicated to the linearity and 12 hour long term measurements were also used to calculate the scaling factor using the longer averaging time provided by the

Table 7: Calibration currents used to measure the scaling factor of each range. The ranges 2 to 4 are calibrated at 80% of their range while range 1 is calibrated at 50% of its range due to the limited maximal current of the source.

Range	Injected current (mA)	Equivalent charges	Approximate LSB value (charges/bin)
4	0.18017	$4 \cdot 10^{11}$	$2.5 \cdot 10^{8}$
3	1.8017	$4 \cdot 10^{12}$	$2.5 \cdot 10^{9}$
2	18.017	$4 \cdot 10^{13}$	$2.5 \cdot 10^{10}$
1	112.61	$2.5 \cdot 10^{14}$	$2.5 \cdot 10^{11}$

sequence. The results of the so called “self” calibrations compared to the standard calibrations performed in 2011 is shown in Fig. 52 for the DCCT system A beam 1. The other DCCT’s are shown in the appendix Fig. 78, 79 and 80.

In conclusion the scaling factors measured with both methods agree within an envelope of $\pm$ 1 LSB (equivalent to $\pm$ 0.06% at 80% of the range) for the ranges 1 to 3 and within $\pm$ 4 LSB ($\pm$ 0.24%) for range 4. No difference can be seen between the two methods. Furthermore there is no difference between the calibrations performed with the source in the tunnel or on the surface excluding a possible current leak in the 500 meter cables and switches between the surface and the calibration rods in the tunnel.

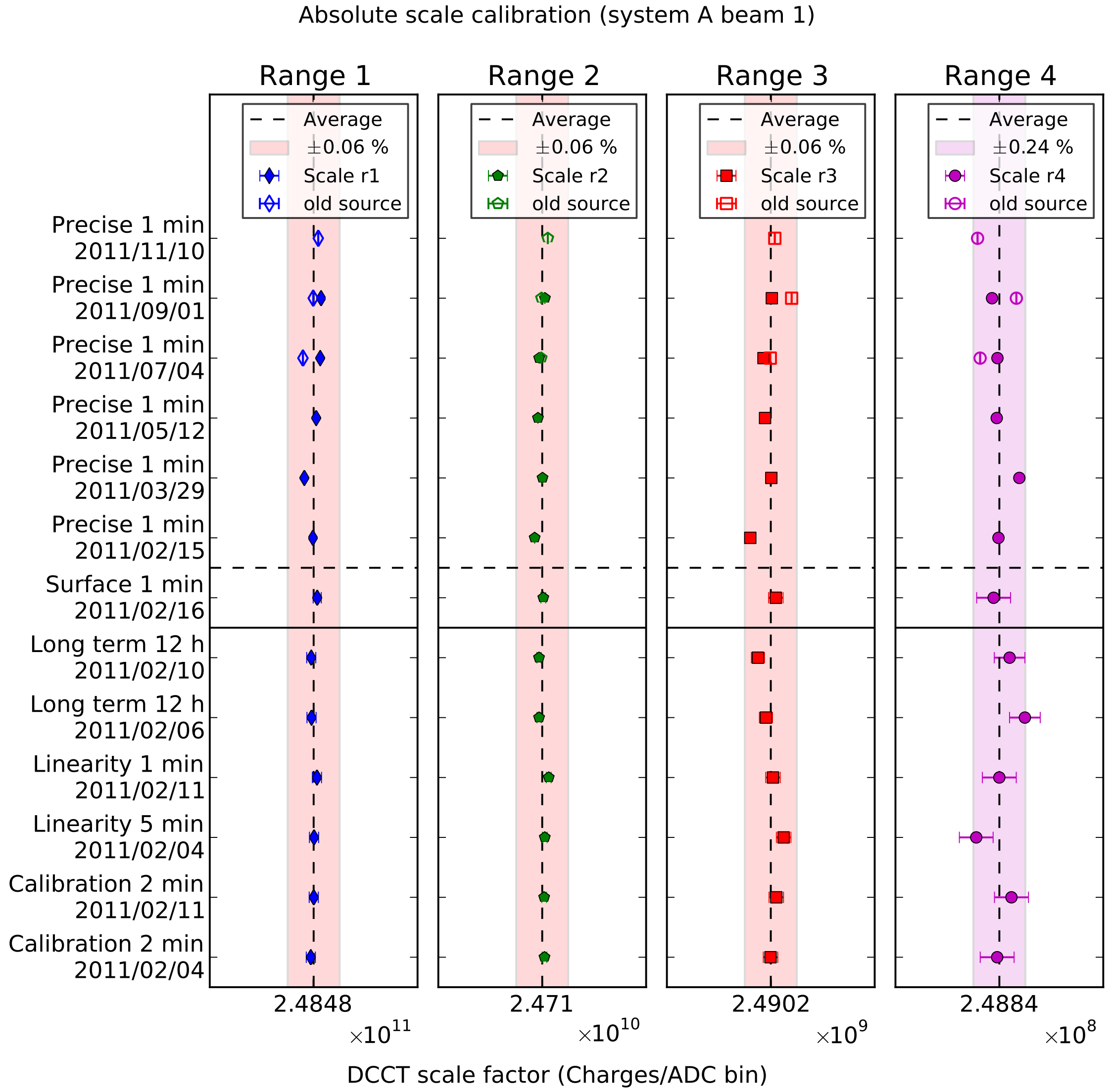

Figure 52: Long term stability of scaling factor. All points below the horizontal dashed line are so called “self” calibrations performed independently from the BI method and software. The points below the continuous horizontal line are calibrations performed with the source in the tunnel instead of on the surface.

6 Difference between systems A and B

As shown in Sec. 4.2, both systems A and B were behaving differently in 2010 due to a dependence on the bunch pattern. The difference can be seen on all train injections in 2010, but is not observed with the corrected hardware in 2011 as shown in Fig. 35. A systematic study of all injections during 2010 and 2011 permits to assert the stability of the new hardware. Indeed the injections during 2011 are performed not only with high intensities up to $2 \cdot 10^{14}$ charges in total, but also with different train length from 8 to 144 bunches per train. Furthermore, during a fill injection each additional train changes the filling pattern and thus the harmonics seen by the DCCT. Additionally, since no error source larger than $\pm$ 1 LSB has been discovered for the ranges 1 to 3, both DCCT systems must agree within $\pm$ 1 LSB in the absence of uncorrelated systematic error.

Each injection step was analyzed for all physics injections of 2010 and 2011, an example of the method used for all fills is shown in Fig. 53 for fill 1459. On the left plot, each injection step of a given fill is detected and the intensity is measured by taking a 60 s average. The standard deviation of data is used as error. The relative difference at each step N(sys A) - N(sys B) / N(average) (%) between system A and B is plotted over time on the right plot. While both systems happen to agree at the end of injection, the erratic behavior during the injection unveil large discrepancies.

The relative difference between system A and B over the course of two years is shown in Fig. 54 for all analyzed fills. A detailed view of all 2011 injections is shown in Fig. 55. With some exceptions, the relative difference between both systems remains within $\pm 0.5\%$ for the majority of the injection steps. On May 24 some points (all from fill 1804) with negative relative difference in beam 2 are clearly visible. The behavior of fill 1804 is not explained yet. The November injections are fills with lead ions. The same 2011 data plotted against the intensity on the x axis is shown in Figs. 56 and 56 for beams 1 and 2 respectively. A relative difference caused by a 1 ADC bin difference is indicated by a dashed line; the four ranges span from range 1 on the right to range 4 on the left. The lower right group of points from beam 2 belongs to fill 1804 which was identified in Fig. 55. On the upper right, some points from beam 2 are above the 1 LSB line at the limit between range 1 and range 2. Those 9 points above 0.5% are spread around the year as can be seen in Fig. 55. No study has been made to understand this rare effect which appears to occur at the range change. A possible explanation is that the switch from range 1 to 2 occurs at a slightly different time for both independent systems and the comparison is made between the high-end of range 2 and low-end of range 1. In all other injection steps throughout 2011, the relative difference between system A and B remains within $\pm$ 1 LSB. At low intensities covered by range 4, the difference is larger which is to be expected with a typical noise of $\pm$ $3-4$ LSB; however, the difference remains within $\pm$ 1 LSB of range 3 which corresponds to $\pm$ 10 LSB of range 4.

In conclusion both independent DCCT systems A and B provided a consistent measurement throughout all physics injections in 2011 within the resolution of the 12-bit ADC or within the noise level of range 4. The DCCT accuracy is therefore at best limited by the 12-bit ADC; furthermore, no other uncorrelated systematic error has been revealed with this consistency check. An envelope error of $\pm$ 1 LSB is taken for the ranges 1 to 3 and of $\pm$ 10 LSB for range 4. However, this additional uncertainty is probably already included in the absolute scale and baseline fluctuations error. In absence of better knowledge, the difference is conservatively added to the total error.

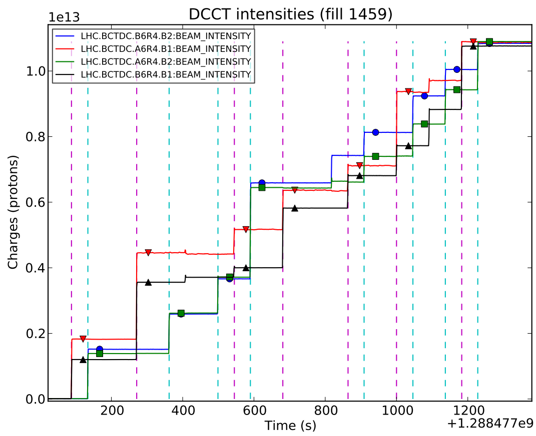

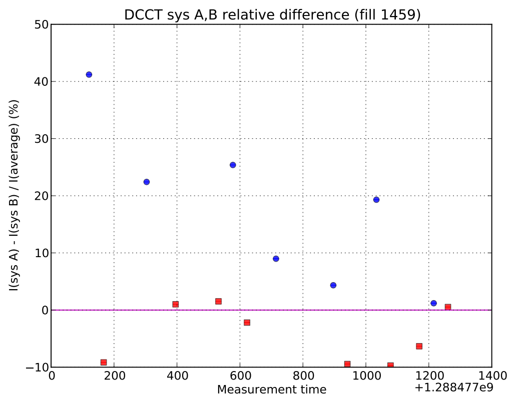

Figure 53: Example of injection steps (fill 1459 in 2010). Each train injection is seen as a step in the beam intensity. In 2010 the DCCT misbehavior can be clearly seen where the systems A and B indicate a different intensity for the same beam.

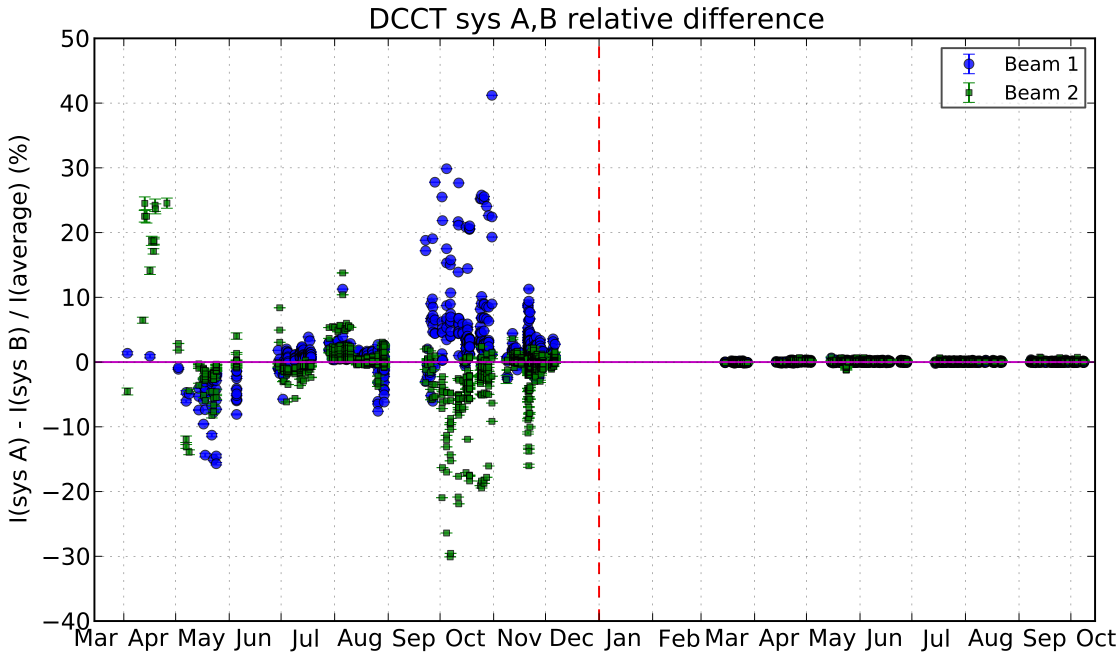

Figure 54: Relative difference between system A and B during all physics injections of 2010 and 2011 using a 60 s average per injection step. The DCCT misbehavior in 2010 is clearly visible.

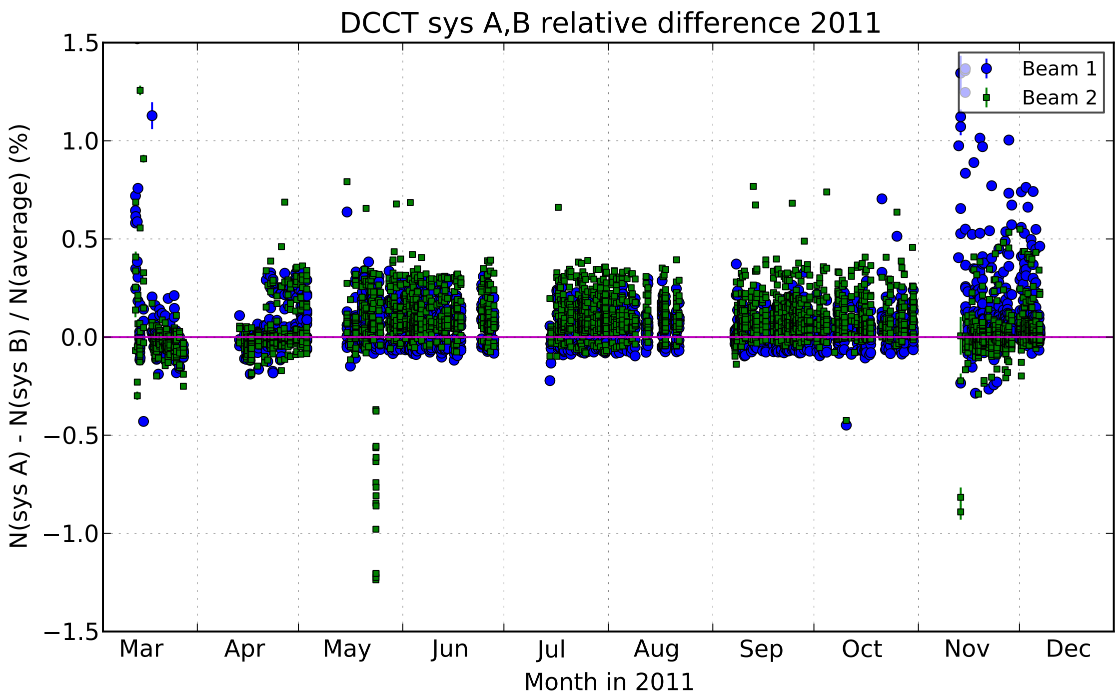

Figure 55: Relative difference between system A and B for 2011 using a 60 s average per injection step.

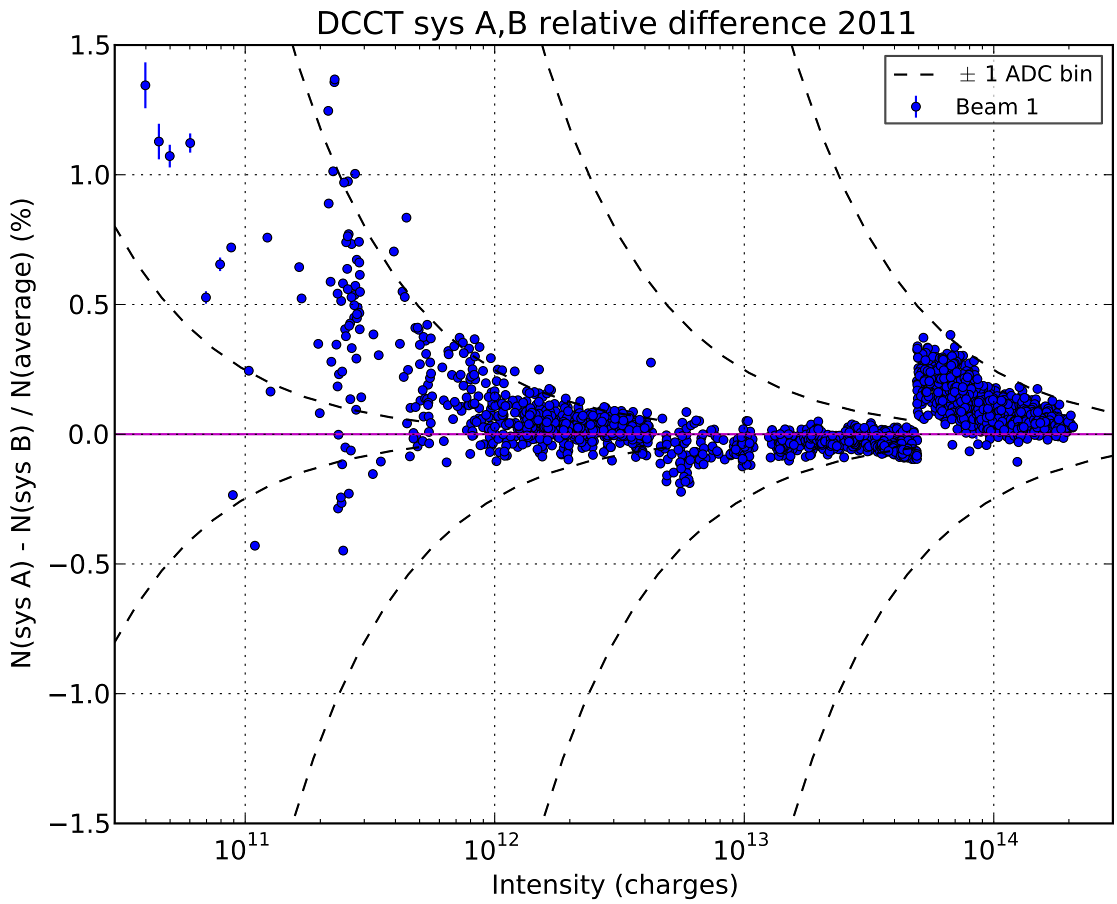

Figure 56: Relative difference between system A and B for 2011 *vs.* beam-1 intensity. Each point is a 60 s average of an injection step.

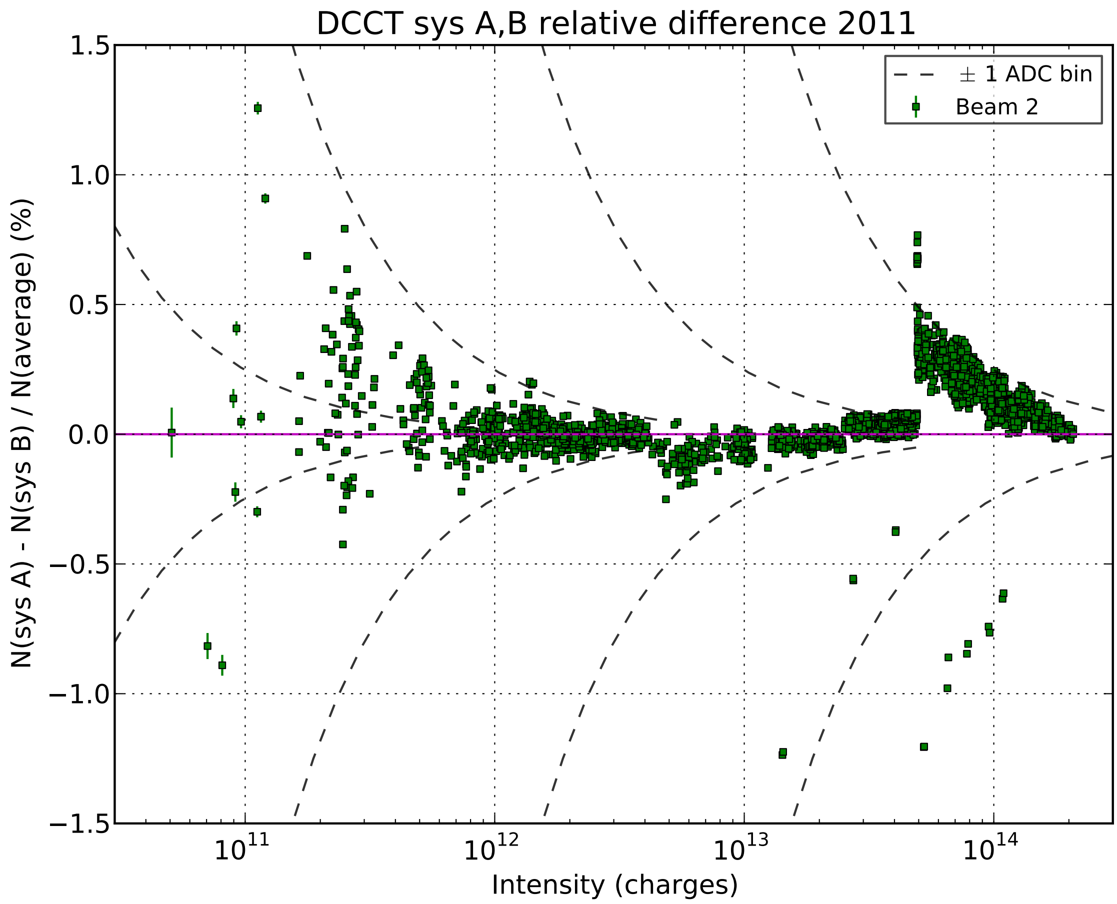

Figure 57: Relative difference between system A and B for 2011 *vs.* beam-2 intensity. Each point is a 60 s average of an injection step.

7 Summary of uncertainties affecting total-intensity measurements

The DCCT system proved to be stable and consistent throughout all tests documented in this work. No sensitivity to external factor or to the beam conditions could be found. The uncertainty of 0.1% attributed to the laboratory measurement of the bunch pattern dependence is probably limited by the instrumentation and components used in the setup. For the DCCT internal effects, the acquisition chain with the 12-bit ADC is limiting the accuracy for the ranges 1 to 3, while the noise level is limiting range 4. No error could be found in the calibration method and the accuracy of both sources was tested down to 0.05% in the laboratory. This uncertainty reflects the limits of the laboratory instrumentation and components and is higher than the specifications provided by the manufacturer.

The source of uncertainties without any measurable effect are listed in Table 8. The listed effects have been analyzed and the fluctuations are either compatible with the noise level or within one LSB. The summary of the DCCT uncertainties used for the final uncertainty on the beam intensities are listed in Table 9. All uncertainties are given as an envelope error (100% confidence level). To interpret the envelope uncertainties below in terms of 68.3% confidence level, the numbers in Table 9 and in the examples below should be multiplied by 0.683. The following errors should be considered as correlated between fills:

- The current source precision, because the same source is used for all calibrations throughout the year.
- The non-linearity of 12-bit ADC, because all fills are acquired with the same ADC.
- The bunch pattern dependence, because the laboratory measurement is applied to all DCCT's and it is not possible to exclude a systematic effect below 0.1%.

The other errors are related to random fluctuations and can be treated as uncorrelated between fills.

Table 8: Summary of tested source of uncertainty without measurable effect.

Source of uncertainty	Range	Relative error (%)	Absolute error
Cross-talk between beams (Sec. 4.1) Noise change during dump of other beam			-
Sensitivity to injected RF sine wave (Sec. 4.2.3) No resonance found between 1 kHz - 110 MHz			-
Sensitivity to LHC energy (Sec. 4.4.1) No correlation observed with LHC energy			-
Sensitivity to LHC RF system (Sec. 4.4.2) No correlation observed with LHC RF cavity field			-
Thermal effect during 24 hours under load No systematic drift of day/night effect (Sec. 3.4.2)			$< 0.01\%$
Current leak during calibration from surface No difference between the source on the surface or in the tunnel (Sec. 5.3)			-
Methodology of calibration procedure No difference between "self" calibration and standard BI procedure (Sec. 5.3)			-
Seasonal fluctuations of calibration factors Calibrations stable within expected ADC bit accuracy, verified over 9 month (Sec. 3.6)			-
Off-center position of calibration rods (Sec. 5.2)			-
Bunch position dependence (MD) No dependence found with beam movement during MD (Sec. 4.3)			-
Bunch pattern dependence (MD) No dependence found during beam debunching with RF off (Sec. 4.2.2)			-

Table 9: Source of uncertainties per beam. All numbers are given as envelope error (100% confidence level). For the baseline correction, the reduced error of $\pm\,1\cdot10^9$ charges can be used if the offset is corrected or smaller than $\pm\,1\cdot10^9$ e. Otherwise the more generic errors dependent on the range must be used. For the long term stability of the baseline, the indicated errors depend on the signal averaging time. A normalization of the beam intensity using a 1 hour average or more can use the lower errors provided in parenthesis. Low intensity fills acquired with range 4 will benefit from a longer averaging time, while the difference is negligible for the other ranges.

Source of uncertainty	Range	Relative error (%)	Absolute error	Correlated btw. beams
Current source precision		$\pm$ 0.05%		yes
accuracy limited by instrumentation (Sec. 5.1)				
Baseline correction				
If data is manually baseline corrected (Sec. 3.1)			$\pm\,1\cdot10^9$ e	
If data is not baseline corrected (Sec. 3.2)	1		$(\pm\,6\cdot10^{10}$ $e)$	
	2		$(\pm\,7\cdot10^9$ $e)$	
	3		$(\pm\,4\cdot10^9$ $e)$	
	4		$(\pm\,4\cdot10^9$ $e)$	
Non-linearity of 12-bit ADC (Sec. 3.4.3)			$\pm$ 1 LSB	yes
non-linearity tue to acquisition chain				
beam 1, 2 and all ranges share same ADC				
Long term stability of baseline				
observed fluctuations within 2×12 hours	1		$\pm\,1.1\cdot10^{11}$ e	
if signal average $\geq$ 1 minute (Sec. 3.4.1)	2		$\pm\,1.0\cdot10^{10}$ e	
	3		$\pm\,2.4\cdot10^9$ e	
	4		$\pm\,2.3\cdot10^9$ e	
observed fluctuations within 2×12 hours	1		$(\pm\,7.3\cdot10^9$ $e)$	
if signal average $\geq$ 1 hour (Sec. 3.4.1)	2		$(\pm\,1.1\cdot10^9$ $e)$	
	3		$(\pm\,1.1\cdot10^9$ $e)$	
	4		$(\pm\,1.0\cdot10^9$ $e)$	
Long term stability of calibration factor	1,2,3		$\pm$ 1 LSB	
envelope observed within 9 month (Sec. 3.6)	4		$\pm$ 4 LSB	
Bunch pattern dependence (laboratory test)		$\pm$0.1%		yes
accuracy limited by instrumentation (Sec. 4.2.1)				
Difference between system A and B	1,2,3		$\pm$ 1 LSB	
observed during all physics injections 2011	4		$\pm$ 10 LSB	
range 4 limited by noise (Sec. 6)				

The final uncertainty on the beam intensity provided by the DCCT depends on the range used for the measurement and the total intensity relative to the full scale of the range. The range used for a given fill can be deduced from Table 2. The acquisition system will select the most sensitive range such that the measurement is lower than the full scale of the range. For example a measurement of $4 \cdot 10^{12}$ charges is acquired with range 3. In case of doubt, the selected range for a DCCT can be retrieved from the logging database using the variable "LHC.BCTDC.A6R4.B1:SELECTED_RANGE" as an example for system A/beam 1. The 12-bit ADC has a total resolution of $2^{12} = 4096$ bins; due to the bipolar mode, only the positive range is used, limiting the full range to 2048 bins. In addition, the automatic offset correction can further reduce the range, therefore, it can be assumed in general that 2000 ADC bins are available to measure values covering the full dynamic of a range. In consequence, the absolute uncertainty corresponding to 1 LSB depends on the full intensity $N_{\text{Full scale}}$ of the range used:

$$1 \text{ LSB} = \frac{N_{\text{Full scale}}}{2000}, \tag{11}$$

Thus, for a beam intensity measured by the DCCT the relative uncertainty corresponding to 1 LSB is

$$\delta N_{LSB} = \frac{1 \text{ LSB}}{N_{\text{DCCT}}}. \tag{12}$$

The full scale of the range and the corresponding LSB value are given in Table 2.

The error on the baseline correction depends on whether the correction is applied or not: without any correction or verification, an absolute error of $\pm\, 5 \cdot 10^9$ charges has to be assumed (see Sec. 3.2). However, if the data is baseline-corrected, or if the absolute value of the baseline before and after the fill is smaller than 10^9 charges, the uncertainty of $\pm\, 1 \cdot 10^9$ charges can be used.

7.1 Example with a VDM fill

The following section is an example for the uncertainty calculation for the VDM fill 1783 on May 15 2011.

The fill started with an intensity of $3.26 \cdot 10^{12}$ protons and ended with $3.16 \cdot 10^{12}$ protons, and the DCCT was acquired with range 3. To be valid for the whole fill, the relative errors are based on the lowest intensity of $3.16 \cdot 10^{12}$ protons, with (12), the relative error of 1 LSB is 0.08%. The acquisition was locked on range 3 during the whole fill including the periods without beam. The absolute value of the baseline before and after the fill is smaller than 10^9 protons, a manual correction is therefore not warranted and the smaller error of 10^9 protons can be used as if the baseline was manually corrected. The relative error of the baseline is $10^9/3.16 \cdot 10^{12} = 0.03\%$. If the normalization is done with a time average shorter than 1 hour, then the error from the long term stability of baseline for range 3 is $2.4 \cdot 10^9$ protons corresponding to a relative error or 0.08%. The smaller error of $1.1 \cdot 10^9$ can be used if the normalization is done over a period of 1 hour or more. The summary of all uncertainties for fill 1783 is presented in Table 10. As with Table 9, all uncertainties are given as an envelope error.

In conclusion the total uncertainty per beam is 0.20% and of 0.34% for the beam product taking into account that the first three listed errors are correlated between beams.

Table 10: Summary of uncertainties for VDM fill 1783

Source of uncertainty (per beam)	Relative error (%)	Correlated btw. beams
Current source precision	$\pm$ 0.05	yes
Bunch pattern dependence (laboratory test)	$\pm$ 0.1	yes
Non-linearity of 12-bit ADC	$\pm$ 0.08	yes
Baseline correction	$\pm$ 0.03	no
Long term stability of baseline on range 3	$\pm$ 0.08	no
Long term stability of calibration on range 3	$\pm$ 0.08	no
Difference between system A and B on range 3	$\pm$ 0.08	no
Total error per beam	$\pm$ 0.20	
Correlated error per beam	($\pm$ 0.138)	yes
Uncorrelated error per beam	($\pm$ 0.143)	no
Total error on beam product	$\pm$ 0.34	

7.2 Example with a typical high intensity fill

The following section provides an example for the uncertainty calculation for a typical high intensity fill acquired in range 1 assuming an intensity of $1.5 \cdot 10^{14}$ protons. Without any analysis of the offset, an error of $\pm 6 \cdot 10^{10}$ protons has to be assumed for the baseline uncertainty, corresponding to a relative error of 0.04%. The long term stability of the baseline has an absolute error of $1.1 \cdot 10^{11}$ protons corresponding to a relative error of 0.07%. The maximal intensity of range 1 is $5 \cdot 10^{14}$ protons, with equation (12), the relative error of 1 LSB is $\pm$0.17%. The summary of all uncertainties given as an envelope error for such fill is presented in Table 11.

Table 11: Summary of uncertainties for a fill acquired with range 1

Source of uncertainty (per beam)	Relative error (%)	Correlated btw. beams
Current source precision	$\pm$ 0.05	yes
Bunch pattern dependence (laboratory test)	$\pm$ 0.1	yes
Non-linearity of 12-bit ADC	$\pm$ 0.17	yes
Baseline correction	$\pm$ 0.04	no
Long term stability of baseline on range 1	$\pm$ 0.07	no
Long term stability of calibration on range 1	$\pm$ 0.17	no
Difference between system A and B on range 1	$\pm$ 0.17	no
Total error per beam	$\pm$ 0.32	
Correlated error per beam	($\pm$ 0.20)	yes
Uncorrelated error per beam	($\pm$ 0.25)	no
Total error on beam product	$\pm$ 0.53	

7.3 Example with a low intensity fill

This section provides an example for the uncertainty calculation for a low intensity fill acquired in range 4 assuming an intensity of $4 \cdot 10^{10}$ protons as example. Provided the offset has been either corrected or is smaller than $1 \cdot 10^{9}$ protons, the reduced error of $\pm 1 \cdot 10^{9}$ protons can be used as baseline error, which corresponds to a relative error of $\pm$2.5%. If the normalization is done with a time average of 1 hour or more, then the absolute error from the long term stability of the baseline for range 4 is $1.0 \cdot 10^{9}$ protons corresponding to a relative error or 2.5%. The maximal intensity of range 4 is $5 \cdot 10^{11}$ protons, with equation (12), the relative error of 1 LSB is $\pm$0.63%. The summary of all uncertainties given as an envelope error for such a fill is presented in Table 12. The resulting beam intensity error is valid for any period during the fill averaged over 1 hour or more. The error is dominated by the difference between system A and B (±10 LSB). A lower error can be achieved by comparing both systems for the same time period.

Table 12: Summary of uncertainties for a fill acquired with range 4

Source of uncertainty (per beam)	Relative error (%)	Correlated btw. beams
Current source precision	± 0.05	yes
Bunch pattern dependence (laboratory test)	± 0.1	yes
Non-linearity of 12-bit ADC	± 0.63	yes
Baseline correction	± 2.50	no
Long term stability of baseline on range 4	± 2.5	no
Long term stability of calibration on range 4	± 2.5	no
Difference between system A and B on range 4	± 6.25	no
Total error per beam	± 7.6	
Correlated error per beam	(± 0.63)	yes
Uncorrelated error per beam	(± 7.6)	no
Total error on beam product	± 10.8	

7.4 Outlook

The laboratory measurement of the bunch pattern dependence is the dominating uncertainty and is probably limited by the instruments and components used in the setup. Furthermore the maximal intensity allowed by the setup could not test the high LHC intensities that can be reached with 25 ns bunch spacing. Therefore, further tests will be carried out in the laboratory to include all possible LHC intensities.

The remaining uncertainties are essentially originating from the noise level together with the baseline stability and the 12-bit limitation of the ADC acquisition. In conclusion, the ideal settings and conditions to minimize the DCCT uncertainties, for example during a van der Meer scan, are as follows.

- Low intensities acquired with range 4 should be avoided due to the dominating influence of the noise level and the baseline and scaling factor fluctuations. Ideally the beam intensities should lie within the ranges 1 to 3. The typical van der Meer scans performed in 2010 and 2011 were acquired in range 3.
- The total beam intensity should be close to the calibration point of the range which is normally set at 80% of each range (notice that range 1 is calibrated at 50% of its range). Therefore, the error induced by the non-linearity of the ADC is minimized near the calibration point; furthermore, at 80% of the range the relative error of 1 LSB is also reduced.
- The expected range should be blocked throughout the fill including periods without beam before and after the fill. Consequently the offset can be evaluated without analyzing the ADC raw values and the manual correction is simplified.

A new single range 24-bit ADC has been installed in the front-end electronics and will acquire the DCCT intensities in parallel to the actual setup starting with the 2012 LHC run. Once fully tested and validated, this new higher resolution acquisition might further reduce the uncertainties quoted in this work. Because the 24-bit is installed directly in the front-end electronics, digital values are send to the surface crates instead of analogue voltages; therefore, a better understanding of the DCCT intrinsic noise level, baseline fluctuations and linearity will be possible. Accordingly, the acquisition chain should not limit the DCCT's accuracy anymore in the future.

A Appendices

A.1 Noise and baseline correction

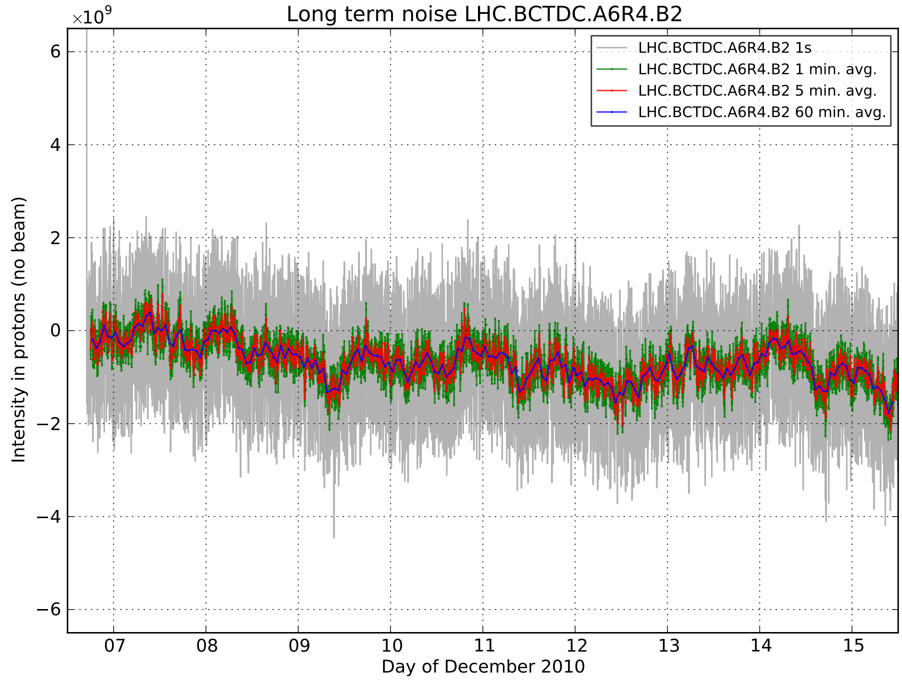

Figure 58: DCCT long term offset for system A/beam 2.

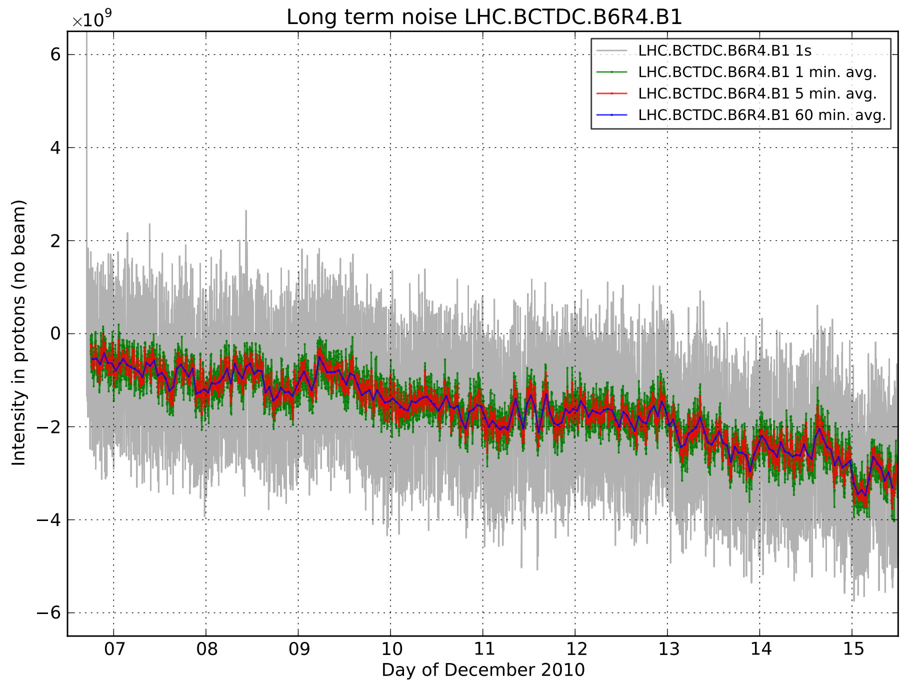

Figure 59: DCCT long term offset for system B/beam 1.

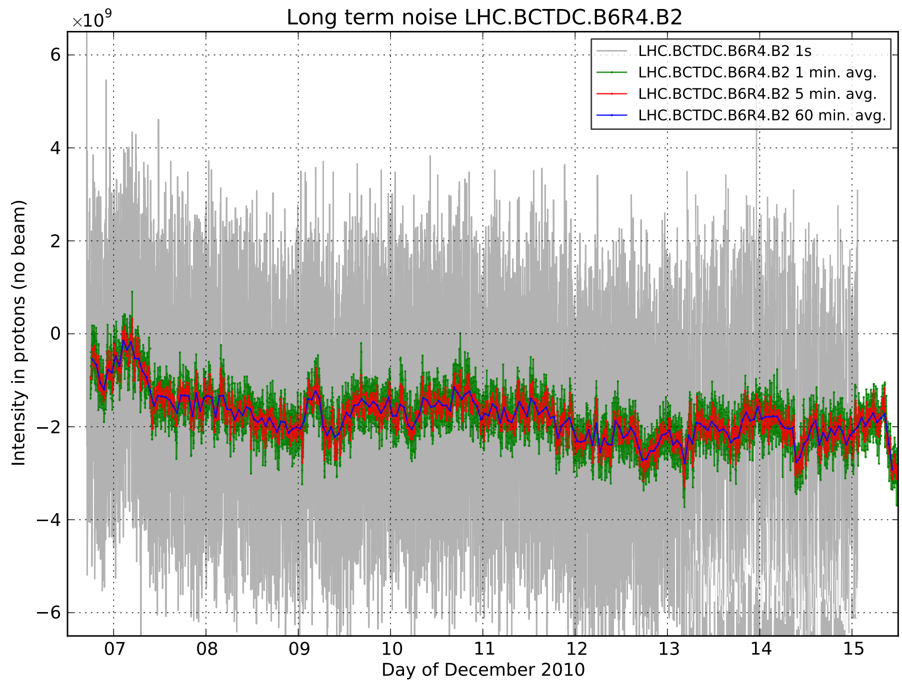

Figure 60: DCCT long term offset for system B/beam 2.

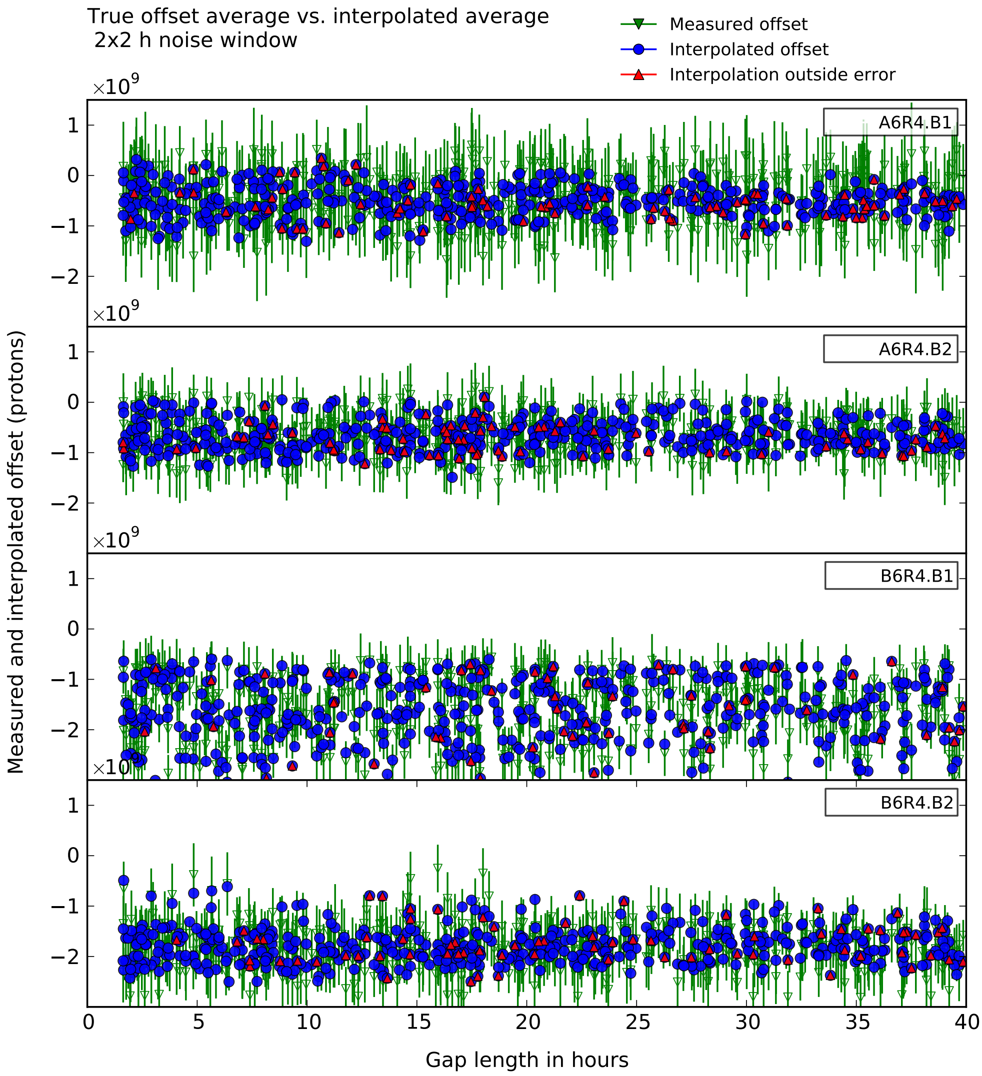

Figure 61: Offset box error test for all DCCT's. A random gap length between 1 h and 40 h is chosen at a random time position within the 9 days of available noise data. The true signal value taken at the center of the gap is compared to the interpolated value. A plain blue dot indicates an interpolated offset inside the error bar. A plain red triangle indicates an interpolated offset value outside of the expected error. 8.2% of the 2000 tests are outside of the peak-to-peak error.

A.2 Long term stability over 12 hours

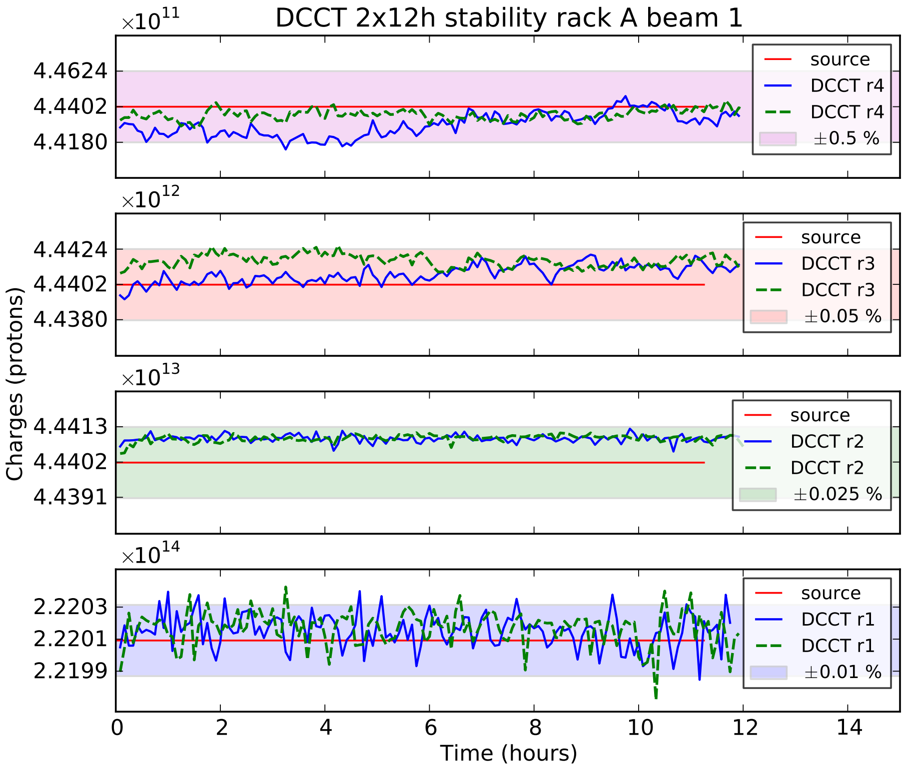

Figure 62: Long term stability under load for all ranges of system A/beam 1.

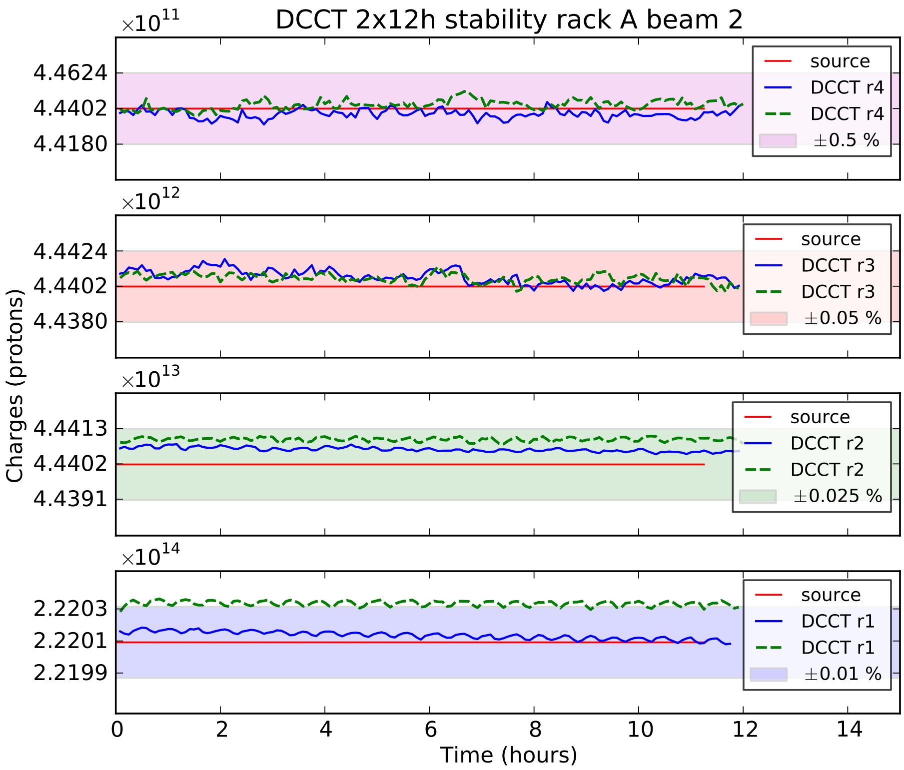

Figure 63: Long term stability under load for all ranges of system A/beam 2.

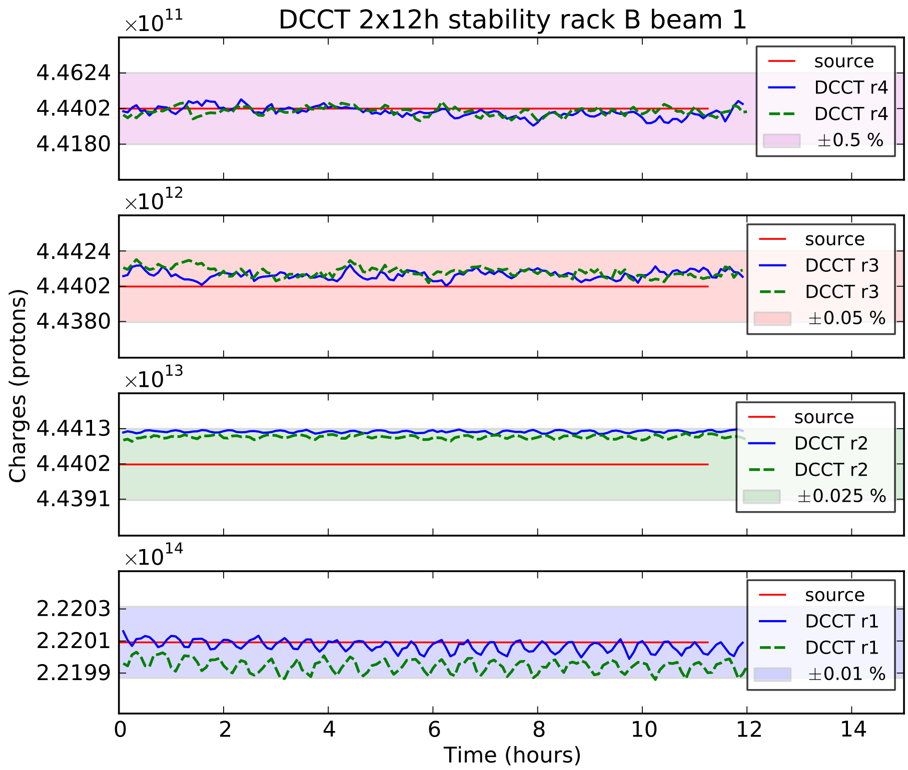

Figure 64: Long term stability under load for all ranges of system B/beam 1.

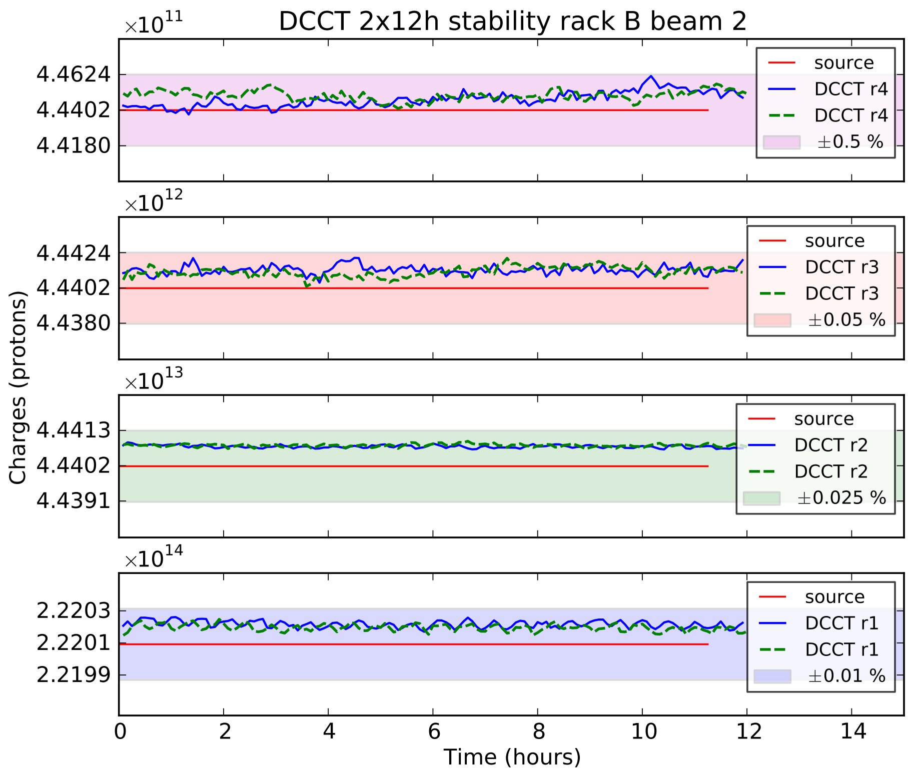

Figure 65: Long term stability under load for all ranges of system B/beam 2.

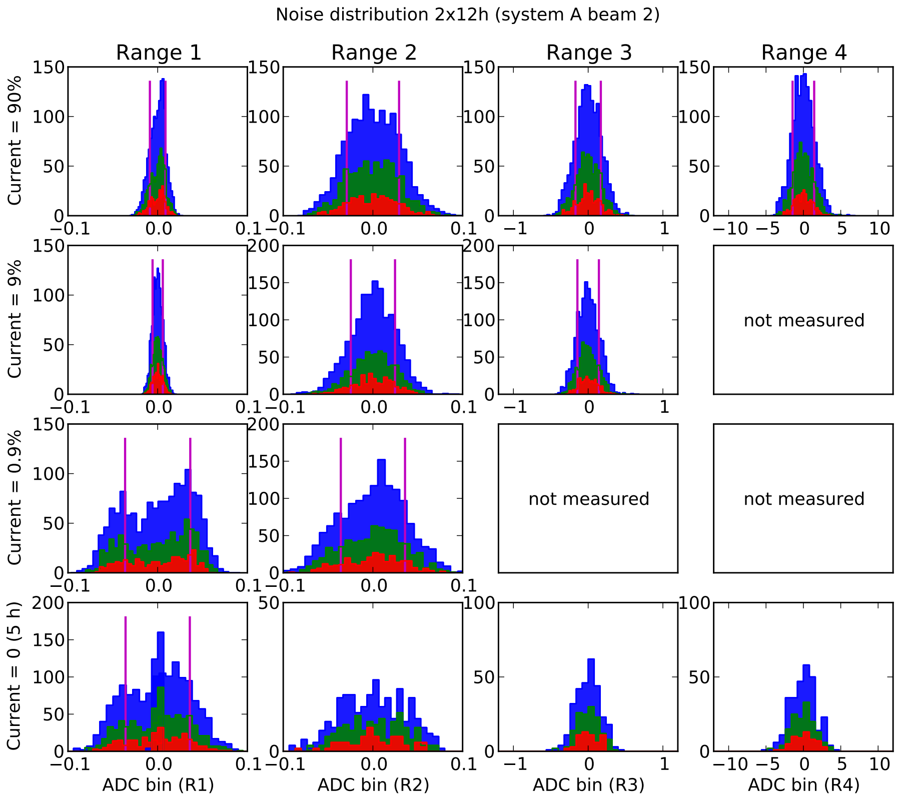

Figure 66: Histograms of 2×12 hours of all ranges for system A/beam 2

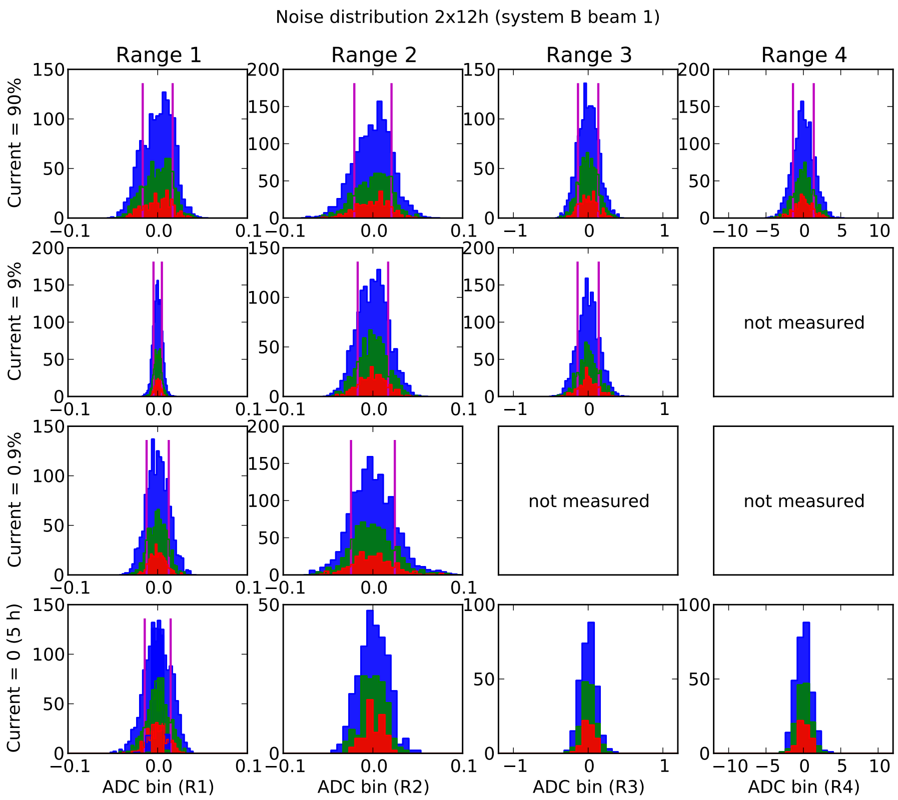

Figure 67: Histograms of 2×12 hours of all ranges for system B/beam 1

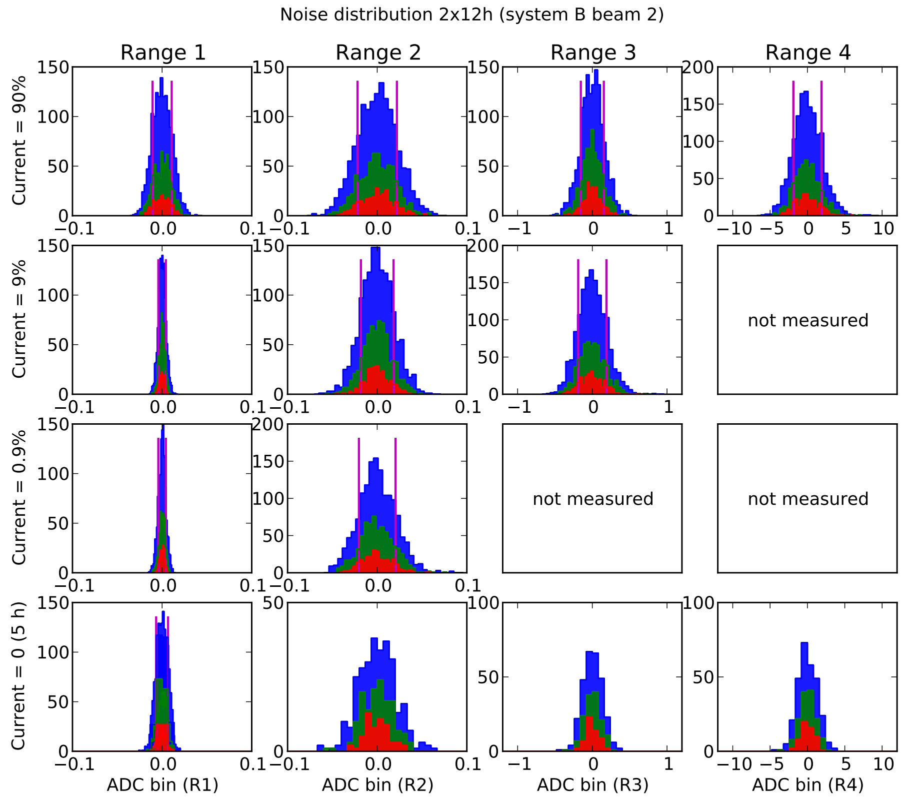

Figure 68: Histograms of 2×12 hours of all ranges for system B/beam 2

A.3 Linearity

A.3.1 Linearity measurements with 12-bit ADC

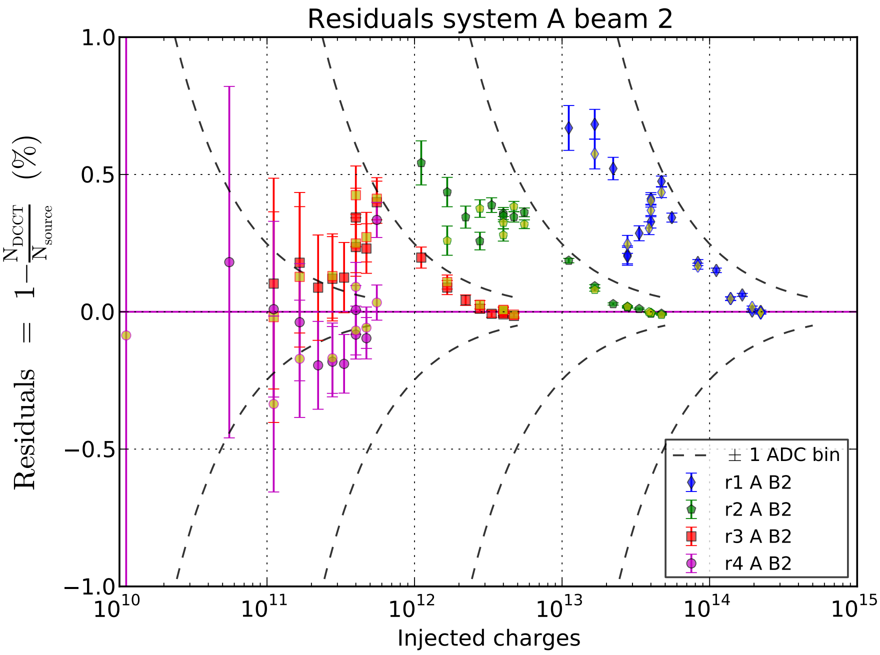

Figure 69: Linearity residuals for system A/beam 2 combining the values from the first measurement (plain dots) and the third measurement (yellow faced dots). Intensities below 2% of the range (about 40 ADC bins) are not shown.

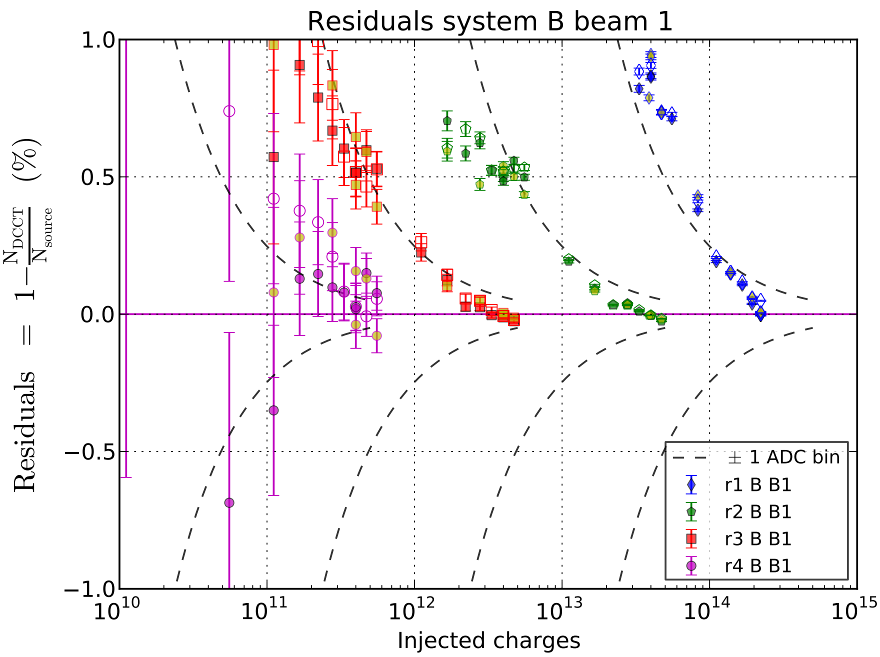

Figure 70: Linearity residuals for system B/beam 1 combining the values from the first measurement (plain dots), the second measurement (open dots) and the third measurement (yellow faced dots). Intensities below 2% of the range (about 40 ADC bins) are not shown.

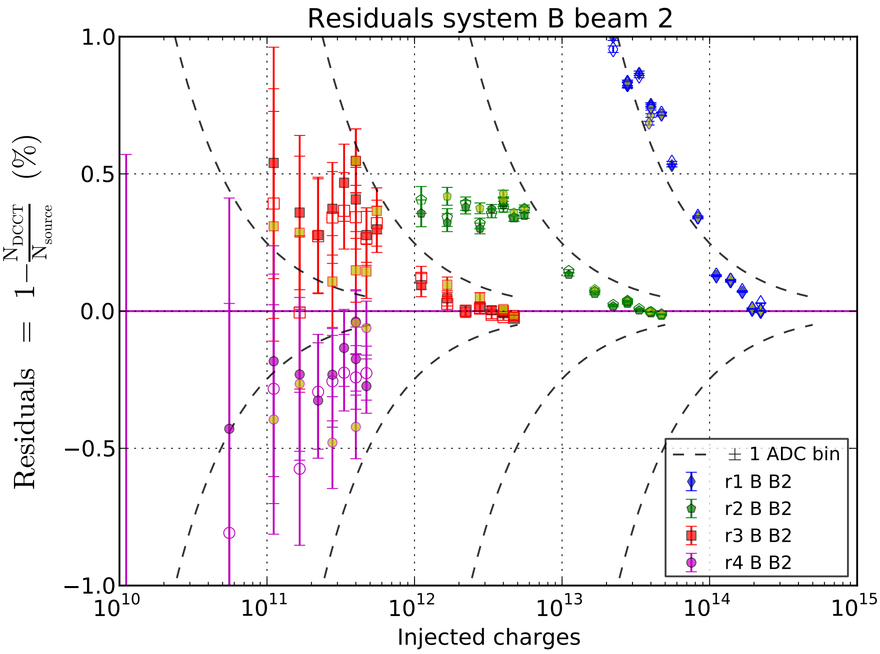

Figure 71: Linearity residuals for system B/beam 2 combining the values from the first measurement (plain dots), the second measurement (open dots) and the third measurement (yellow faced dots). Intensities below 2% of the range (about 40 ADC bins) are not shown.

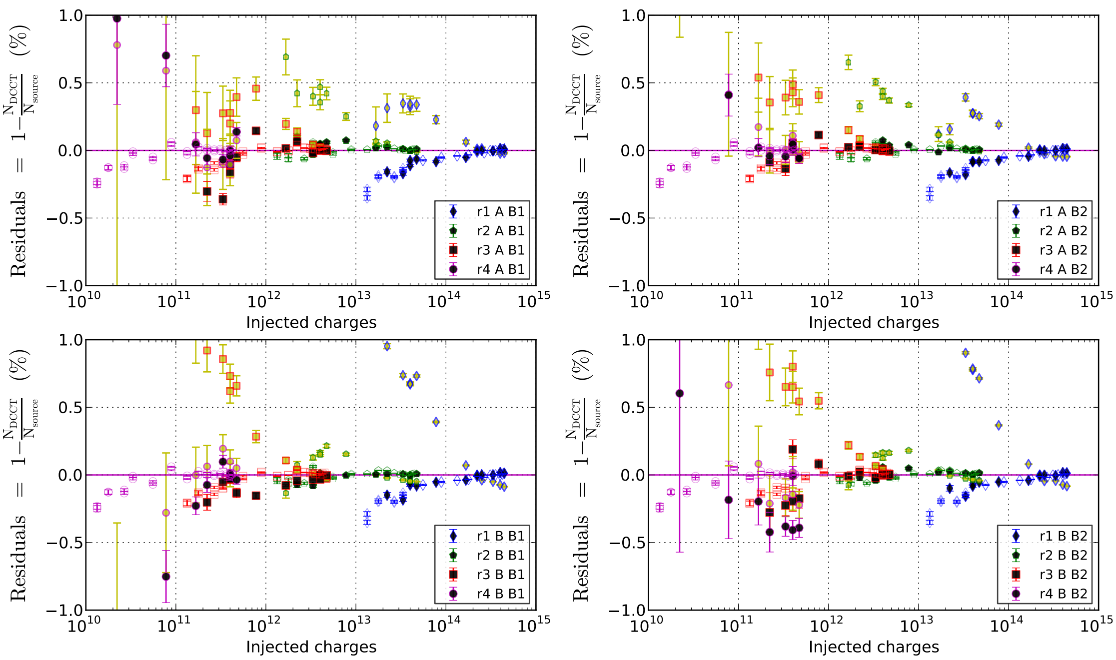

Figure 72: Linearity residuals measured with both ADC's. The empty markers are the laboratory reference response of the 16 bit NI ADC, the yellow filled markers are the DCCT response measured with the standard 12-bit ADC and the black filled markers are the DCCT response measured with the 16 bit NI ADC. With the ranges 1 and 2, the DCCT response measured with the NI ADC clearly follow the laboratory reference while the response measured with the 12-bit ADC shows the same positive residuals pattern as observed before (see above and Fig. 24). The larger fluctuations on range 3 still allow to see that the 16 bit measurement tends to follow the reference; however, range 4 is too noisy and difficult to measure as before. The observed non linearity is therefore due to the acquisition chain and not due to the DCCT itself.

A.3.2 Linearity measurements with 24-bit ADC

The scaling factors of the 24-bit acquisition were measured with a similar setup as used in Sec. 3.4.3. The source Yokogawa 7651 was used to inject a current trough the DCCT's in preprogrammed steps of 5 minutes. Due to the limited maximal output of 120 mA, the cable carrying the current passed one time through both systems A to test injections at low intensities and four times through both systems B to test injections at higher intensities. The maximal nominal current of the DCCT is 1 A. The measurement was performed three times within 24 hours and consisted of 31 steps of 5 minutes in a sequence similar to Fig. 22 in Sec. 3.4.3. The results are shown in Figures 73 to 76. The errors include the source uncertainty as specified by the manufacturer, the data fluctuations within one measurement step and the fluctuations due to the offset corrections.

The scaling factors are constant within $\pm 0.1\%$ for intensities larger than $5 \cdot 10^{11}$ protons. For lower intensities, the noise level and baseline fluctuations start to decrease the accuracy resulting in larger fluctuations as seen on both systems A. In general no systematic bias can be observed and the non-linearity measured in Sec. 3.4.3 is not observed with the 24-bit ADC acquisition.

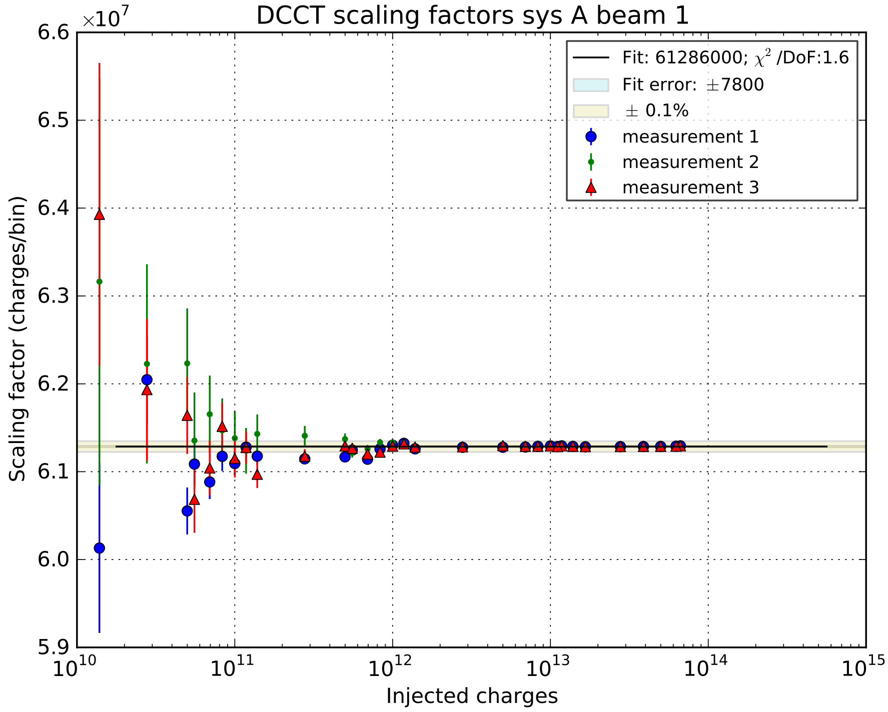

Figure 73: Scaling factor of 24-bit acquisition for system A/beam 1 combining the values from three measurements.

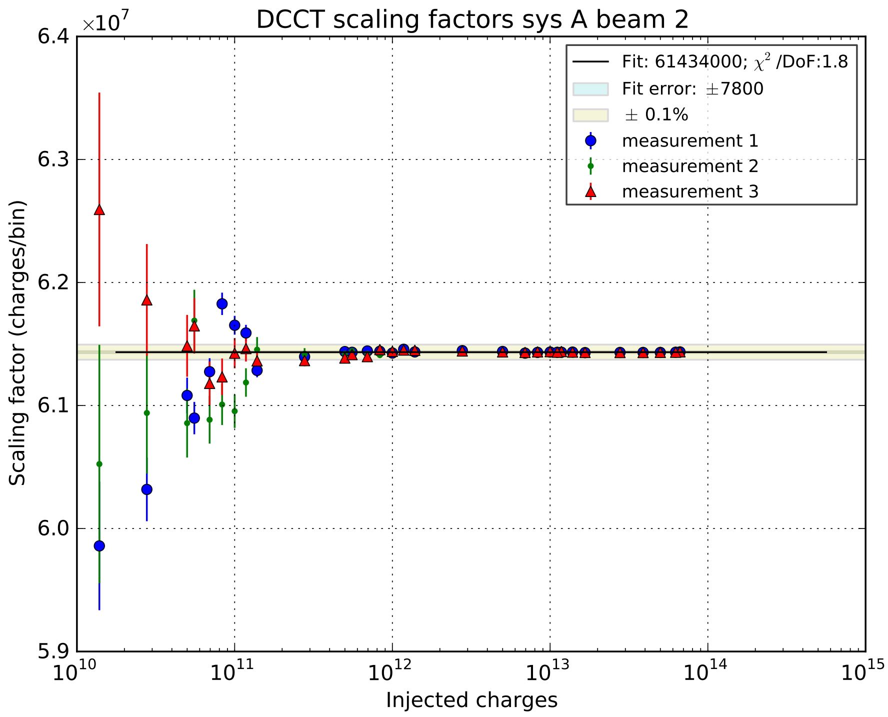

Figure 74: Scaling factor of 24-bit acquisition for system A/beam 2 combining the values from three measurements.

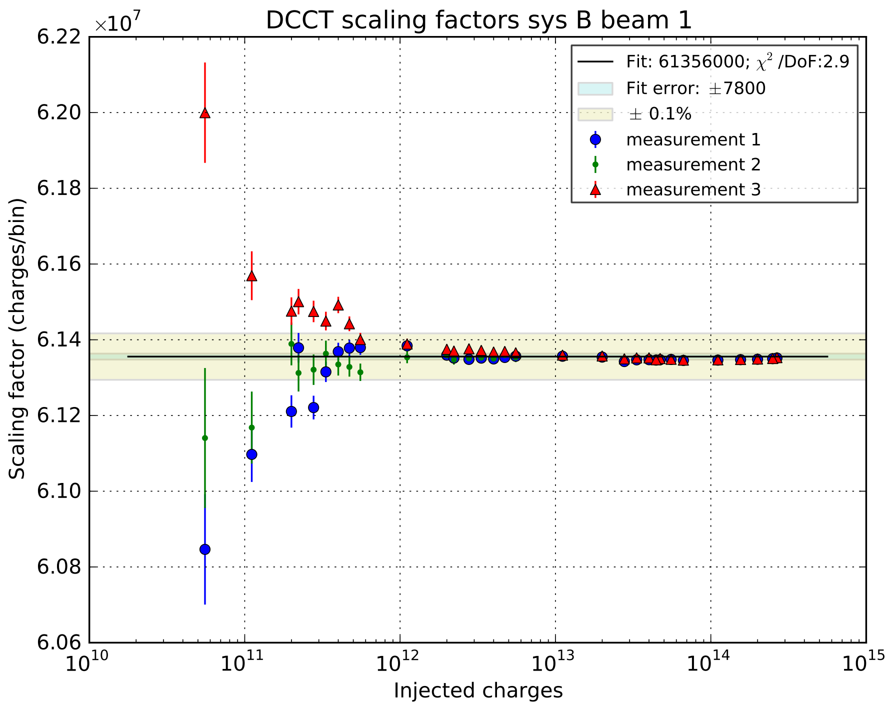

Figure 75: Scaling factor of 24-bit acquisition for system B/beam 1 combining the values from three measurements.

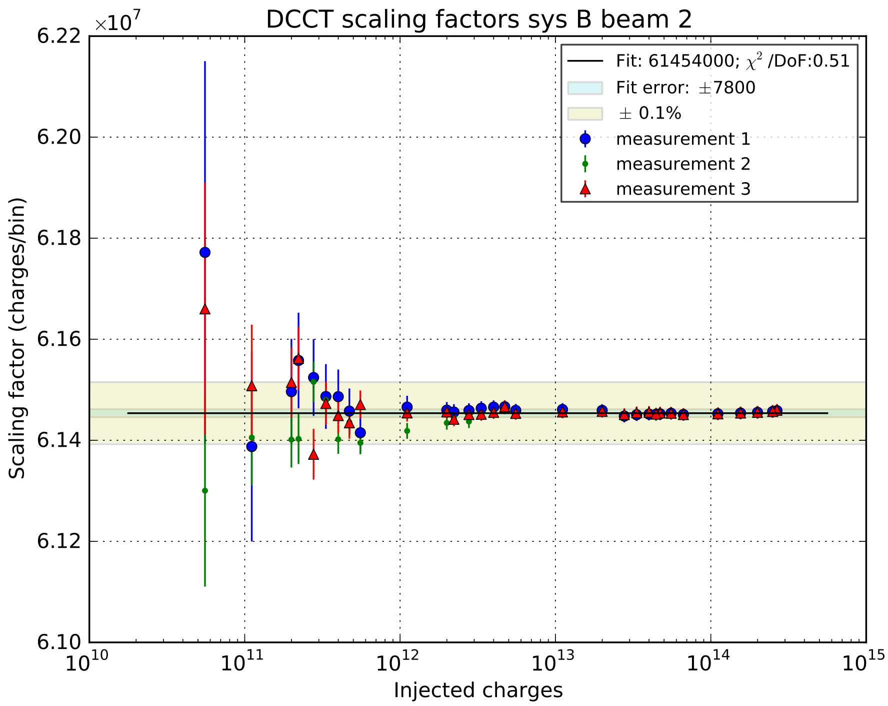

Figure 76: Scaling factor of 24-bit acquisition for system B/beam 2 combining the values from three measurements.

A.4 Cross talk between rings

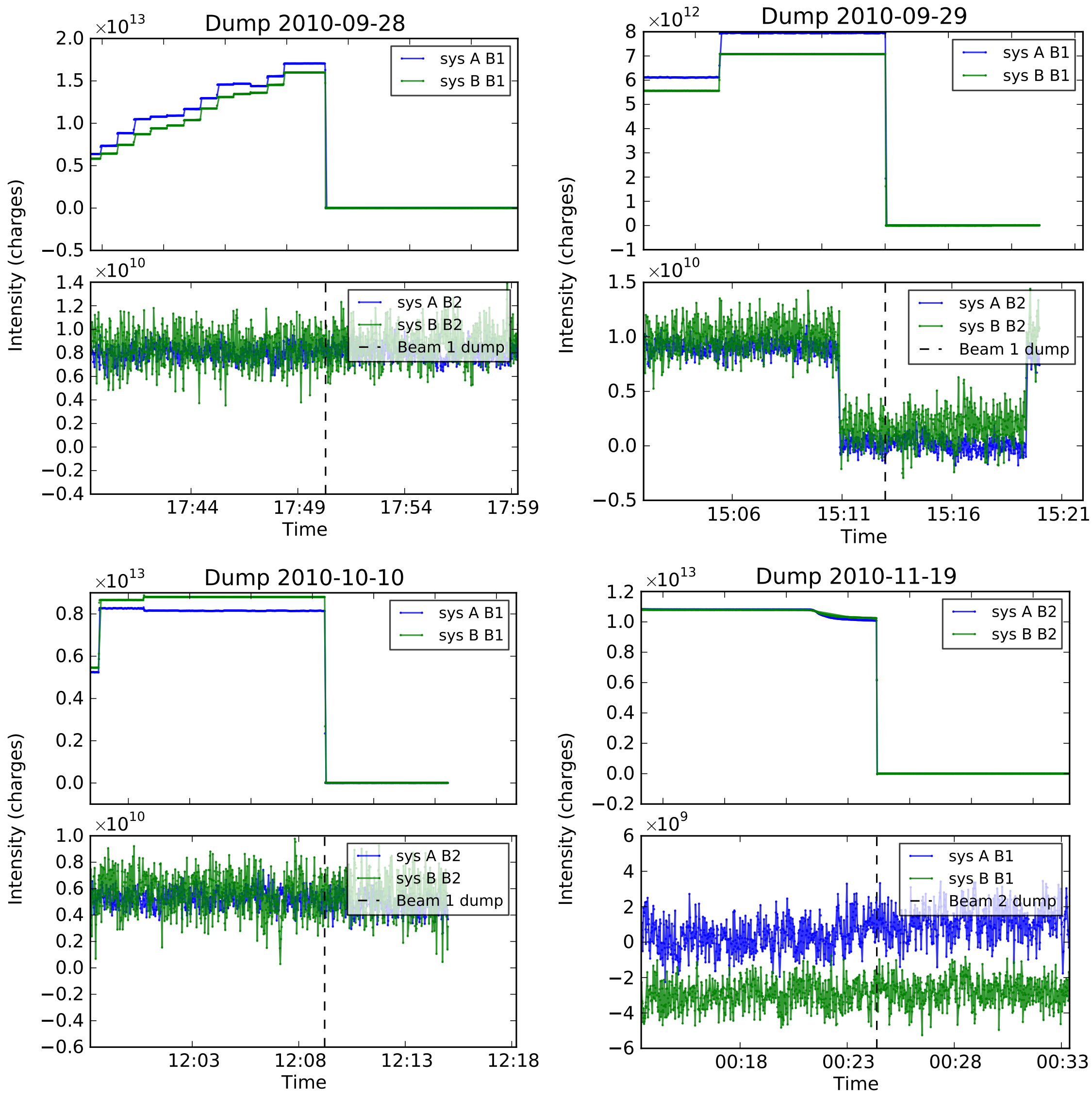

Figure 77: Cross talk between rings

A.5 Calibration

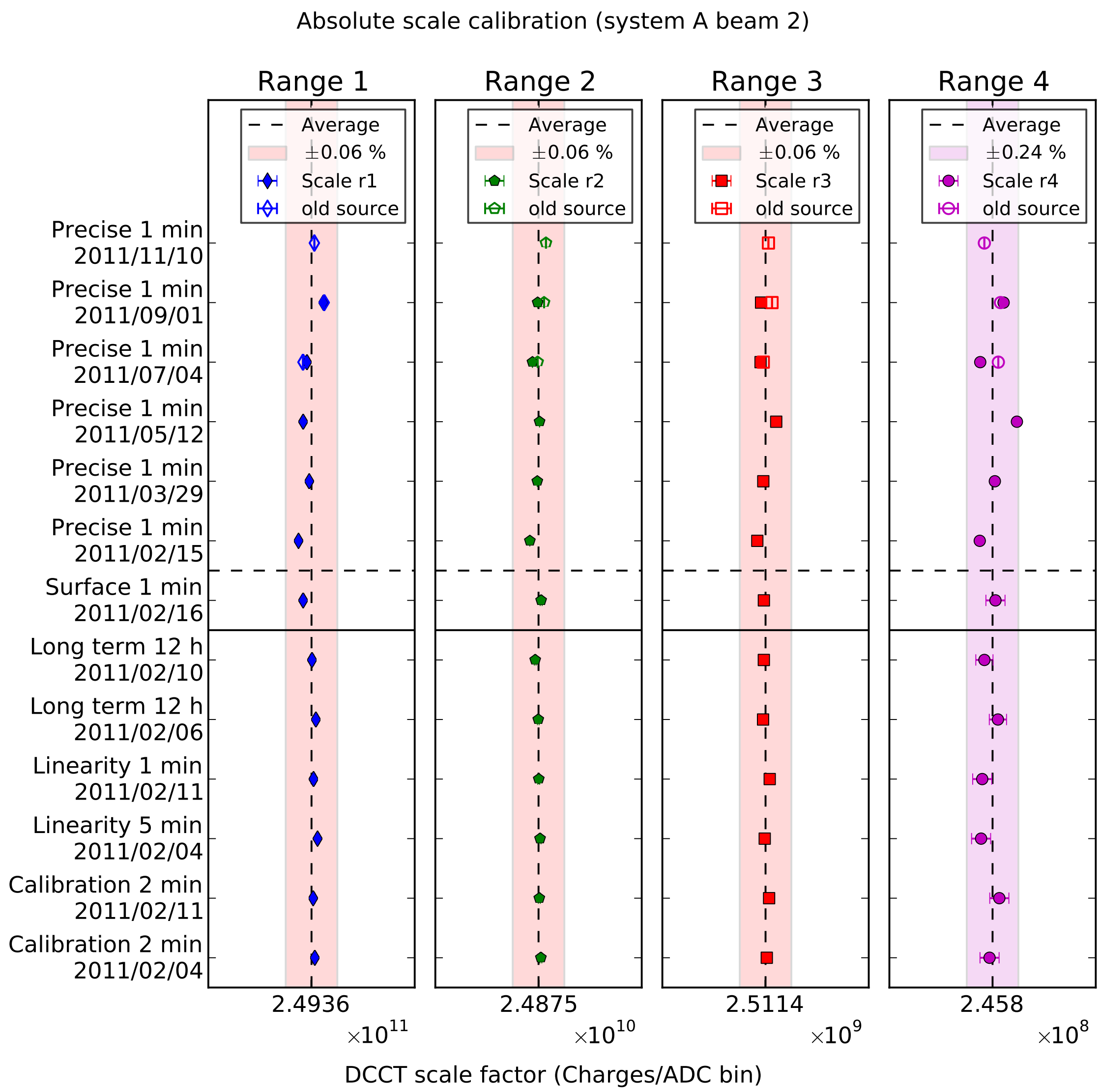

Figure 78: Calibration stability of all ranges of system A/beam 2.

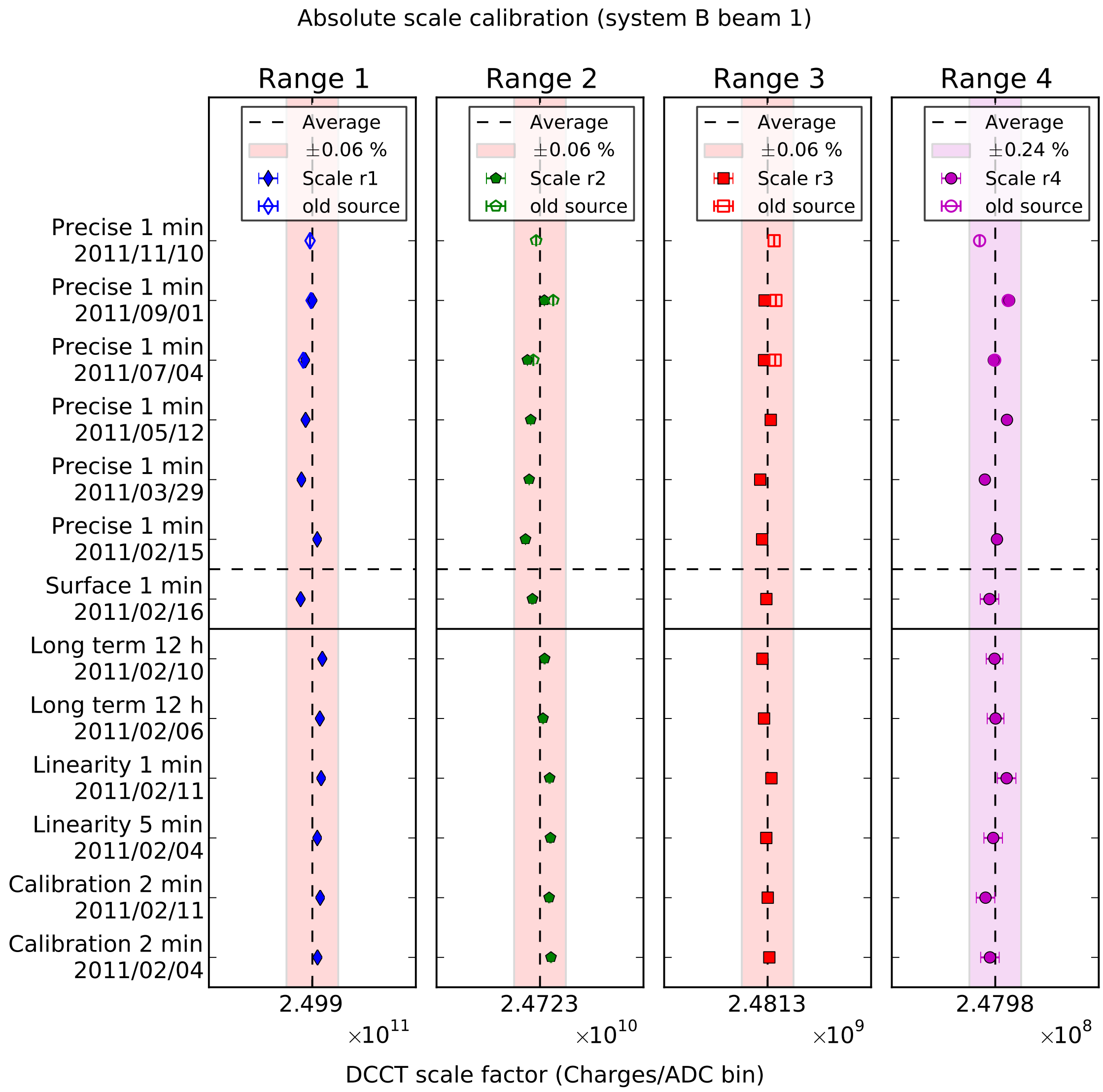

Figure 79: Calibration stability of all ranges of system B/beam 1.

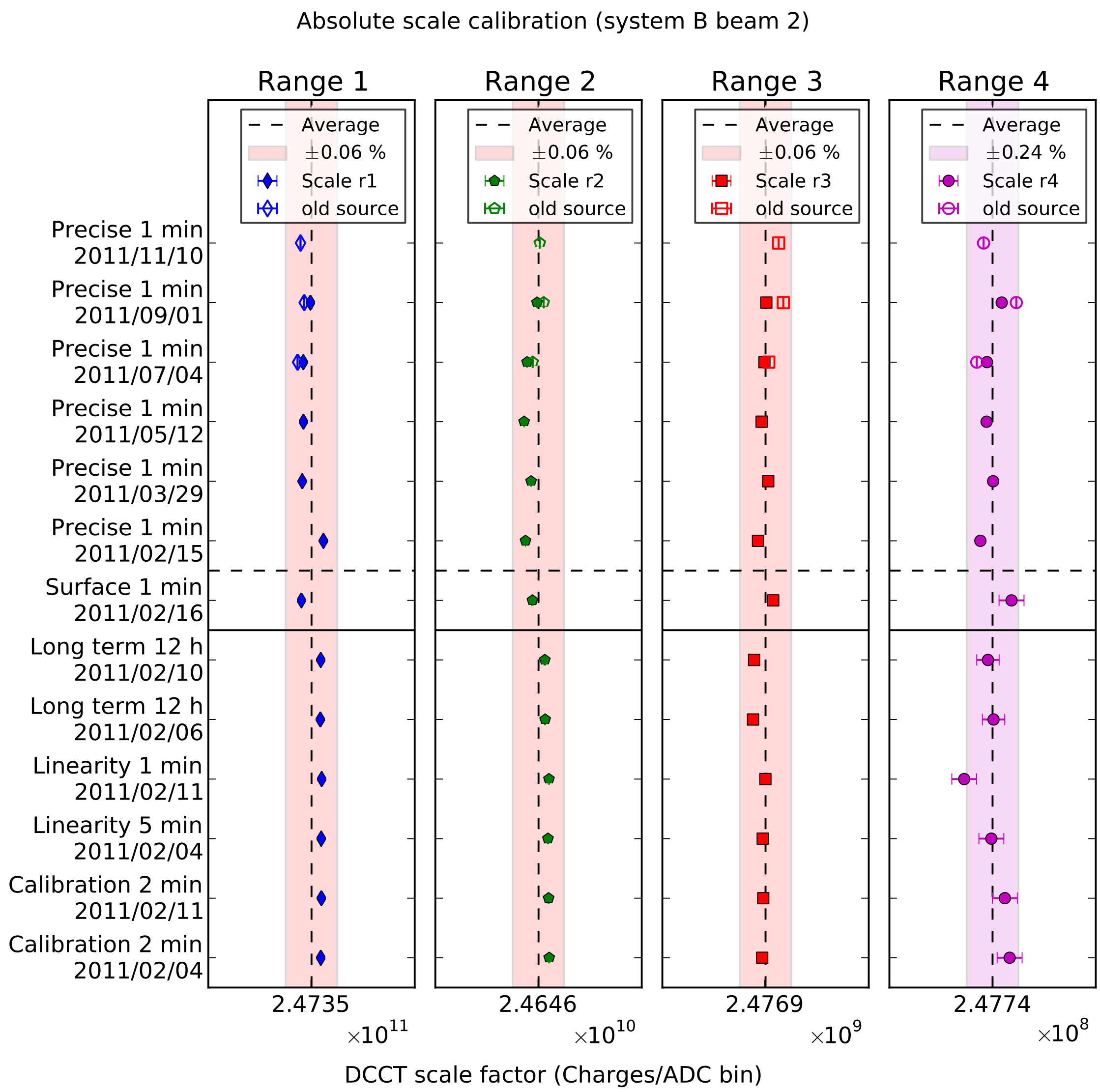

Figure 80: Calibration stability of all ranges of system B/beam 2.

References

[1] G. Anders, *et al. LHC Bunch Current Normalisation for the April-May 2010 Luminosity Calibration Measurements*. CERN-ATS-Note-2011-004 PERF, (BCNWG note1) (2011).
URL `http://cdsweb.cern.ch/record/1325370`

[2] G. Alici, *et al. LHC Bunch Current Normalisation for the October 2010 Luminosity Calibration Measurements*. CERN-ATS-Note-2011-016 PERF, (BCNWG note1) (2011).
URL `http://cdsweb.cern.ch/record/1333997`

[3] G. Anders, *et al. Study of the Relative LHC Bunch Populations for Luminosity Calibration*. CERN-ATS-Note-2012-028 PERF, (BCNWG Note 3) (2012).
URL `http://cdsweb.cern.ch/record/1427726`

[4] A. Alici, *et al. Study of the LHC Ghost Charge and Satellite Bunches for Luminosity Calibration*. CERN-ATS-Note-2012-029 PERF, (BCNWG Note 4) (2012).
URL `http://cdsweb.cern.ch/record/1427728`

[5] P. Odier, *et al. The DCCT for the LHC Beam Intensity Measurement*. Proceedings of DIPAC09, Basel, Switzerland. (2009).

[6] P. Odier, *et al. Operational Experience and Improvements of the LHC Beam Current Transformers*. Proceedings of DIPAC11, Hamburg, Germany (2011).

[7] P. Odier. *DCCT Technology Review*. In *2nd meeting in the framework of the CARE-HHH-ABI networking* (2004).